



<https://theses.gla.ac.uk/>

Theses Digitisation:

<https://www.gla.ac.uk/myglasgow/research/enlighten/theses/digitisation/>

This is a digitised version of the original print thesis.

Copyright and moral rights for this work are retained by the author

A copy can be downloaded for personal non-commercial research or study,  
without prior permission or charge

This work cannot be reproduced or quoted extensively from without first  
obtaining permission in writing from the author

The content must not be changed in any way or sold commercially in any  
format or medium without the formal permission of the author

When referring to this work, full bibliographic details including the author,  
title, awarding institution and date of the thesis must be given

Enlighten: Theses

<https://theses.gla.ac.uk/>  
[research-enlighten@glasgow.ac.uk](mailto:research-enlighten@glasgow.ac.uk)

U N I V E R S I T Y   O F   G L A S G O W

CHEMISTRY   DEPARTMENT

HALOGEN NUCLEAR QUADRUPOLE  
RESONANCE STUDIES OF SOME  
PHOSPHAZANE- AND PHOSPHAZENE-DERIVATIVES

Being

A thesis submitted in part fulfilment  
of the requirements for the

DEGREE OF DOCTOR OF PHILOSOPHY

by

KAREEM SHAREEF AHMED

MAY 1981

ProQuest Number: 10984240

All rights reserved

INFORMATION TO ALL USERS

The quality of this reproduction is dependent upon the quality of the copy submitted.

In the unlikely event that the author did not send a complete manuscript and there are missing pages, these will be noted. Also, if material had to be removed, a note will indicate the deletion.



ProQuest 10984240

Published by ProQuest LLC (2018). Copyright of the Dissertation is held by the Author.

All rights reserved.

This work is protected against unauthorized copying under Title 17, United States Code  
Microform Edition © ProQuest LLC.

ProQuest LLC.  
789 East Eisenhower Parkway  
P.O. Box 1346  
Ann Arbor, MI 48106 – 1346

## ACKNOWLEDGEMENTS

I would like to express my sincere thanks to Dr. A.L. Porte for his constant guidance and advice during all my work, and I am also grateful to Professor G.A. Sim for providing all necessary facilities in the laboratories, and Dr. R. Keat for providing several samples.

Special thanks are reserved for mechanical workshop staff for their co-operation during the construction of the "Pressure Vessel", and I wish to record my appreciation of all my friends and colleagues, who gave me helpful advice and co-operation during my work. My acknowledgements also due to Mrs. June Anthony for typing this thesis so quickly and so efficiently and so pleasantly.

It is a matter of great pride to dedicate my thesis to my wife and my children and my father. Their continual encouragement and happy home have always sustained me.

Finally, I must thank the University of Basrah and the Ministry of Higher Education of the Republic of Iraq for awarding me a scholarship and thereby enabling the higher studies described in this thesis to be carried out.

KAREEM SHAREEF AHMED

MAY 1981

## PREFACE

This thesis is concerned with some chemical aspects of nuclear quadrupole resonance spectroscopy applied to the study of some solid compounds containing phosphorus-halogen bonds. It is made up of seven chapters.

The first deals with the basic theory of the quadrupolar interactions of  $I = \frac{3}{2}$  nuclei.

In Chapter 2 the effects of changes of temperature and pressure on quadrupole resonance frequencies are considered in detail. The Bayer-Kushida theory is presented and the volume dependence of quadrupole resonance frequencies are discussed. Isothermal volume dependence of these frequencies and their temperature dependence under constant pressure conditions is considered in more detail in Appendix - 2A, at the end of this chapter.

Chapter 3 deals with Zeeman splitting of quadrupole resonance spectra of  $I = \frac{3}{2}$  nuclei. The "zero-splitting locus" and the "frequency-field" methods, which enable the asymmetry parameters to be obtained in single crystals, are presented, and the theory developed by Morino and Toyama, for polycrystalline specimens, is discussed in detail.

The experimental techniques for detecting nuclear quadrupole resonance transitions are discussed in Chapter 4. The super-regenerative oscillator, used in the present work, is described in some detail and other techniques, including Double Resonance with Level Crossing, are briefly mentioned in this chapter.

The work described in Chapters 5, 6 and 7 is unique. Chapter 5 is concerned with the effects of temperature variation on the chlorine-35 and bromine-79 quadrupole resonance frequencies in some acyclic compounds of phosphorus. The procedures for preparing these derivatives are described in detail in Appendix - 5A. The nitrogen gas-flow system, used to control the temperature in the present work, is described in Appendix - 5B.

Halogen quadrupole resonance spectra of some cyclophosph(III)-azane derivatives are examined over wide ranges of temperature in Chapter 6. The pressure dependence of bromine-79 N.Q.R. frequencies in  $(\text{BrPNBu}^t)_2$  is also examined. Chlorine-35 and bromine-79 quadrupole spectra of  $(\text{ClPNBu}^t)_2$  and of  $(\text{BrPNBu}^t)_2$ , respectively, are investigated in applied magnetic fields, and halogen asymmetry parameters are estimated. The N.Q.R. data are then used to obtain information about the  $\pi$ -characters in the P-Cl and P-Br bonds in these molecules. Procedures for preparing these cyclophosph(III)azane derivatives are presented in Appendix - 6A, while Appendices 6B and 6C describe the experimental aspects of the pressure and Zeeman experiments, respectively.

Chapter 7 is concerned with the effects of temperature and pressure variations on the bromine-79 and/or bromine-81 N.Q.R. spectra of some bromocyclophosphazatriene derivatives: these data enable molecular conformations to be assigned to these molecules. Furthermore, asymmetry parameters are approximately estimated and thence information is deduced about the  $\pi$ -characters of the P-Br bonds in  $\text{N}_3\text{P}_3\text{Br}_6$ . The N.Q.R. data has also been used to place electro-negativities of substituents in these cyclophosphazane and cyclophosphazene derivatives in a relative order, and the bromine frequencies

## TABLE OF CONTENTS

### CHAPTER 1

#### NUCLEAR QUADRUPOLE RESONANCE SPECTROSCOPY

	<u>Page</u>
1.1 INTRODUCTION	1
1.2 THE QUADRUPOLE ENERGY LEVELS	3

### CHAPTER 2

#### THE EFFECTS OF TEMPERATURE AND PRESSURE ON PURE NUCLEAR QUADRUPOLE RESONANCE FREQUENCIES

2.1 INTRODUCTION	14
2.2 THE BAYER-KUSHIDA THEORY : TEMPERATURE DEPENDENCE OF N.Q.R. FREQUENCIES UNDER CONSTANT VOLUME CONDITIONS	16
2.3 THE VOLUME DEPENDENCE OF QUADRUPOLE RESONANCE FREQUENCIES	30

APPENDIX - 2A

2A.1	ISOTHERMAL VOLUME DEPENDENCE OF QUADRUPOLE RESONANCE FREQUENCIES	35
2A.2	TEMPERATURE DEPENDENCE OF QUADRUPOLE RESONANCE FREQUENCIES UNDER CONSTANT PRESSURE CONDITIONS	39

CHAPTER 3

ZEEMAN SPLITTING OF QUADRUPOLE RESONANCE SPECTRA FOR  
SPIN  $\frac{3}{2}$  NUCLEI

3.1	INTRODUCTION	42
3.2	ZEEMAN EFFECTS ON QUADRUPOLE RESONANCE SPECTRA FOR $I = \frac{3}{2}$ NUCLEI	43

## CHAPTER 4

### EXPERIMENTAL DETECTION OF NUCLEAR QUADRUPOLE

#### RESONANCE ABSORPTION

	<u>Page</u>
4.1 INTRODUCTION	56
4.2 THE SUPER-REGENERATIVE OSCILLATOR	58

## CHAPTER 5

### HALOGEN NUCLEAR QUADRUPOLE RESONANCE STUDIES OF SOME

ACYCLIC COMPOUNDS OF PHOSPHORUS:  $\text{CH}_3\text{N}(\text{PCl}_2)_2$ ,  $\text{PhPCl}_2$ ,

$\text{PhPBr}_2$  AND  $\text{C}_6\text{H}_5\text{NPOCl}_2$

5.1 INTRODUCTION	70
5.2 THE EFFECTS OF TEMPERATURE VARIATION ON HALOGEN N.Q.R. SPECTRA OF $\text{CH}_3\text{N}(\text{PCl}_2)_2$ , $\text{PhPCl}_2$ , $\text{PhPBr}_2$ AND $\text{C}_6\text{H}_5\text{NPOCl}_2$	72

APPENDIX - 5A

Page

PREPARATION OF THE ACYCLIC COMPOUNDS

5A.1 Preparation of $\text{CH}_3\text{N}(\text{PCl}_2)_2$	89
5A.2 Preparation of $\text{PhPBr}_2$	90
5A.3 Preparation of $\text{Cl}_3\text{PNPOCl}_2$	91

APPENDIX - 5B

THE NITROGEN GAS-FLOW SYSTEM	92
------------------------------	----

CHAPTER 6

HALOGEN QUADRUPOLE RESONANCE STUDIES OF SOME  
CYCLOPHOSPH(III)AZANE DERIVATIVES

6.1 INTRODUCTION	95
6.2 TEMPERATURE DEPENDENCE OF CHLORINE-35 N.Q.R. FREQUENCIES IN $(\text{ClPNEt})_3$ , $(\text{ClPNPh})_2$ AND $(\text{ClPNBu}^t)_2$	97
6.3 PRESSURE DEPENDENCE OF BROMINE-79 QUADRUPOLE RESONANCE FREQUENCIES IN $(\text{BrPNBu}^t)_2$	108
6.4 TEMPERATURE DEPENDENCE OF BROMINE-79 QUADRUPOLE RESONANCE FREQUENCIES IN $(\text{BrPNBu}^t)_2$	113
6.5 THE HALOGEN QUADRUPOLE RESONANCE SPECTRA OF $(\text{ClPNBu}^t)_2$ AND $(\text{BrPNBu}^t)_2$ IN APPLIED MAGNETIC FIELDS	120

APPENDIX - 6A

Page

PREPARATION OF CYCLOPHOSPH(III)AZANE DERIVATIVES

6A.1 Preparation of $(C\&PNET)_3$	132
6A.2 Preparation of $(C\&PNPh)_2$	133
6A.3 Preparation of $(C\&PNBu^t)_2$	134
6A.4 Preparation of $(BrPNBu^t)_2$	135

APPENDIX - 6B

BROMINE QUADRUPOLE SPECTRA AT HIGH PRESSURES	136
----------------------------------------------	-----

APPENDIX - 6C

EXPERIMENTAL ASPECTS OF ZEEMAN N.Q.R. STUDIES	148
-----------------------------------------------	-----

CHAPTER 7

BROMINE QUADRUPOLE RESONANCE STUDIES OF SOME  
BROMOCYCLOTRIPHOSPHAZATRIENE DERIVATIVES

7.1 INTRODUCTION	153
------------------	-----

	<u>Page</u>
7.2 BROMINE QUADRUPOLE RESONANCE SPECTRA OF $N_3P_3Br_6$ , $N_3P_3Br_5NHPr^i$ , $cis-N_3P_3Br_4(NMe_2)_2$ AND $cis-N_3P_3Br_3Ph_3$ SUBJECTED TO HYDROSTATIC PRESSURES	155
7.3 TEMPERATURE DEPENDENCE OF BROMINE QUADRUPOLE RESONANCE SPECTRA OF $N_3P_3Br_6$ , $N_3P_3Br_5NHPr^i$ , $cis-N_3P_3Br_4(NMe_2)_2$ AND $cis-N_3P_3Br_3Ph_3$	166
7.4 THE EFFECTS OF WEAK MAGNETIC FIELDS ON BROMINE-81 N.Q.R. SPECTRA OF $N_3P_3Br_6$	187

#### APPENDIX - 7

##### PREPARATION OF THE BROMOCYCLOTRIPHOSPHAZATRIENE

##### DERIVATIVES

7.1 Preparation of $N_3P_3Br_6$	193
7.2 Preparation of $cis-N_3P_3Br_4(NMe_2)_2$	195
7.3 Preparation of $cis-N_3P_3Br_3Ph_3$	196
7.4 Preparation of $N_3P_3Br_5NMe_2$	198
7.5 Preparation of $N_3P_3Br_5NHPr^i$	199

REFERENCES	200
------------	-----

CHAPTER 1

NUCLEAR QUADRUPOLE RESONANCE SPECTROSCOPY

1.1. INTRODUCTION

All nuclei are charged and some possess angular momentum. Spinning charges generate magnetic fields and so a magnetic moment can be associated with this angular momentum.

The quantum mechanics of angular momentum and its operators show that the maximum component of the angular momentum of a spinning nucleus can be written in the form  $I \frac{h}{2\pi}$  where  $h$  is Planck's constant and  $I$  is a spin quantum number.  $I$  must be either half-integral or integral. Each nuclear ground state has its own characteristic value of  $I$ . The total angular momentum of the nucleus,  $\underline{I}$ , can be shown to be  $\sqrt{I(I+1)}$  in units of  $\frac{h}{2\pi}$  and there are only certain permitted values for the components of total angular momentum projected, for example, along the direction of an applied magnetic field. These permitted values are given by  $m_I \frac{h}{2\pi}$ , where

$$m_I = (+I), (I-1), (I-2) \dots (-I) \quad 1.1$$

There are obviously  $(2I+1)$  allowed orientations or states for the nucleus, all of which have the same energy in the absence of a magnetic field, but have different potential energies in the presence of a uniform magnetic field.

A large assembly of nuclei in equilibrium with its environment distributes itself over these energy levels in accordance with Boltzmann's distribution law; an excess number of nuclei lie in the lower levels.

In nuclear magnetic resonance spectroscopy, magnetic nuclei are made to undergo transitions between allowed states, by coupling radio frequency radiation with the nuclear magnetic dipole moments.

In nuclear quadrupole resonance spectroscopy, another branch of radio frequency spectroscopy, the radio frequency radiation is also coupled to nuclear magnetic dipole moments. This branch of spectroscopy is concerned with nuclei for which the spin quantum number  $I \geq 1$ . The charge distribution in such nuclei is not spherical, and so these nuclei also possess electric quadrupole moments which enable them to interact with the electric field gradient tensor which is produced by nearby charges. This interaction is quantized and it is the transitions between the levels allowed for the electrostatic interaction, which cause absorption of radio frequency radiation. Although the interaction of a nuclear quadrupole moment is an electrostatic interaction, its coupling to the radiation field is magnetic dipolar in character and so nuclear quadrupole resonance can be considered to be a branch of magnetic resonance spectroscopy. Provided care is taken, nuclear quadrupole resonance spectroscopy offers a unique means for studying chemical bonding and electron distributions in molecular solids since it provides information about the electric field gradient tensor and about the degree of asymmetry of this tensor at the nuclear site in the ground state of the system. Before discussing the interpretation of quadrupole resonance spectra, it is worth while considering

in more detail the nature of the nuclear quadrupole moment and its interaction with the electric field gradients produced by all charged particles in its environment.

## 1.2 THE QUADRUPOLE ENERGY LEVELS

Let  $\rho(r)$  be the charge density in a small volume element  $d\tau$  inside a nucleus at a distance  $r$  from the nuclear centre of mass, and let the centre of mass be the origin of a Cartesian coordinate system. The incremental charge  $\rho(r)d\tau$  interacts with the external potential  $V(r)$  generated by all charged particles, both electrons and nuclei, that surround the nucleus in any chemically interesting situation and the contribution made by this interaction to the energy of nucleus is given by

$$E = \int \rho(r)V(r)d\tau \quad 1.2$$

where the integral is taken over the nuclear volume.

When the charge distribution is small and the potential does not change rapidly over the volume, as is the case for the nuclear volume, the potential  $V(r)$  can be expanded in a Taylor series about the nuclear centre of mass, as origin, to give

$$V(r) = V(o) + \sum_{\alpha} V_{\alpha} X_{\alpha} + \frac{1}{2} \sum_{\alpha\beta} X_{\alpha} X_{\beta} V_{\alpha\beta} + \text{higher order terms} \quad 1.3$$

where  $\alpha, \beta = 1, 2, 3$  and  $X_\alpha$  and  $X_\beta = x, y$  and  $z$

$$V_{\alpha} = \left( \frac{\partial V}{\partial X_{\alpha}} \right)_{r=0} \quad 1.4$$

$$V_{\alpha\beta} = \left( \frac{\partial^2 V}{\partial X_{\alpha} \partial X_{\beta}} \right)_{r=0} \quad 1.5$$

hence

$$E = V(0) \int \rho(r) d\tau + \sum_{\alpha} V_{\alpha} \int X_{\alpha} \rho(r) d\tau + \frac{1}{2} \sum_{\alpha\beta} V_{\alpha\beta} \int X_{\alpha} X_{\beta} \rho(r) d\tau + \text{higher order terms.} \quad 1.6$$

The first term in this expression is simply the Coulomb monopole contribution to the electrostatic energy of the nucleus and it is of no interest to us since it is independent of nuclear orientation. In the second term the integral involves the first moment of the nuclear charge i.e. the second term represents the contribution made by the electric dipole moment to the electrostatic energy of the nucleus. This is effectively zero since the nucleus is effectively centrosymmetric when it is in a state of definite parity. Therefore to fourth order, the orientational contribution to the electrostatic energy of the nucleus is given by the third term in this expression. This involves interactions concerning second moments of nuclear charge distribution, i.e. it concerns the electric quadrupolar contribution,  $E_Q$ , to the electrostatic energy of the nucleus. In general nine terms contribute to  $E_Q$  but in practice a set of principal axes for the potential function  $V(r)$

can always be chosen so that only the three diagonal terms

$$\left(\frac{\partial^2 V}{\partial x^2}\right)_{r=0}, \left(\frac{\partial^2 V}{\partial y^2}\right)_{r=0} \text{ and } \left(\frac{\partial^2 V}{\partial z^2}\right)_{r=0} \text{ are non-zero, i.e. in the}$$

principal axes system, the quadrupole energy term can be written as

$$E_Q = \frac{1}{2} \sum_{\alpha\beta} V_{\alpha\beta} \int X_{\alpha} X_{\beta} \rho(r) d\tau \quad 1.7$$

It is now convenient to introduce the  $Q_{\alpha\beta}$  functions which are defined by

$$Q_{\alpha\beta} = \int_{\text{nuclear volume}} (3X_{\alpha} X_{\beta} - \delta_{\alpha\beta} r^2) \rho(r) d\tau \quad 1.8$$

where

$$\delta_{\alpha\beta} = 1 \text{ if } \alpha = \beta \ ; \ \delta_{\alpha\beta} = 0 \text{ if } \alpha \neq \beta$$

and the quadrupolar energy can then be recast in the form

$$E_Q = \frac{1}{6} \sum_{\alpha\beta} V_{\alpha\beta} Q_{\alpha\beta} + \frac{1}{6} \sum_{\alpha\beta} V_{\alpha\beta} \delta_{\alpha\beta} \int r^2 \rho(r) d\tau \quad 1.9$$

The last term in this expression is independent of nuclear orientation. Since in pure nuclear quadrupole resonance spectroscopy we are concerned with transitions between different allowed nuclear orientations, the last term therefore does not affect the energy differences as long as the orientations involved belong to the same nuclear spin quantum number,  $I$ , of the nucleus under investigation. It is, therefore, customary in N.Q.R. spectroscopy to simplify the electric quadrupolar contribution to the energy of a nucleus to

$$E_Q = \frac{1}{6} \sum_{\alpha\beta} V_{\alpha\beta} Q_{\alpha\beta} \quad 1.10$$

Furthermore, if we neglect the effects of a very small electronic charge distribution within the nucleus then we may use Laplace's equation,

$$\sum_{\alpha} V_{\alpha\alpha} = V_{xx} + V_{yy} + V_{zz} = 0 \quad 1.11$$

and only two quantities are then needed to define the electric field gradient at the nucleus.

In the quantum mechanical description of the quadrupolar interaction, a Hamiltonian is obtained by replacing the classical  $V_{\alpha\beta}$  and  $Q_{\alpha\beta}$  functions by their appropriate operators. An integral is just the limit of a sum, and therefore the operator for  $Q_{\alpha\beta}$  becomes

$$Q_{\alpha\beta}^{op} = e \sum_{\text{protons}} (3X_{\alpha}X_{\beta} - \delta_{\alpha\beta} r^2) \quad 1.12$$

where the summation is taken over the protons in the nucleus. Neutrons do not contribute since they have no charge. It should be noticed that  $Q_{\alpha\beta}^{op}$  is an operator which operates only on nuclear eigenfunctions.

The quadrupolar Hamiltonian can be written in the form

$$\mathcal{H}_Q = \frac{1}{6} \sum_{\alpha\beta} V_{\alpha\beta}^{op} Q_{\alpha\beta}^{op} \quad 1.13$$

where  $V_{\alpha\beta}^{op}$  is an operator equivalent for the classical tensor components of the electric field gradient generated by charged particles external to the nucleus of interest.

N.Q.R. spectroscopy is concerned with nuclear states which all have the same nuclear spin quantum number,  $I$ , but have different  $m_I$  values and so the appropriate nuclear eigenfunctions can be written as linear combinations of the basis functions  $\phi_i$  labelled by the magnetic quantum number  $m_I$ , i.e.

$$\psi_{\text{nucl.}} = \sum_i C_i \phi_i \quad 1.14$$

There are obviously  $2I+1$  terms in the linear combination. The allowed nuclear eigenfunctions and eigenvalues can be obtained from the classical quantum mechanical procedures applied to the wave equation,

$$\mathcal{H} \psi_{\text{nucl.}} = E \psi_{\text{nucl.}} \quad 1.15$$

Making use of variation procedure,  $(2I+1)$  secular equations and a  $(2I+1) \times (2I+1)$  secular determinant of the usual form can be obtained. The secular determinant involves diagonal matrix elements  $(\mathcal{H}_{m_I m_I} - E)$  and off-diagonal elements  $\mathcal{H}_{m_1 m_2}$  where

$$\mathcal{H}_{m_1 m_2} = \int \phi_{m_1}^* \mathcal{H} \phi_{m_2} d\tau = \frac{1}{6} \sum_{\alpha\beta} V_{\alpha\beta}^{\text{OP}} \int \phi_{m_1}^* Q_{\alpha\beta}^{\text{OP}} \phi_{m_2} d\tau \quad 1.16$$

where  $m_1$  and  $m_2$  refer to basis states whose  $m_I$  values are  $m_1$  and  $m_2$  respectively.

Evaluation of matrix elements in this expression can be made by making use of the Wigner-Eckart theorem, which in the present context states that the matrix elements of  $Q_{\alpha\beta}^{\text{OP}}$  are proportional to those of

analogous angular momentum operators, thus

$$\int \phi_{m_1}^* Q_{\alpha\beta}^{op} \phi_{m_2} d\tau = C \langle m_1 | \frac{3}{2} (I_\alpha I_\beta + I_\beta I_\alpha) - \delta_{\alpha\beta} I^2 | m_2 \rangle \quad 1.17$$

where C is a constant of proportionality. This constant can be obtained by considering the matrix element for which  $m_1 = m_2 = I$  and  $\alpha = \beta = z$ , so that

$$\int \phi_I^* Q_{zz}^{op} \phi_I d\tau = C \int \phi_I^* (3I_z^2 - I^2) \phi_I d\tau = CI(2I-1) \quad 1.18$$

The integral on the left hand side of this expression is a constant characteristic of the nucleus being considered. It can be replaced, therefore, by eQ where

$$Q = \int \phi_I^* \sum_k r_k^2 (3\cos^2\theta_k - 1) \phi_I d\tau \quad 1.19$$

This is the spectroscopist's definition of the nuclear quadrupole moment. It is the expectation value of the classical and purely geometric quantity

$$\sum_{k\text{-protons}} r_k^2 (3\cos^2\theta_k - 1) \quad 1.20$$

evaluated for the nucleus when it is in the state  $m_I = I$ . The constant C can now be given by the expression

$$C = \frac{eQ}{I(2I-1)} \quad 1.21$$

In the principal-axes system of the electric field gradient tensor, where  $V_{\alpha\beta} = 0$  for  $\alpha \neq \beta$ , taking account of Laplace's equation, the quadrupole Hamiltonian becomes

$$\mathcal{H}_Q = \frac{eQ}{4I(2I-1)} \left[ V_{zz} (3I_z^2 - I^2) + (V_{xx} - V_{yy}) (I_x^2 - I_y^2) \right] \quad 1.22$$

where  $I_x$ ,  $I_y$  and  $I_z$  are x, y and z components of the spin operator respectively.

Sometimes it becomes necessary to discuss quadrupole resonance phenomena in a coordinate framework which does not coincide with the principal axes of the electric field gradient tensor. In such cases it can be shown that equation 1.22 then takes the more general form as

$$\mathcal{H}_Q = \frac{eQ}{2I(2I-1)} \left[ V_{xx} I_x^2 + V_{yy} I_y^2 + V_{zz} I_z^2 + V_{xy} (I_x I_y + I_y I_x) \right. \\ \left. + V_{xz} (I_x I_z + I_z I_x) + V_{yz} (I_y I_z + I_z I_y) \right] \quad 1.23$$

Equation 1.22 emphasizes that only two parameters are needed to characterize the second derivatives of the potential. The two parameters customarily used for this purpose are the electric field gradient,  $-q$ , and the asymmetry parameter,  $\eta$ , defined by

$$-q = \frac{\partial^2 V}{\partial z^2} = V_{zz} \quad \text{and} \quad \eta = \frac{V_{xx} - V_{yy}}{V_{zz}} \quad 1.24$$

The quantity  $-q$  is, by definition, that component of the electric field gradient, E.F.G., tensor having the largest magnitude, and  $\eta$  is the asymmetry parameter which measures the departure of the

E.F.G. tensor from axial symmetry. The axes are chosen such that  $|V_{zz}| \gg |V_{yy}| \gg |V_{xx}|$  and, thus  $1 \gg \eta \gg 0$ . The familiar form of the quadrupole Hamiltonian, using the principal directions of the electric field gradient tensor as the frame of reference, therefore can be written as

$$\mathcal{H}_Q = \frac{eqQ}{4I(2I-1)} \left[ (3I_z^2 - I^2) + \eta (I_x^2 - I_y^2) \right] \quad 1.25$$

This expression can now be recast into a more useful form involving the ladder operators  $I_+$  and  $I_-$

$$\mathcal{H}_Q = \frac{eqQ}{4I(2I-1)} \left[ (3I_z^2 - I^2) + \frac{\eta}{2} (I_+^2 - I_-^2) \right] \quad 1.26$$

where the quantity  $eqQ$  is the quadrupole coupling constant and  $I_+$  and  $I_-$  are raising and lowering operators respectively

$$I_+ = I_x + iI_y \quad \text{and} \quad I_- = I_x - iI_y \quad 1.27$$

The Hamiltonian in equation 1.26 enables the matrix elements in the secular determinant to be evaluated. Basis states differing by  $\Delta m_I = \mp 2$  are mixed because of the presence of the shift operators in the quadrupolar Hamiltonian, except in the absence of asymmetry.

Because of this, it turns out that closed solutions cannot be found for  $I \gg \frac{5}{2}$  except in the absence of asymmetry. In the case of  $I = \frac{3}{2}$ , as is the case for  $^{35}\text{Cl}$ ,  $^{37}\text{Cl}$ ,  $^{79}\text{Br}$  and  $^{81}\text{Br}$  nuclei, the secular determinant has the form

$m_I \backslash m_I'$	$  -\frac{3}{2} \rangle$	$  +\frac{1}{2} \rangle$	$  -\frac{1}{2} \rangle$	$  +\frac{3}{2} \rangle$
$  -\frac{3}{2} \rangle$	$(\frac{3}{12} \text{ eqQ} - E)$	$(\frac{\sqrt{3}}{12} \text{ eqQ}\eta)$	$( 0 )$	$( 0 )$
$  +\frac{1}{2} \rangle$	$(\frac{\sqrt{3}}{12} \text{ eqQ}\eta)$	$(\frac{-3}{12} \text{ eqQ} - E)$	$( 0 )$	$( 0 )$
$  -\frac{1}{2} \rangle$	$( 0 )$	$( 0 )$	$(\frac{-3}{12} \text{ eqQ} - E)$	$(\frac{\sqrt{3}}{12} \text{ eqQ}\eta)$
$  +\frac{3}{2} \rangle$	$( 0 )$	$( 0 )$	$(\frac{\sqrt{3}}{12} \text{ eqQ}\eta)$	$(\frac{3}{12} \text{ eqQ} - E)$

= 0    1.28

i.e. the asymmetry in the E.F.G. mixes the basis state  $\phi_{\frac{3}{2}}$  with  $\phi_{-\frac{1}{2}}$  and the basis state  $\phi_{\frac{1}{2}}$  with  $\phi_{-\frac{3}{2}}$ .

The secular determinant can easily be solved exactly to give the energy eigenvalues

$$E_{\pm\frac{3}{2}} = + \frac{\text{eqQ}}{4} \left( 1 + \frac{\eta}{3} \right)^{\frac{1}{2}} \quad 1.29$$

$$E_{\pm\frac{1}{2}} = - \frac{\text{eqQ}}{4} \left( 1 + \frac{\eta}{3} \right)^{\frac{1}{2}} \quad 1.30$$

and the associated eigenfunctions. The schematic diagram for the energy levels, in zero magnetic field, is shown in figure 1.1.

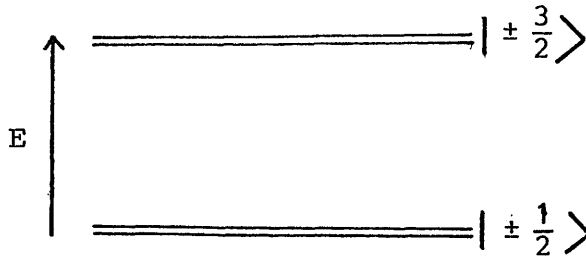


Figure 1.1 Quadrupolar energy levels for  $I = \frac{3}{2}$  in the absence of magnetic field. eqQ assumed to be positive.

The eigenfunctions are obviously the linear combinations

$$c_1 \left| -\frac{3}{2} \right\rangle + c_2 \left| +\frac{1}{2} \right\rangle \quad \text{and} \tag{1.31}$$

$$c'_1 \left| -\frac{1}{2} \right\rangle + c'_2 \left| +\frac{3}{2} \right\rangle$$

where  $c_1$ ,  $c_2$ ,  $c'_1$  and  $c'_2$  can easily be derived from the secular equations. The degree of mixing depends on the value of  $\eta$  and for small  $\eta$  labelling of the eigenstates with the magnetic quantum numbers  $m_I$  is a reasonably good approximation.

The quadrupolar nuclei distribute themselves between these sets of doubly degenerate levels according to the Boltzmann distribution law. The quadrupolar nuclei also have magnetic dipole moments, so magnetic dipolar transition between these levels can be brought about by bathing the nuclei in suitably circularly polarized electromagnetic radiation, i.e. transitions for which  $\Delta m_I = \pm 1$  are allowed, and therefore when  $I = \frac{3}{2}$ , transitions take place at a frequency given by

$$\nu = \frac{1}{2} \frac{eqQ}{h} \left(1 + \frac{\eta^2}{3}\right)^{\frac{1}{2}} \quad 1.32$$

Detection of this frequency obviously does not permit the quadrupole coupling constant and asymmetry parameter to be obtained separately. Determination of  $\eta$ , and hence  $\frac{eqQ}{h}$ , need experiments to be performed in the presence of a weak magnetic field. This subject will be considered in chapter 3 in this thesis.

The conclusion which can be drawn now, is that the quadrupolar nucleus, has a spin quantum number  $I \geq 1$ , spins about its axis in an asymmetric electric field gradient, and the interaction energy of the nucleus depends on its orientation relative to the direction of the electric field gradient. Thus the nucleus is forced to precess about the direction of the maximum component of the electric field gradient tensor, that is about the z-axis direction. The nuclear magnetic dipole moment vector must undergo the same precession, and so the situation is now very similar to that encountered in N.M.R. spectroscopy. A pure N.Q.R. transition may be induced by superimposing an appropriate circularly polarized magnetic field in the plane at right angles to the z-axis direction of the electric field gradient. The transition takes place when the frequency of this magnetic field equals the precession frequency of the quadrupolar nucleus.

## CHAPTER 2

### THE EFFECTS OF TEMPERATURE AND PRESSURE ON PURE NUCLEAR

#### QUADRUPOLE RESONANCE FREQUENCIES

##### 2.1 INTRODUCTION

Nuclear quadrupole resonance frequencies generally, though not always, decrease in magnitude with increasing temperature. The negative temperature coefficient of the quadrupole resonance frequency can be attributed to the thermal motions in the solid. In any solid, nuclei are agitated by molecular and lattice vibrations at frequencies that are much greater than the nuclear quadrupole resonance frequency.<sup>(1)</sup> Any general motion can be decomposed into three major components. The first concerns translational motions in which the centers of mass of the molecules, acting as rigid bodies, are displaced. The second involves rotational motions and the third vibrational motions. The last two components include librational, stretching and bending modes of vibration which alter the orientation of the rigid molecule in the crystal lattice. In most solids at temperatures much below their melting points it is mainly the low frequency librational modes that affect the quadrupolar interaction of the nucleus. They act to turn the orientation of the electric field gradient tensor with respect to the nuclear gyroscope and the quadrupolar nucleus therefore sees electric field gradient components averaged over the amplitude of the librational motions. The average component of the electric field gradient tensor in any

particular direction decreases as the amplitudes of the vibrational modes increase. When free rotation occurs at elevated temperatures, or complete tumbling in a liquid takes place, the electric field gradient is time-averaged to zero, and then no quadrupole resonance transitions can be detected.

In the theory of the temperature dependence of the quadrupole resonance frequency developed by Bayer<sup>(2)</sup> and extended by Kushida,<sup>(3)</sup> the increase in the amplitude of the thermal vibrations with increasing temperature is the only reason for the negative temperature coefficient of the quadrupole resonance frequency. However, Kushida, Benedek and Bloembergen<sup>(4)</sup> extended Bayer and Kushida's original work and showed that the effects of temperature variation on quadrupole resonance frequencies at atmospheric pressure essentially arise from two contributions, the first of which is the explicit temperature dependence of the vibration amplitudes, considered by Bayer and Kushida, and the second originates from the effects of the volume expansion on the static electric field gradient tensor, the vibrational frequencies and the amplitudes of vibration.

The pressure dependence of quadrupole resonance frequencies can itself be expressed in terms of the volume dependence of the vibration amplitudes and the static value of the electric field gradient tensor.

These developments will be considered in their turn in the following sections of this chapter.

2.2. THE BAYER-KUSHIDA THEORY: TEMPERATURE DEPENDENCE OF N.Q.R.

FREQUENCIES UNDER CONSTANT VOLUME CONDITIONS

Pure nuclear quadrupole resonance frequencies correspond to transitions between the energy levels of the Hamiltonian describing the interaction of the electric field gradient tensor,  $V_{\alpha\beta}$ , and the nuclear quadrupole moment,  $Q$ , and given generally by<sup>(4,5)</sup>

$$\mathcal{H} = \frac{eQ}{2I(2I-1)} \left[ V_{xx} I_x^2 + V_{yy} I_y^2 + V_{zz} I_z^2 + V_{xy} (I_x I_y + I_y I_x) + V_{xz} (I_x I_z + I_z I_x) + V_{yz} (I_y I_z + I_z I_y) \right] \quad 2.1$$

where  $e$ ,  $Q$ ,  $I$ ,  $I_x$ ,  $I_y$ ,  $I_z$  and  $V_{\alpha\beta}$  have been defined in chapter 1.

The Bayer-Kushida theory<sup>(3)</sup> begins by considering a molecule in which the electric field gradient tensor around the quadrupolar nucleus is axially symmetric in the absence of molecular motions i.e. the electric field gradient tensor has the symmetric form

	X	Y	Z	
X	$-\frac{1}{2}$	0	0	x q
Y	0	$-\frac{1}{2}$	0	
Z	0	0	1	

2.2

where X, Y and Z are the principal directions of the electric field gradient tensor of the stationary molecule.

Molecular and lattice vibrations are assumed to cause the following effects:

1. The tensor  $V_{\alpha\beta}$  deviates by a small amount from axial symmetry.
2. The averaged directions of the  $V_{\alpha\beta}$  tensor incline by small Eulerian angles,  $\theta$ ,  $\phi$ , and  $\psi$  from the original directions, i.e. from the directions of the X, Y and Z axes respectively, the principal axes of the electric field gradient tensor in the stationary molecule.
3. The magnitude of the maximum component of the electric field gradient tensor varies in time about its equilibrium value.

With respect to the inclined coordinate system,  $X'$ ,  $Y'$  and  $Z'$ , the principal axes of the electric field gradient tensor of the vibrating molecule, the elements of the  $V_{\alpha\beta}$  tensor now become

	$X'$	$Y'$	$Z'$	
$X'$	$-\frac{1}{2} + a$	$b$	$0$	$x \ q$
$Y'$	$b$	$-\frac{1}{2} - a$	$0$	$2.3$
$Z'$	$0$	$0$	$1$	

where  $a$  and  $b$  are first-order infinitesimal changes caused by molecular motions. On transforming back from the inclined coordinate system,  $X'$ ,  $Y'$ ,  $Z'$  to the original stationary frame,  $X$ ,  $Y$ ,  $Z$ , the  $V_{\alpha\beta}$  tensor elements become

	X	Y	Z	
X	$-\frac{1}{2} + \frac{3}{2} \theta^2 + a - 2b(\psi + \varphi)$	$2a(\psi + \varphi) + b$	$\frac{3}{2} \theta - a\theta$	x q 2.4
Y	$2a(\psi + \varphi) + b$	$-\frac{1}{2}a + 2b(\psi + \varphi)$	$\frac{3}{2} \theta\varphi - b\theta$	
Z	$\frac{3}{2} \theta - a\theta$	$\frac{3}{2} \theta\varphi - b\theta$	$1 - \frac{3}{2} \theta^2$	

Inserting 2.4 into the Hamiltonian in equation 2.1 gives

$$\begin{aligned}
 \mathcal{H} = \frac{2I(2I-1)}{eqQ} = & \left[ \left(1 - \frac{3}{2} \theta^2\right) \left(\frac{3}{2} I_z^2 - \frac{1}{2} I_-^2\right) \right. \\
 & + \left[ \frac{3}{4} \theta^2 + a - 2b(\psi + \varphi) \right] \frac{1}{2} (I_+^2 + I_-^2) \\
 & + \left[ 2a(\psi + \varphi) + b \right] \frac{1}{2i} (I_+^2 - I_-^2) \\
 & + \left( \frac{3}{2} \theta - a\theta \right) \frac{1}{2} \left[ (I_+ + I_-) I_z + I_z (I_+ + I_-) \right] \\
 & + \left( \frac{1}{2} \theta\varphi - b\theta \right) \frac{1}{2i} \left[ (I_+ - I_-) I_z + I_z (I_+ - I_-) \right] \quad 2.5
 \end{aligned}$$

The first term in this expression corresponds to the effect of molecular and lattice vibrations on the quadrupole resonance frequency. The other terms are concerned with the spin-lattice relaxation. It should be noticed that only changes in the orientation of  $V_{zz}$  affect the quadrupole resonance frequency, i.e. only variation of the Euler angle  $\theta$  affects the frequency. The Hamiltonian describing the reduction of the quadrupole resonance frequency due to the molecular and lattice vibrations can therefore be written as

$$\nu = \frac{eqQ}{4I(2I-1)} (3I_z^2 - I^2) (1 - \frac{3}{2} \theta^2) + \text{Terms related with spin-lattice relaxation.} \quad 2.6$$

Molecular and lattice vibrations occur at frequencies much higher than that of pure quadrupole resonance, and hence  $\theta^2$  in this expression can be replaced by  $\langle \theta^2 \rangle$ , the time average value of the square of the angle of inclination of the maximum principal axis of the electric field gradient tensor relative to its equilibrium direction, and similarly  $q$  can be replaced by  $\langle q \rangle$ , the time average value of the magnitude of the maximum component of the electric field gradient tensor, in calculating the resonance frequency, i.e. the pure quadrupole resonance frequency can now be expressed as

$$\nu = \text{constant} (1 - \frac{3}{2} \langle \theta^2 \rangle) \langle q \rangle \quad 2.7$$

In Kushida's original paper<sup>(3)</sup> and in later developments, notably by McEnnan and Schempp<sup>(6-8)</sup>  $\langle \theta^2 \rangle$  and  $\langle q \rangle$  are expressed in terms of the normal vibrational modes appropriate to the solid.

In general, a small amplitude external coordinate,  $\theta$ , can be described as a linear combination of the normal coordinates  $\xi_i$  of the vibrational modes in the form<sup>(3)</sup>

$$\theta = \sum_i \alpha_i \xi_i + \dots \quad 2.8$$

where  $\alpha_i$  are appropriate expansion coefficients. Hence the mean-square displacements,  $\langle \theta^2 \rangle$ , are given by

$$\langle \theta^2 \rangle = \left\langle \sum_{ij} \alpha_i \alpha_j \xi_i \xi_j \right\rangle \quad 2.9$$

For nondegenerate and for orthogonalised degenerate normal modes  $\xi_i$  of frequencies  $\nu_i$  this expression reduces to

$$\langle \theta^2 \rangle = \sum_i \alpha_i^2 \langle \xi_i^2 \rangle \quad 2.10$$

Furthermore the maximum component of the electric field gradient tensor,  $q$ , can similarly be expanded in terms of these coordinates as

$$q = q_0 (1 + \sum_i \beta_i \xi_i + \sum_{ij} \delta_{ij} \xi_i \xi_j + \dots) \quad 2.11$$

where  $q_0$  is the maximum component of the electric field gradient in the stationary molecule,  $\beta_i$  and  $\delta_{ij}$  are also expansion coefficients. Higher order terms in these expansions may be neglected for small angles  $\theta \ll 1$ .

It now follows that the relationship 2.7 becomes

$$\nu = \nu_0 \left( 1 - \frac{3}{2} \sum_i \alpha_i^2 \langle \xi_i^2 \rangle + \left\langle \sum_i \beta_i \xi_i \right\rangle + \left\langle \sum_{ij} \delta_{ij} \xi_i \xi_j \right\rangle \right) \quad 2.12$$

where  $\nu_0$  is the quadrupole resonance frequency in the absence of even zero-point vibration. Since  $\langle \beta_i \xi_i \rangle = 0$  this equation reduces to

$$\begin{aligned} \nu &= \nu_0 \left( 1 - \frac{3}{2} \sum_i \alpha_i^2 \langle \xi_i^2 \rangle + \sum_i \delta_{ii} \langle \xi_i^2 \rangle \right) \\ &= \nu_0 \left( 1 - \frac{3}{2} \sum_i A_i \langle \xi_i^2 \rangle \right) \end{aligned} \quad 2.13$$

where 
$$A_i = \alpha_i^2 - \frac{2}{3} \delta_{ii} \quad 2.14$$

In order to make use of equation 2.13, expressions for the average value of  $\langle \xi_i^2 \rangle$  must now be derived.

If the mean energy of each normal mode considered is equated with the mean energy of the corresponding Planck's oscillator it can be shown<sup>(7,8)</sup> that

$$\langle \xi_i^2 \rangle = \frac{h}{4\pi^2 \nu_i} \left[ \frac{1}{2} + \frac{1}{e^{h\nu_i/kT_{-1}}} \right] \quad 2.15$$

Hence the resonance frequency can be written as

$$\nu = \nu_0 \left[ 1 - \frac{3}{2} \sum_{i=1}^N \frac{A_i h}{4\pi^2 \nu_i} \left( \frac{1}{2} + \frac{1}{e^{h\nu_i/kT_{-1}}} \right) \right] \quad 2.16$$

where  $\nu_i$  is the frequency of the  $i$  th normal mode of vibration, and  $A_i$  are the constants arising from the series expansions mentioned above.  $A_i^{-1}$  has the dimensions and order of magnitude of the moment of inertia of the molecular vibration about the axis associated with the motion.

The coefficients  $A_i$  can always be obtained if a normal mode analysis of the vibrations are made in each particular situation. Kushida,<sup>(3)</sup> and McEnnan and Schemp<sup>(6-8)</sup> have discussed the estimation of  $A_i$  for particular cases.

Kushida has estimated  $\alpha_i$  for the simple case of bending motion shown in figure 2.1

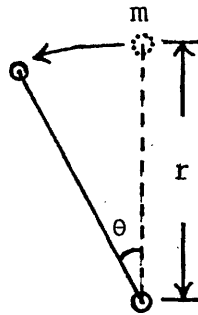


Figure 2.1 The simple case of bending motion.

It follows from equation 2.8 that

$$\alpha_i = \frac{\partial \theta}{\partial \xi_i} \quad 2.17$$

where  $\theta$  is a function of the displacement coordinates; and it can be shown that

$$\alpha_i = \frac{\partial \theta}{\partial \xi_i} = \sum_j \frac{\partial \theta}{\partial X_j} X_j^{(i)} \quad 2.18$$

For the simple motion in figure 2.1, when  $j = 1$

$$\frac{\partial \theta}{\partial X_j} = \frac{1}{r} \quad 2.19$$

$X_j^{(i)}$  can be obtained from the normalization condition of the particular normal coordinate, when  $j = 1$ .

$$x_1^{(1)} = \frac{1}{\sqrt{m}} \quad 2.20$$

and hence

$$\alpha_1 = \frac{1}{r} * \frac{1}{\sqrt{m}} = \frac{1}{\sqrt{I}} \quad 2.21$$

where  $m$  is the mass of the atom,  $r$  is the distance between the centres of mass of the two bonded atoms, and  $I$  is the moment of inertia of the bending motion considered. Hence  $A_1$ , for a simple bending mode of vibration, is

$$A_i = \alpha_i^2 = \frac{1}{I_i} \quad 2.22$$

Accordingly, equation 2.16 reduces to Bayer's equation

$$\nu = \nu_0 \left[ 1 - \frac{3}{2} \sum_{i=1}^N \frac{h}{4\pi^2 I_i \nu_i} \left( \frac{1}{2} + \frac{1}{e^{h\nu_i/kT} - 1} \right) \right] \quad 2.23$$

Similarly it follows from equation 2.11 that the  $\delta_{ii}$  coefficients are given by

$$\delta_{ii} = \frac{1}{2q_0} \frac{\partial^2 q}{\partial \xi_i^2} = \frac{1}{2q_0} \sum_{jk} \frac{\partial^2 q}{\partial X_j \partial X_k} x_j^{(i)} x_k^{(i)} \quad 2.24$$

If  $q$  is approximated to  $\frac{e}{r^3}$ , then for  $j = 1$  in the case of a simple stretching motion of a bond, it can be shown that

$$\delta_1 \approx \frac{6}{I} \quad 2.25$$

McEnnan and Schempp have extended Kushida's ideas to a slightly more complicated case of solid chlorine.<sup>(6,7)</sup> In this case it turns out that again  $A_i^{-1}$  represents the effective moment of inertia,  $I_i$ , for the  $i$ th mode of vibration, provided it is assumed that only librational modes are involved in the averaging of the electric field gradient tensor at the quadrupolar nucleus. The mean square amplitude of vibration,  $\langle \theta^2 \rangle$ , in McEnnan and Schempp's analysis again turns out to be given by

$$\begin{aligned} \langle \theta^2 \rangle &= \sum_{i=1}^N \frac{A_i h}{4\pi^2 \nu_i} \left( \frac{1}{2} + \frac{1}{e^{h\nu_i/kT_{-1}}} \right) \\ &= \sum_{i=1}^N \frac{h}{4\pi^2 I_i \nu_i} \left( \frac{1}{2} + \frac{1}{e^{h\nu_i/kT_{-1}}} \right) \end{aligned} \quad 2.26$$

and again equation 2.16 follows.

The lattice vibrations can be classified into high- and low-frequency modes depending on whether their frequencies are higher or lower than

$$\nu = \frac{kT_M}{h} \quad 2.27$$

where  $T_M$  is the lowest temperature used in the experiments.<sup>(4)</sup>

Equation 2.16 shows explicitly that the low-frequency modes of vibration dominate the temperature dependence of quadrupole resonance frequency. The temperature variation of quadrupole resonance frequency due to the low-frequency modes can be expressed simply by making use of

the expansion , valid in the range

$$x = \frac{h\nu_i}{kT} \ll 1 ,$$

$$\left(\frac{1}{2} + \frac{1}{e^x - 1}\right) = \frac{1}{x} + \frac{x}{12} + o(x^3) \quad 2.28$$

and hence equation 2.16 can be written as

$$\nu = \nu_o \left[ 1 - \frac{3kT}{8\pi^2} \sum_{i=1}^M \frac{A_i}{\nu_i^2} - \frac{h^2}{32\pi^2 kT} \sum_{i=1}^M A_i + \Omega(T) \right] \quad 2.29$$

$$\text{where } \Omega(T) = -\frac{3}{2} \sum_{i=M+1}^N \frac{A_i h}{4\pi^2 \nu_i} \left( \frac{1}{2} + \frac{1}{e^{h\nu_i/kT} - 1} \right) \quad 2.30$$

$\Omega(T)$  represents the contribution of the high-frequency modes to  $\nu$ .

The summation is taken over all modes of vibration with frequencies fulfilling the condition  $h\nu_i \ll kT$ .<sup>(9)</sup> The high-frequency terms,  $\Omega(T)$ , can be completely neglected, and hence equation 2.29 can be recast into the form

$$\nu = a \left( 1 + bT + \frac{c}{T} \right) \quad 2.31$$

$$\text{where } a = \nu_o = \frac{eq_o Q}{2h} \quad 2.32$$

$$b = -\frac{3k}{8\pi^2} \sum_{i=1}^M \frac{A_i}{\nu_i^2} \quad 2.33$$

$$\text{and } c = -\frac{h^2}{32\pi^2 k} \sum_{i=1}^M A_i \quad 2.34$$

At room temperature, the rate of change of quadrupole resonance frequency with temperature under constant volume conditions can therefore be approximately expressed as<sup>(10)</sup>

$$\left(\frac{\partial \nu}{\partial T}\right)_V \approx - \frac{3k\nu_0}{8\pi^2} \sum_{i=1}^M \frac{A_i}{\nu_i^2} \quad 2.35$$

It follows from equation 2.35 that the temperature coefficient increases with increasing resonance frequency,  $\nu_0$ . However this coefficient also decreases with increasing frequency,  $\nu_i$ , of the librational motion involved.

Equation 2.35 enables the variation of quadrupole resonance frequency with temperature under constant volume conditions to be correlated with vibrational or librational data obtained from Raman or infra-red experiments.

Kushida has extended the consideration of the effects of molecular and lattice vibrations on the resonance frequencies of quadrupolar nuclei to situations where the electric field gradient is not symmetric.<sup>(3)</sup>

All oscillations introduce asymmetry into the electric field gradient tensor although in practice only librations about the principal X and Y directions affect  $q$ . It has been shown that if  $\theta_X$ ,  $\theta_Y$  and  $\theta_Z$  are angular displacements brought about by libration about the respective principal axes, X, Y and Z, then average value of  $q$  and  $\eta$  is given by<sup>(6-8)</sup>

$$\langle q \rangle = q_0 \left[ 1 - \frac{3}{2} (\langle \theta_X^2 \rangle + \langle \theta_Y^2 \rangle) + \frac{1}{2} \eta_0 (\langle \theta_Y^2 \rangle - \langle \theta_X^2 \rangle) \right] \quad 2.36$$

$$\langle \eta \rangle = \frac{q_0}{q} \left[ \eta_0 \left\{ 1 - \frac{1}{2} (\langle \theta_X^2 \rangle + \langle \theta_Y^2 \rangle) - 2 \langle \theta_Z^2 \rangle \right\} + \frac{3}{2} (\langle \theta_Y^2 \rangle - \langle \theta_X^2 \rangle) \right] \quad 2.37$$

These equations enable 1.32 to be recast to take account of librational motions in more general situations. Furthermore Kushida<sup>(3)</sup> showed, in the case of an asymmetric electric field gradient, that equation 2.7 becomes

$$v = (\text{constant})' \left[ 1 - \left( \frac{3}{2} - \frac{\eta_0}{2} \right) \langle \theta^2 \rangle \right] \langle q \rangle \quad 2.38$$

and  $A_i$  becomes

$$A_i = \left( 1 - \frac{\eta_0}{3} \right) \alpha_i^2 - \frac{2}{3} \delta_{ii} \quad 2.39$$

and hence equation 2.13 can be written, in this case, as

$$v = v'_0 \left( 1 - \frac{3}{2} \sum_i A_i \langle \xi_i^2 \rangle \right) \quad 2.40$$

where

$$v'_0 = \frac{eq_0 Q}{2h} \left( 1 + \frac{\eta_0^2}{3} \right)^{\frac{1}{2}} \quad 2.41$$

However since in the compounds to be considered later in this thesis, the effects of the asymmetry parameter,  $\eta$ , are believed to be very small, this situation is therefore not considered here in any detail.

The treatment discussed so far provides an explanation of the, usually observed, negative temperature coefficients of quadrupole resonance frequencies in molecular solids in which librational motions dominate the overall temperature dependence. However this treatment is

no longer valid when the molecule undergoes a complete rotation, as happens in the gas phase, where the quadrupole coupling constant,  $eqQ$ , depends on the vibrational state of the molecule. Observed rotational spectra, for a number of diatomic molecules,<sup>(11)</sup> show that the quadrupole coupling constant, and hence the resonance frequency, can increase or decrease with increasing vibrational quantum number, and it follows that the intramolecular vibrations can give rise to both negative and positive temperature dependences of quadrupole resonance frequencies.

The Bayer-Kushida theory<sup>(2,3)</sup> and its extension<sup>(4)</sup> only consider the effects of small librational motions of the molecule in the solid that occur at frequencies much higher than the quadrupole resonance frequencies, and so this theory does not provide an adequate explanation of the temperature dependence of quadrupole resonance frequency when complete reorientations of the molecule occur between the equilibrium positions in the crystal lattice, or when a complete rotation of a fragment of the molecule takes place. These motions occur in the solid at different frequencies and so different effects can be expected.<sup>(12)</sup> Slow molecular reorientations or rotations, that occur at frequencies lower than quadrupole resonance frequencies, cause serious broadening of the observed resonance line to take place. However when these molecular motions occur at much higher frequencies then noticeable changes in the corresponding quadrupole resonance frequencies can be expected. Very detailed descriptions of the effect of such molecular motions are present in the paper published by Lotfullin and Semin.<sup>(12)</sup>

The development just outlined does not consider the effects of volume changes on quadrupole resonance frequencies. In measuring frequencies under constant pressure conditions volume changes must undoubtedly take place and so their effects on the resonance frequencies must now be considered in some detail.

### 2.3. THE VOLUME DEPENDENCE OF QUADRUPOLE RESONANCE FREQUENCIES

The twin dependence of quadrupole resonance frequencies on temperature and volume leads to the total differential

$$\partial v = \left(\frac{\partial v}{\partial T}\right)_V dT + \left(\frac{\partial v}{\partial V}\right)_T dV \quad 2.42$$

Under constant pressure conditions it therefore follows that

$$\left(\frac{\partial v}{\partial T}\right)_P = \left(\frac{\partial v}{\partial T}\right)_V + \left(\frac{\partial v}{\partial V}\right)_T \left(\frac{\partial V}{\partial T}\right)_P \quad 2.43$$

and hence

$$\left(\frac{\partial v}{\partial T}\right)_P = \left(\frac{\partial v}{\partial T}\right)_V + \alpha V_0 \left(\frac{\partial v}{\partial V}\right)_T \quad 2.44$$

where  $\alpha$  is the volume coefficient of the thermal expansion of the solid considered, <sup>(13)</sup> and  $V_0$  is its volume at absolute zero of temperature and zero pressure.

The first term on the right hand side of equation 2.44 represents the Bayer effect which has already been considered in section 2.2. The last term involves the isothermal volume dependence of the resonance frequency and it can be estimated if measurements of the pressure dependence of quadrupole resonance frequencies are made under constant temperature conditions. This follows from equation 2.42, since under isothermal conditions

$$\partial v = \left(\frac{\partial v}{\partial V}\right)_T dV \quad 2.45$$

and therefore

$$\left(\frac{\partial v}{\partial P}\right)_T = \left(\frac{\partial v}{\partial V}\right)_T \left(\frac{\partial V}{\partial P}\right)_T \quad 2.46$$

Hence

$$\left(\frac{\partial v}{\partial P}\right)_T = -\chi V_0 \left(\frac{\partial v}{\partial V}\right)_T \quad 2.47$$

where  $\chi$  is the isothermal volume compressibility coefficient for the solid.

It now follows from equations 2.44 and 2.47 that<sup>(9)</sup>

$$\left(\frac{\partial v}{\partial T}\right)_V = \left(\frac{\partial v}{\partial T}\right)_P + \frac{\alpha}{\chi} \left(\frac{\partial v}{\partial P}\right)_T \quad 2.48$$

The Bayer term,  $\left(\frac{\partial v}{\partial T}\right)_V$ , and the isothermal volume dependence of the resonance frequency,  $\left(\frac{\partial v}{\partial V}\right)_T$ , can now easily be obtained via 2.48 and 2.47 from the temperature and pressure measurements of the resonance frequency, provided the coefficients of the thermal expansion,  $\alpha$ , and the compressibility,  $\chi$ , for the solid are known.

Furthermore since the Bayer effect is determined by the effects of the temperature variation on the amplitudes,  $\xi_i^0$ , of the normal modes of lattice vibration, it can be expressed in the form<sup>(4)</sup>

$$\left(\frac{\partial \nu}{\partial T}\right)_V = \sum_i \frac{\partial \nu}{\partial \xi_i^O} \left(\frac{\partial \xi_i^O}{\partial T}\right)_V \quad 2.49$$

Similarly, if the field gradient is axially symmetric at the nucleus, then the last term in equation 2.44 can be recast into the form

$$\left(\frac{\partial \nu}{\partial V}\right)_T = \frac{\partial \nu}{\partial q_O} \frac{dq_O}{dV} + \sum_i \frac{\partial \nu}{\partial \xi_i^O} \left(\frac{\partial \xi_i^O}{\partial V}\right)_T \quad 2.50$$

i.e. the volume dependence of the resonance frequency is determined by the volume dependence of both  $q_O$  and  $\xi_i^O$ .

In order to obtain some idea about the relative importance of the explicit temperature dependence of  $\xi_i^O$  compared with the effects of the volume changes on  $q_O$  and  $\xi_i^O$ , it is necessary to consider in more detail the volume dependence of resonance frequencies under constant temperature conditions.

This has been done in a classic paper by Kushida, Benedek and Bloembergen who correlated the volume dependences of the experimental parameters  $a$ ,  $b$  and  $c$  in equation 2.31 with the volume dependences of  $q_O$ ,  $\nu_i$  and  $A_i$ .<sup>(4)</sup> These authors derived a relationship between the volume,  $V$ , of the solid and its volume compressibility,  $\chi(T,V)$ , at temperature  $T$ , of the form

$$\chi(T,V) = -\frac{1}{V} \frac{\partial V}{\partial P} = \frac{V_O}{V} \chi_{O0} \left[ \frac{1}{1 - \zeta \left(\frac{V-V_O}{V_O}\right)} \right] \quad 2.51$$

where  $\chi_{O0}$  is the initial compressibility at absolute zero temperature

and zero pressure,  $\frac{V}{V_0}$  is the volume of the solid under study at any temperature,  $T$ , and pressure,  $P$ , relative to its volume at absolute zero temperature and zero pressure, and  $\zeta$  is a constant whose value depends on the nature of the solid.

If 2.51 is integrated at constant temperature, and use is made of relationships connecting volume,  $V$ , pressure,  $P$ , and volume coefficients of thermal expansion,  $\alpha$ , and compressibility,  $\chi$ , then the equation of state

$$\chi_T P = - \ln \frac{V}{V_0} + \alpha T \quad 2.52$$

can be derived for the solid in question.

Equation 2.52 then enables the isothermal pressure dependence of resonance frequencies to be recast in terms of the isothermal volume dependence of these frequencies and thence the experimental parameters  $a$ ,  $b$  and  $c$  can be used to test the theoretical treatment developed by Kushida, Benedek and Bloembergen. A detailed description of the way in which this can be done is discussed in Appendix 2A.1.

It should be noted that Kushida, Benedek and Bloembergen's paper<sup>(4)</sup> focuses attention only on the volume dependences of the parameters  $a$ ,  $b$  and  $c$ . It, obviously, is defective since it neglects the effects of temperature changes on these parameters which are shown to vary significantly with temperature.<sup>(14,15)</sup>

Brown<sup>(16)</sup> has introduced modifications into the Kushida, Benedek and Bloembergen treatment by making allowance for the fact that the molecular libration frequencies,  $\nu_i$ , vary with temperature. He

assumed that change in volume has only negligibly small effect on  $\nu_0$  and  $A_i$  and that  $\nu_i$  varies with temperature according to

$$\nu_i = \nu_i^0 (1 - g_i t) \quad 2.53$$

where  $\nu_i$  is the frequency of the  $i$  th normal mode of the librational motion of the molecule,  $\nu_i^0$  is the frequency at  $t=0$ ,  $g_i$  are constants, and  $t$  is the temperature measured from any fixed temperature. Thence, as explained in Appendix 2A.2 he derived relationships that connect the first and second temperature derivatives of quadrupole resonance frequency with  $A_i$ ,  $\nu_i$  and  $g_i$ ; where  $A_i$  is given by expression 2.14.  $\nu_i^0$  and  $g_i$  have been deduced from Raman<sup>(17)</sup> and X-ray<sup>(14)</sup> sources for a number of compounds, for example, the  $\alpha$ -phase of *p*-dichlorobenzene<sup>(16)</sup> and  $(\text{CH}_2)_6\text{N}_4$ <sup>(14)</sup> and in each case incorporation of Brown modification appears to improve the agreement between experimental N.Q.R. measurements and their theoretical interpretations.

APPENDIX - 2A

2A.1 ISOTHERMAL VOLUME DEPENDENCE OF QUADRUPOLE RESONANCE

FREQUENCIES

The theory developed by Kushida, Benedek and Bloembergen concerning the effects of volume changes on quadrupole resonance frequencies has already been discussed briefly in section 2.3 and it will now be considered in more detail.

In this theory it has been pointed out that the parameters  $a$ ,  $b$  and  $c$  in equation 2.31 are volume dependent as a result of the volume dependence of  $q_o$ ,  $v_i$  and  $A_i$ . Kushida, Benedek and Bloembergen assumed that these volume dependences have the forms<sup>(4)</sup>

$$q_o = q_{o0} \left(\frac{V}{V_o}\right)^n$$

$$v_i = v_{i0} \left(\frac{V}{V_o}\right)^{-\gamma} \quad 2A-1.1$$

$$A_i = A_{i0} \left(\frac{V}{V_o}\right)^\sigma$$

where  $q_{o0}$ ,  $v_{i0}$  and  $A_{i0}$  are respectively the values of  $q_o$ ,  $v_i$  and  $A_i$  at absolute zero temperature and zero pressure, and  $\frac{V}{V_o}$  is the volume of the solid under study at any temperature and pressure relative to its volume at absolute zero temperature and zero pressure.

It now follows from equations 2.32-2.34 that the volume dependence of  $a$ ,  $b$  and  $c$  are related to the parameters,  $n$ ,  $\gamma$  and  $\sigma$  by

$$\frac{d \ln a}{d \ln V} = n$$

$$\frac{d \ln |b|}{d \ln V} = 2\gamma + \sigma \quad 2A-1.2$$

$$\frac{d \ln |c|}{d \ln V} = \sigma$$

i.e. if the isothermal volume dependence of quadrupole resonance frequencies is measured at, at least, three distinct temperatures then in principle the parameters  $n$ ,  $\gamma$  and  $\sigma$  can be obtained and thence complete analysis and interpretation can be made for the quadrupole resonance data. In practice however this information can be more easily obtained by measuring the pressure dependence of the resonance frequency under constant temperature conditions and then converting these data into the form of isothermal volume dependence of the resonance frequency by making use of a suitably equation of state for the solid.

In this context Kushida, Benedek and Bloembergen used the following relationship between the compressibility and the volume of the solid

$$\chi(T,V) = -\frac{1}{V} \frac{\partial V}{\partial P} = \frac{V_0}{V} \chi_{00} \frac{1}{\left[1 - \zeta \left(\frac{V-V_0}{V_0}\right)\right]} \quad 2A-1.3$$

where, as before,  $\chi(T,V)$  is the volume compressibility of the solid at temperature  $T$ ,  $\chi_{00}$  is the initial compressibility at absolute zero temperature and zero pressure, and  $\zeta$  is a constant. Equation 2A-1.3 can be recast at constant temperature to give

$$\chi_T \int_0^P dP = - \int_{V_T}^V \frac{dV}{V} \quad 2A-1.4$$

where  $V_T$  is the volume of the solid at temperature  $T$  and zero pressure, and  $V$  is the volume of the solid at temperature  $T$  and pressure  $P$ .

Therefore equation 2A-1.4 gives

$$\chi_T P = - \ln \frac{V}{V_T} \quad 2A-1.5$$

But  $V_T$  is related to the volume coefficient of the thermal expansion,  $\alpha$ ,<sup>(9)</sup> by

$$V_T = V_0 \exp. \int_0^T \alpha (T) dT \quad 2A-1.6$$

and  $V$  is given by

$$V = V_T \exp. (- \chi_T P) \quad 2A-1.7$$

Hence equation 2A-1.5 becomes the equation of state

$$\chi_T P = - \ln \frac{V}{V_0} + \alpha T \quad 2A-1.8$$

This equation of state enables experimentally obtained data of the isothermal  $v$  vs.  $P$  to be transformed in terms of  $v$  vs.  $V$  at constant temperature,<sup>(9,14,18,19)</sup> and these results enable the magnitudes and the volume dependences of  $a$ ,  $b$  and  $c$ , in equation 2.31, to be obtained and hence the parameters  $n$ ,  $\gamma$  and  $\sigma$  can be calculated.

A knowledge of the volume dependence of a, b and c now enables estimates to be made of the changes that occur in  $q_0$  and in the amplitude of the lattice vibrations,  $\langle \theta'^2 \rangle$ , when the volume of the solid changes, and also enables information to be obtained about the relative importance of these two contributions to the volume dependence of quadrupole resonance frequencies.

This can be clearly shown in the following equation which is derived from equation 2.31

$$\begin{aligned} \frac{\partial \ln v}{\partial \ln V} &= \frac{d \ln a}{d \ln V} + \left[ \frac{db}{d \ln V} T + \frac{dc}{d \ln V} \times \frac{1}{T} \right] / (1 + bT + \frac{c}{T}) \\ &= \frac{d \ln q_0}{d \ln V} + \frac{\partial \ln v}{\partial \ln \langle \theta'^2 \rangle} \frac{\partial \ln \langle \theta'^2 \rangle}{\partial \ln V} \end{aligned} \quad 2A-1.9$$

where  $\langle \theta'^2 \rangle = \langle \sum_i A_i \xi_i^{O^2} \rangle$  2A-1.10

The relative importance of the Bayer effect,  $(\frac{\partial v}{\partial T})_V$ , and of the effects of the volume expansion,  $(\frac{\partial v}{\partial V})_T$ , can be observed directly if a comparison is made between the curves of  $v$  vs.  $T$  at constant atmospheric pressure, obtained experimentally, and  $v$  vs.  $T$  under constant volume,  $\frac{V}{V_0} = 1$ , conditions deduced by following the procedures outlined above.

2A.2 TEMPERATURE DEPENDENCE OF QUADRUPOLE RESONANCE FREQUENCIES UNDER  
CONSTANT PRESSURE CONDITIONS

In molecular crystals, the frequencies,  $\nu_i$ , of the librational motions depend on the intermolecular force constants whereas  $\nu_0$  and  $A_i$  depend mainly on intramolecular properties and force constants. (14)

Furthermore the parameters a and b in equation 2.31 have been shown to vary significantly with temperature (14,15) although this variation has been neglected in the Kushida, Benedek and Bloembergen treatment.

Brown (16) modified the Kushida, Benedek and Bloembergen theory assuming that the volume dependences of  $\nu_0$  and  $A_i$  are negligibly small and that  $\nu_i$  is a function of temperature according to

$$\nu_i = \nu_i^0 (1 - g_i t) \quad 2A-2.1$$

where  $\nu_i$  is the frequency of the i th normal mode of the librational motion,  $\nu_i^0$  is the frequency at  $t = 0$ ,  $g_i$  are constants and  $t$  is the temperature measured from any fixed temperature,  $T'$ , i.e.  $T = t + T'$ .

It is assumed that equation 2A-2.1 is valid for all molecular crystals. It now follows from equations 2A-2.1, 2.31 and 2.33 that the parameter b is temperature dependent and the quadrupole resonance frequencies,  $\nu$ , vary nonlinearly with temperature under constant pressure conditions. The temperature dependence of the resonance frequency can be expressed in terms of  $\nu_i$  as

$$\frac{d\nu}{dT} = \left(\frac{\partial \nu}{\partial T}\right) + \sum_{i=1}^M \left(\frac{\partial \nu}{\partial \nu_i}\right) \left(\frac{d\nu_i}{dT}\right) \quad 2A-2.2$$

It now follows from equations 2.31, 2.33, 2A-2.1 and 2A-2.2 that the first and second temperature derivatives of the resonance frequencies,  $\nu$ , can be expressed, at any temperature  $T = T'$  as

$$\frac{1}{\nu_0} \left( \frac{d\nu}{dT} \right)_0 = (1 + 2\langle g \rangle T) b_0 \quad 2A-2.3$$

$$\frac{1}{\nu_0} \left( \frac{d^2\nu}{dT^2} \right)_0 = (4\langle g \rangle + 6\langle g^2 \rangle T) b_0 \quad 2A-2.4$$

where  $b_0$  is the value of  $b$  at  $t = 0$  and the weighted averages  $\langle g \rangle$  and  $\langle g^2 \rangle$  are defined by

$$\langle g \rangle = \left[ \sum_{i=1}^M \frac{A_i}{\nu_{i0}^2} \times g_i \right] / \left[ \sum_{i=1}^M \frac{A_i}{\nu_{i0}^2} \right] \quad 2A-2.5$$

$$\langle g^2 \rangle = \left[ \sum_{i=1}^M \frac{A_i}{\nu_{i0}^2} \times g_i^2 \right] / \left[ \sum_{i=1}^M \frac{A_i}{\nu_{i0}^2} \right] \quad 2A-2.6$$

Assuming that  $\langle g \rangle = g$  and  $\langle g^2 \rangle = g^2$ , equations 2A-2.3 and 2A-2.4 can easily be solved to obtain the parameters  $g$  and  $b_0$  if experimental values of both derivatives are available.

The value of  $b_0$  obtained in this way for the  $\alpha$ -phase of *p*-dichlorobenzene<sup>(16)</sup> shows a close agreement with the value calculated by Wang<sup>(20)</sup> using data obtained from Raman spectra<sup>(17)</sup> and even closer to the value obtained by Kushida, Benedek and Bloembergen.<sup>(4)</sup> Furthermore the temperature and pressure dependence of the resonance frequency of

$^{14}\text{N}$  in  $(\text{CH}_2)_6\text{N}_4$  <sup>(14)</sup> has been analyzed using both the Brown <sup>(16)</sup> and Kushida, Benedek and Bloembergen <sup>(4)</sup> methods. Both results turned out to give an excellent fit to the experimentally obtained temperature dependence of the resonance frequency under constant atmospheric pressure, however the fit of simple Bayer theory to the temperature dependence is poor. These imply that Brown's method improves the consistency of the experimental data with theoretical treatments used to interpret them.

CHAPTER 3

ZEEMAN SPLITTING OF QUADRUPOLE RESONANCE SPECTRA

FOR SPIN  $\frac{3}{2}$  NUCLEI

3.1 INTRODUCTION

Zeeman nuclear quadrupole resonance has turned out to be a useful method for measuring the nuclear electric quadrupole parameters for  $I = \frac{3}{2}$  nuclei. In this context, the nuclear Zeeman interaction observed on application of a magnetic field, removes the degeneracy of the levels and permits the observation of four transitions whose frequencies are centered about the original pure quadrupole single line. These frequencies enable the asymmetry parameter of the field gradient,  $\eta$ , and the quadrupole coupling constant,  $eQq$ , to be obtained.

Zeeman splitting of quadrupole resonance spectra can be studied using both single crystal<sup>(1-4)</sup> and polycrystalline<sup>(5-9)</sup> specimens.

In the case of single crystals, the frequency separations and intensities of the four Zeeman components depend on the value of  $\eta$  and on the orientation of the applied magnetic field,  $H_0$ , relative to the directions of the principal axes of the field gradient at the nucleus. Two single-crystal methods have been developed; they are known as the "zero-splitting locus"<sup>(10,11)</sup> and the "frequency-field"<sup>(4)</sup> methods.

Morino and Toyama<sup>(5)</sup> developed the Zeeman nuclear quadrupole resonance line shape theory for polycrystalline specimens.

These methods will now be considered in their turn in this chapter.

3.2 ZEEMAN EFFECTS ON QUADRUPOLE RESONANCE SPECTRA FOR  $I = \frac{3}{2}$  NUCLEI

---

If the case of an axially symmetric electric field gradient tensor is considered and a static magnetic field,  $H_0$ , is applied at an angle  $\theta$  with respect to the symmetry axis, then the net Hamiltonian can be written as

$$\mathcal{H} = \mathcal{H}_Q + \mathcal{H}_Z \quad 3.1$$

where  $\mathcal{H}_Q$  is given by expression 1.25 and  $\mathcal{H}_Z$  given by<sup>(12)</sup>

$$\mathcal{H}_Z = -\gamma \hbar H_0 (I_z \cos\theta + I_x \sin\theta \cos\varphi + I_y \sin\theta \sin\varphi) \quad 3.2$$

where  $\varphi$  is the azimuthal angle made by  $H_0$  for a particular choice of X and Y axes of the principal system of the electric field gradient tensor. If the magnetic field,  $H_0$ , is weak, i.e.  $\gamma \hbar H_0 \ll e q Q$ , its effect can be regarded as a perturbation on the quadrupolar interaction.

The presence of the  $I_x$  and  $I_y$  terms in equation 3.2 introduce some mixing between the adjacent basis states,  $\Delta m_I = \pm 1$ , but this mixing can be neglected for  $m_I = \pm \frac{3}{2}$ , and so to first order only the component of the magnetic field in the z-axis direction contributes in the perturbation of these basis states and the resulting Zeeman pattern depends only on  $\theta$ . The Zeeman field removes the degeneracy of the  $\psi_{\frac{3}{2}}^{\pm \frac{3}{2}}$  states producing two energy levels,

$$E_{\pm \frac{3}{2}} = A[3m_I^2 - I(I+1)] \mp m_I \hbar \gamma H_0 \cos\theta \quad 3.3$$

where  $A = \frac{eqQ}{4I(2I-1)} \quad 3.4$

However the Zeeman field causes a zero-order mixing of the states  $\psi_{+\frac{1}{2}}$  and  $\psi_{-\frac{1}{2}}$  to form new eigenstates  $\psi_+$  and  $\psi_-$  which are obtained by degenerate perturbation theory to be

$$\psi_+ = \psi_{+\frac{1}{2}} \sin\alpha + \psi_{-\frac{1}{2}} \cos\alpha \quad 3.5$$

$$\psi_- = \psi_{-\frac{1}{2}} \sin\alpha - \psi_{+\frac{1}{2}} \cos\alpha$$

where  $\tan\alpha = \left[ \frac{f+1}{f-1} \right]^{\frac{1}{2}} \quad 3.6$

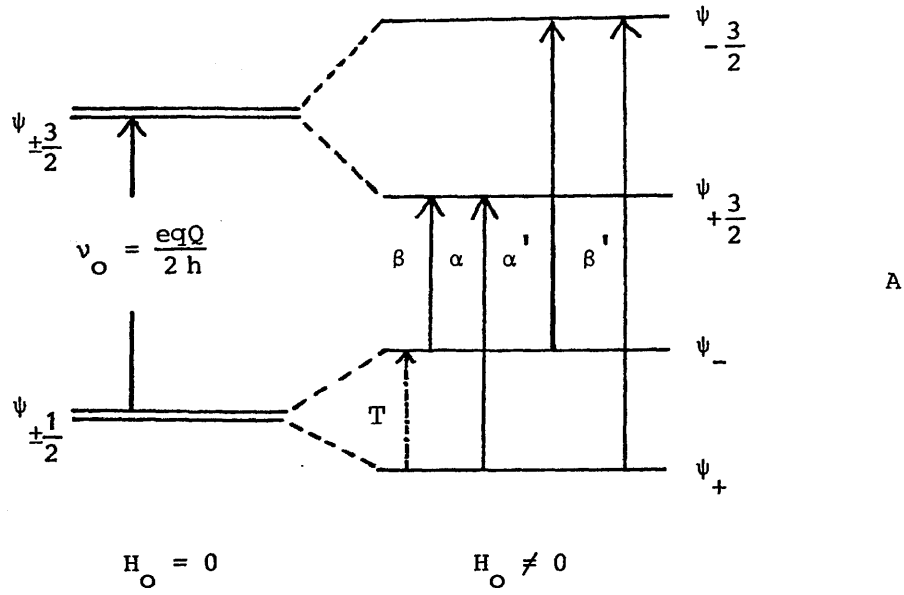
and  $f = \left[ 1 + (I + \frac{1}{2})^2 \tan^2\theta \right]^{\frac{1}{2}} \quad 3.7$

These new eigenstates have energies given by

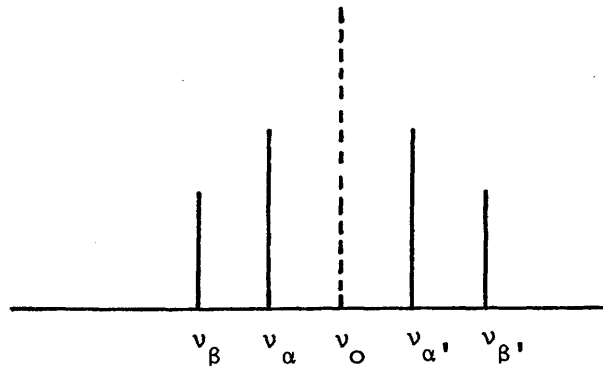
$$E_{\pm} = A \left[ \frac{3}{4} - I(I+1) \right] \mp \frac{1}{2} f \hbar \gamma H_0 \cos\theta \quad 3.8$$

The resultant energy level diagram is shown in figure 3.1.

The applied radio frequency field induces  $\Delta m_I = \pm 1$  transitions between the new states  $\psi_{\pm}$  and the  $m_I = \pm \frac{3}{2}$  states giving two pairs of lines, shown in figure 3.1, whose frequencies are



A



B

**Figure 3.1** A. Zeeman splitting of quadrupolar energy levels for  $I = \frac{3}{2}$  when  $\eta = 0$ .  
 B. Observed N.Q.R. spectrum for  $I = \frac{3}{2}$  and  $\eta = 0$  in the presence of a weak static magnetic field,  $H_0$ .

$$v_{\alpha} = \frac{eqQ}{2h} - \frac{3-f}{4\pi} \gamma H_0 \cos\theta$$

$$v_{\beta} = \frac{eqQ}{2h} - \frac{3+f}{4\pi} \gamma H_0 \cos\theta$$

3.9

$$v_{\alpha'} = \frac{eqQ}{2h} + \frac{3-f}{4\pi} \gamma H_0 \cos\theta$$

$$v_{\beta'} = \frac{eqQ}{2h} + \frac{3+f}{4\pi} \gamma H_0 \cos\theta$$

These lines are symmetric about the original unperturbed resonance frequency,  $v_0$ , and the components of each pair have equal intensities. However the intensity ratio of the outer,  $\beta$ , pair to the inner,  $\alpha$ , pair of these lines found to be  $(f-1)/(f+1)$  confirming that the  $\alpha$  pair is always stronger, and that the intensities are orientation dependent. It follows from equations 3.9 that the separations of these lines also vary with the orientation of the field and so the direction of the symmetry axis of the electric field gradient tensor can be identified from separation measurements of these lines.

When  $\theta_0 = \tan^{-1} [2\sqrt{2}/(I+\frac{1}{2})]$  i.e.  $\theta_0 = 54^\circ 44'$  for  $I = \frac{3}{2}$ , then equations 3.3 and 3.8 show that the energy separations between the states  $\psi_{\frac{3}{2}+\frac{3}{2}}$  and  $\psi_{\frac{3}{2}-\frac{3}{2}}$  and between  $\psi_+$  and  $\psi_-$  are equal, and the splitting between the two components in each pair obtained from 3.9, are then

$$\Delta v_{\alpha\alpha'} = 0$$

3.10

$$\Delta v_{\beta\beta'} = \frac{3\gamma}{\pi} H_0 \cos\theta$$

Hence the locus of zero splitting of the  $\alpha, \alpha'$  Zeeman components is defined by  $H_0$  lying in a right circular cone with semivertical angle  $\theta_0$  and having an axis which coincides with the symmetry axis of the electric field gradient tensor. It therefore follows that the orientation of the symmetry axis of the field gradient can easily be obtained since the lines  $\alpha$  and  $\alpha'$  overlap to form a single strong line at the original pure quadrupole resonance frequency.

It should be noted that a transition, denoted T in figure 3.1, between the states  $\psi_+$  and  $\psi_-$  is also allowed to occur at a frequency given by<sup>(9)</sup>

$$\nu = \frac{\gamma}{2\pi} H_0 \cos\theta \quad 3.11$$

but this is too low to be observed in pure quadrupole resonance experiments.

If the Zeeman interaction is considered in the case of an asymmetric electric field gradient, it can be shown that once again the magnetic field removes the degeneracy of the  $\pm m_I$  levels and the energies are given by<sup>(12)</sup>

$$E_{m\pm} = E_{m(0)} \pm \frac{\gamma \hbar H_0}{2} \left[ a_m^2 \cos^2 \theta + (b_m^2 + c_m^2 + 2b_m c_m \cos 2\varphi) \sin^2 \theta \right]^{\frac{1}{2}} \quad 3.12$$

where  $E_{m(0)}$  are the energy values in the absence of any magnetic field and are given by equations 1.29 and 1.30. Dean<sup>(11)</sup> found that the coefficients in this equation for  $I = \frac{3}{2}$  are given by

$$\begin{aligned}
 a_{\pm\frac{3}{2}} &= -1 - \frac{2}{\rho} & a_{\pm\frac{1}{2}} &= -1 + \frac{2}{\rho} \\
 b_{\pm\frac{3}{2}} &= 1 - \frac{1}{\rho} & b_{\pm\frac{1}{2}} &= 1 + \frac{1}{\rho} \\
 c_{\pm\frac{3}{2}} &= \frac{\eta}{\rho} = -c_{\pm\frac{1}{2}} & \rho &= \left(1 + \frac{\eta^2}{3}\right)^{\frac{1}{2}}
 \end{aligned}
 \tag{3.13}$$

It now follows from equation 3.12 that again two pairs of Zeeman components can be observed at frequencies given by

$$\nu = \nu_0 (m_1 \mp m_2) \pm \frac{\gamma H_0}{4\pi} ([m_1] \pm [m_2])
 \tag{3.14}$$

where  $\nu_0 (m_1 \mp m_2)$  is the original pure quadrupole resonance frequency given by equation 1.32, and

$$[m] = + [a_m^2 \cos^2 \theta + (b_m^2 + c_m^2 + 2b_m c_m \cos 2\varphi) \sin^2 \theta]^{\frac{1}{2}}
 \tag{3.15}$$

and each pair is symmetric about  $\nu_0$ .

The inner,  $\alpha$ , pair are again strong and the outer,  $\beta$ , pair are weak, and all lines in the spectrum depend on the value of  $\eta$ .

The locus of zero-splitting of the  $\alpha$  pair occurs when  $[m_1] = [m_2]$  in equation 3.14 and can be expressed as <sup>(11)</sup>

$$\sin^2 \theta_0 = \frac{2}{3 - \eta \cos 2\varphi_0}
 \tag{3.16}$$

The locus of zero-splitting, is therefore, defined by an elliptic cone around the Z-axis. If  $\theta_0$  is known in two perpendicular planes,  $\theta_0(\varphi = 0^\circ)$  and  $\theta_0(\varphi = 90^\circ)$ , the asymmetry parameter,  $\eta$ , of the electric field gradient tensor can be obtained from the expression (11)

$$\eta = \frac{3[\sin^2\theta_0(0^\circ) - \sin^2\theta_0(90^\circ)]}{[\sin^2\theta_0(0^\circ) + \sin^2\theta_0(90^\circ)]} \quad 3.17$$

Although this, zero-splitting locus method of determining  $\eta$  can be used with any magnitude of the static magnetic field, the more accurate values of  $\eta$  can be obtained by making use of the frequency-field method. (4) In this method the static magnetic field,  $H_0$ , is applied perpendicular to the Z-axis, the axis of the maximum component of the field gradient in its principal axis coordinate system, and the frequency separation between the  $\alpha$  and  $\beta$  components is measured,  $\eta$  can then be calculated using the expression

$$v_\alpha - v_\beta \cong \frac{\gamma H_0 \eta}{2\pi} \left[ 1 + \frac{\eta}{6} (\cos 2\varphi - \eta) \right] \quad 3.18$$

Thus in order to obtain  $\eta$ , using this method, a preliminary investigation is needed to determine the principal axis direction of the electric field gradient tensor.

It should be noted that the main source of error in single crystal Zeeman nuclear quadrupole resonance measurements often comes from the misalignment of the crystal with respect to the direction of the applied magnetic field. Furthermore a single crystal of about one cubic centimetre in size is needed which cannot be obtained for a very wide range

of compounds. Such restrictions can be overcome if a polycrystalline specimen is used in the Zeeman studies.

Morino and Toyama<sup>(5)</sup> developed an alternative technique that enables the asymmetry parameter,  $\eta$ , to be obtained in polycrystalline materials. Their method has been employed by several workers<sup>(6-8)</sup> to measure the quadrupole parameters in powdered materials. The characteristic orientational dependence of the transition frequencies and probabilities of the four Zeeman components observed in single crystals<sup>(3,13,14)</sup> confirm that the spectrum obtained from a polycrystalline sample consists of a superposition of the spectra associated with each orientation, weighted in proportion to the probability of finding the crystallite at that particular orientation. Morino and Toyama<sup>(5)</sup> predicted the line shape of the spectrum and its derivative in a polycrystalline sample in the situation that the weak static magnetic field,  $H_0$ , is applied parallel to the radio frequency field,  $H_r$ , used to induce the transitions, and they found that the resulting resonance shape is sensitive to the value of  $\eta$ . It has been shown that the resonance shapes and their positions are insensitive to  $\eta$  when  $H_0$  and  $H_r$  are applied perpendicular to each other,<sup>(15)</sup> and so  $\eta$  is best obtained under the former conditions.

In calculating the envelope shape of the spectrum for spin  $\frac{3}{2}$  nuclei in polycrystalline samples, first order perturbation theory is employed and it is assumed that;<sup>(5)</sup> (i) the sample consists of a large number of single crystals oriented at random and (ii), that the absorption signal is very sharp in the absence of the field. Furthermore (iii) the applied magnetic field is assumed to be homogeneous over the entire sample.

In the parallel fields, when  $\eta = 0$ , the splitting frequency,  $\nu_{\pm}(\theta, \varphi)$ , and the intensity,  $P_{\pm}(\theta, \varphi)$  of each Zeeman component can be expressed as<sup>(13)</sup>

$$|\nu_{\pm}(\theta, \varphi)| = \frac{1}{2} \nu_L \left[ (4 - 3\cos^2\theta)^{\frac{1}{2}} \mp 3|\cos\theta| \right] \quad 3.19$$

$$P_{\pm}(\theta, \varphi) = \frac{3}{8} \sin^2\theta \left[ 1 \pm \frac{|\cos\theta|}{(4 - 3\cos^2\theta)^{\frac{1}{2}}} \right] \quad 3.20$$

where  $\theta$  and  $\varphi$  are the polar coordinates of the external field with respect to the principal axes of the field gradient at each nucleus.  $\nu_{\pm}(\theta, \varphi)$  is the difference between the pure resonance frequency,  $\nu_0$ , and the transition frequency in the weak static field, and the intensities,  $P_{\pm}(\theta, \varphi)$ , are measured in an arbitrary scale. The + and - signs in the suffixes of  $\nu$  and  $P$  indicate the inner,  $\alpha$ , and the outer,  $\beta$ , pairs of the Zeeman components respectively, and  $\nu_L$  is the Larmor frequency for the nuclei in the applied field and is given by

$$\nu_L = \left| \frac{\gamma H_0}{2\pi} \right| \quad 3.21$$

The shape function,  $I(\nu)$ , of the absorption line broadened by the static field can be expressed as

$$I(\nu)d\nu = \frac{N}{4\pi} \int \int_{\nu}^{\nu+d\nu} P(\theta, \varphi) \sin\theta d\theta d\varphi \quad 3.22$$

where  $N$  is the normalization constant.

It now follows from equations 3.19, 3.20 and 3.22 that

$$I(v) = \frac{N}{12v_L} (4 - f^2) \quad \text{for } |f| \leq 1 \quad 3.23$$

and

$$I(v) = \frac{N}{24v_L} \left[ (4-f^2) + |f| \{3(4-f^2)\}^{\frac{1}{2}} \right] \quad \text{for } 1 < |f| \leq 2 \quad 3.24$$

where

$$f = \frac{v \pm v_L}{v_L}$$

The envelope shape predicted by equations 3.23 and 3.24 shows only two kinks at  $v = \pm v_L$  which is shown in figure 3.2a below.

In the case of  $\eta \neq 0$  the resonance shape function is given by

$$I(v) = \frac{N}{2\pi v_L} \left[ \frac{|\epsilon|}{1+|\epsilon|} \right] \times F \left[ \frac{\pi}{2}, \frac{2|\epsilon|^{\frac{1}{2}}}{1+|\epsilon|} \right] \quad 3.25$$

where

$$\epsilon = \frac{|f|-1}{\eta} = \frac{|v|-v_L}{\eta v_L} \quad 3.26$$

and

$$F(\varphi, k) = \int_0^\varphi \frac{dx}{(1-k^2 \sin^2 x)^{\frac{1}{2}}} \quad 3.27$$

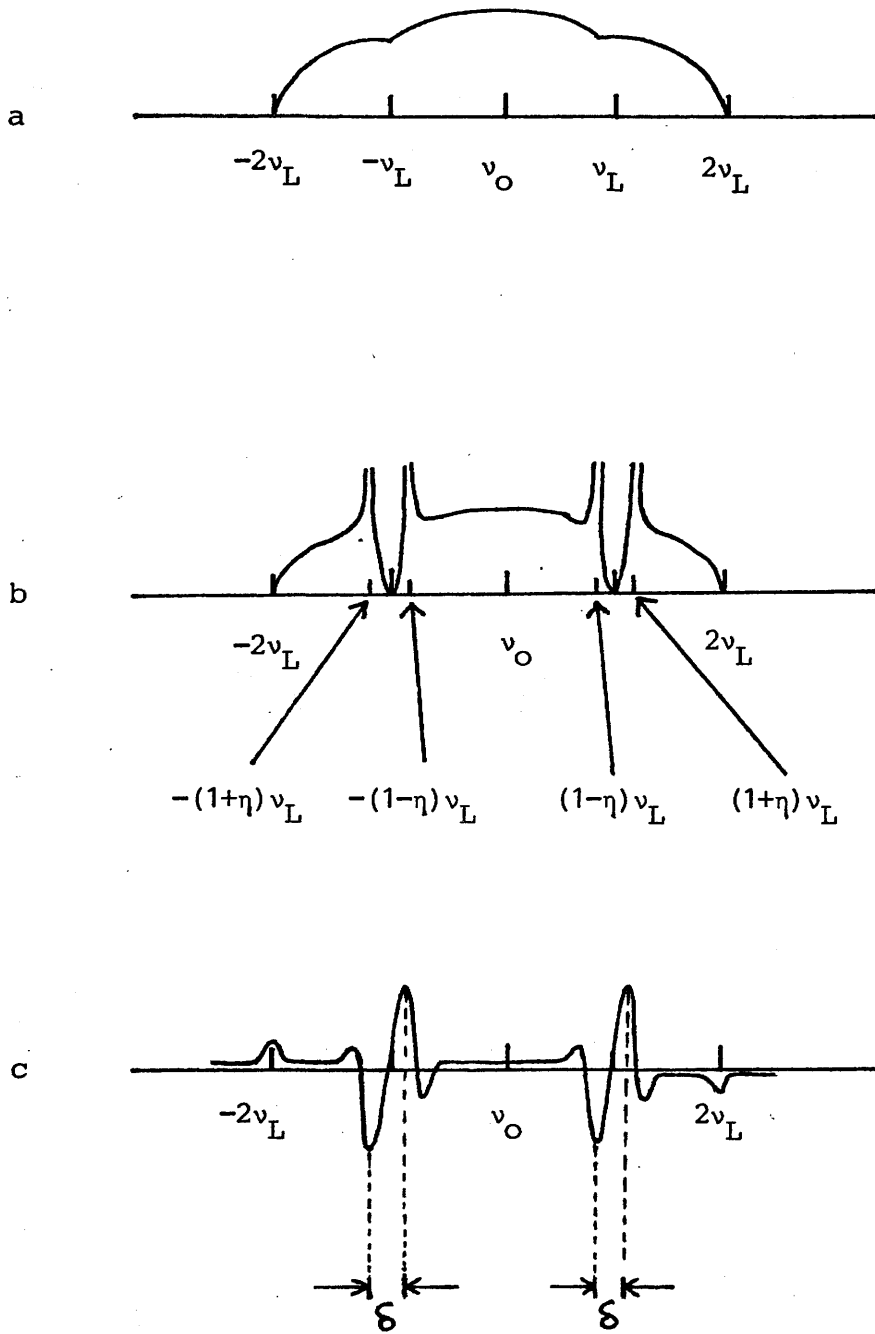


**Figure 3.2** Envelope shape of Zeeman N.Q.R. spectrum for a poly crystalline sample.

(a) when  $\eta = 0$ , (b) for small  $\eta$ , and (c) the first derivative of (b)

The shape function expected through these equations and its derivative are shown in figure 3.2 . Two pairs of sharp maxima at  $\pm (1-\eta)v_L$  and at  $\pm (1+\eta)v_L$  and one pair of sharp minima at  $\pm v_L$  are produced in the envelope shape of the absorption line, and so  $\eta$  can be estimated if the frequencies of these singularities are measured. If the original, zero-field, linewidth,  $\Delta\nu$ , is negligible, the asymmetry parameter can be estimated from

$$\eta = \frac{\delta}{2v_L} \quad 3.28$$

where  $\delta$  is the linewidth parameter which corresponds to the peak to peak separation of the derivative spectrum in the  $\pm v_L$  regions. However in practice  $\eta$  is measured from the plot of  $\frac{\delta}{2v_L}$  versus  $\frac{1}{H_0}$  and extrapolating to infinite field strength, where the effect of the intrinsic linewidth would be negligible. (5) It is necessary to apply a magnetic field strong enough to overcome the influence of the original linewidth, and it can be shown that the field required to make the splitting due to  $\eta$  greater than  $\Delta\nu$ , is given by

$$H_0 \geq \frac{2\pi\Delta\nu}{\eta|\gamma|} \quad 3.29$$

where the peak intensity of the line shape decreases to  $I_{\min}$  which is given by

$$I_{\min} \leq \frac{\eta}{4} I_0 \quad 3.30$$

where  $I_0$  is the intensity of the unperturbed signal.

The very marked broadening of the envelope by the applied magnetic field restricts this method to compounds that exhibit very sharp signals in the absence of the field. Furthermore, this technique is valid only for  $\eta < 0.2$ . These shortcomings of Morino and Toyama's method can obviously be overcome if the complete line shape function, given by equations 3.23-3.25, is calculated by adjusting its parameters until an exact match with the observed spectrum envelope is obtained. Darville et al have devised computer programs that enable Zeeman-broadened polycrystalline spectra<sup>(16,17)</sup> to be calculated from which an accurate value of  $\eta$  and then  $eqQ$  can be obtained.

If the asymmetry parameter is too small, e.g.  $\eta < 0.1$ , to be measured by any of these methods, then to a good approximation  $\eta$  can be neglected in equation 1.32 and then the quadrupole coupling constant can essentially be obtained directly from the pure quadrupole resonance spectrum.

## CHAPTER 4

### EXPERIMENTAL DETECTION OF NUCLEAR QUADRUPOLE

#### RESONANCE ABSORPTION

##### 4.1 INTRODUCTION

Nuclear magnetic resonance spectra are usually obtained by sweeping a magnetic field and using an applied, fixed, radio frequency. However the quadrupole resonance frequency is determined by the electric field gradient within the molecule and the crystal, and so a variable frequency technique is necessary to detect quadrupole resonance signals. Furthermore, pure quadrupole resonance transitions must be induced and detected in the same coil, i.e. a crossed-coil mechanism cannot be used in detecting quadrupole resonance transitions in zero magnetic field since the degeneracy of quadrupolar energy levels,  $\pm m_I$ , cancels the nuclear induction in a direction perpendicular to the transmitting coil.

Quadrupole resonance frequencies of nuclei, in general, range from a few hundred K.Hz. to about 1000 M.Hz. In fact no quadrupole resonance spectrometer is yet able to cover this range of frequency and so the design of the spectrometer depends on the frequency range of interest. Marginal oscillators are known to reproduce good lineshapes, and this type of instrument is sometimes used to detect resonance frequencies below 10 M.Hz. However at all frequencies up to about 700 M.Hz. super-regenerative oscillators are more sensitive and are widely used.

Pulse techniques have also been adapted in detecting quadrupole

resonance signals, and a great deal of information is obtained from them about relaxation phenomena and molecular motions in solids.

Several double resonance, particularly double resonance with level crossing, techniques have been developed recently to detect quadrupole resonance signals in the low frequency region.

The Decca Radar, super-regenerative type of quadrupole resonance spectrometer has been used in this work, and is briefly described in the following section.

#### 4.2 THE SUPER-REGENERATIVE OSCILLATOR

The super-regenerative type of N.Q.R. spectrometer consists, essentially, of an ordinary radio-frequency oscillator which is quenched periodically by an internal or external quenching mechanism, at a rate that corresponds to a small fraction of the R.F. frequency. (1,2)

If an appropriate quenching rate is applied so that the successive oscillations are allowed to build up to their limiting amplitude, the oscillator is then working in the so-called logarithmic mode, in which the coherence of oscillation can be varied by changing the quench frequency.

The successive pulses build up either from the thermal noise or from the tail of the preceding pulse (1-4) and it is the relative amplitudes of these two sources that determine the degree of the phase coherence between R.F. pulses. (4) Fully coherent or incoherent modes of oscillation are obtained when the next pulse is initiated by the tail of the preceding pulse or by thermal noise, respectively.

The oscillation, in the fully coherent mode transmits a power spectrum that consists of a set of sharp peaks at frequencies given by  $f_o \pm n f_q$  where  $f_o$  represents the fundamental, unquenched, frequency of the oscillator having the maximum intensity,  $n$  is an integer, and  $f_q$  is the quench frequency. However each line broadens as the coherence is reduced and eventually, in the fully incoherent state, a broad line centred on the fundamental frequency is observed in the power spectrum. Thus in the super-regenerative oscillator different types of the radio-frequency power spectrum are obtained depending on the degree of coherence of the oscillations. Furthermore, the gain of the circuit

and its efficiency in exciting the quadrupole resonance signals depend on the degree of coherence. The gain increases with increasing incoherence of the system, <sup>(4,5)</sup> while the efficiency, as an exciter, is usually higher in the coherent mode. The maximum efficiency is obtained when the line width in the power spectrum is comparable with that of the quadrupole resonance line. <sup>(6)</sup>

In the coherent mode, the presence of the quadrupole resonance signal slightly increases the amplitude of the exponential rise of the following pulse and this therefore is initiated slightly earlier than it otherwise would be. This increases the overall area of the R.F. envelope and hence changes the average anode current of the oscillator valve, i.e. the quadrupole resonance signal introduces an additional voltage across the anode impedance. The R.F. envelope during one quench cycle is shown in the following figure. <sup>(4)</sup>

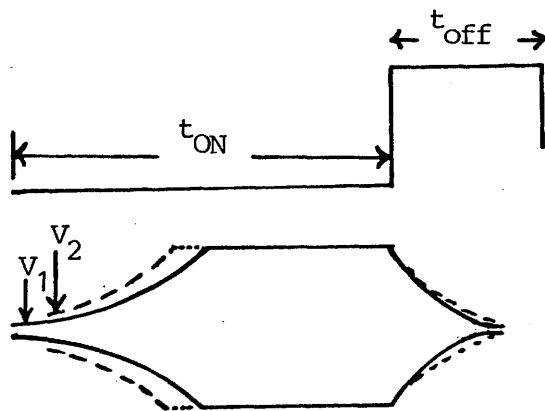


Figure 4.1 The R.F. envelope of a super-regenerative oscillator.

$t_{ON}$  and  $t_{off}$  are the time periods in which the R.F. pulses are ON and OFF respectively.

In the operating range of the super-regenerative oscillator the output voltage,  $V_{out}$ , of the system is approximately described by<sup>(1,4,7)</sup>

$$V_{out} \approx f_q \ln \frac{V_2}{V_1} \quad 4.1$$

where  $V_2$  is the R.F. voltage in the pulse tail in the presence of the resonance signal and  $V_1$  is the voltage without the signal.

Equation 4.1 shows an inverse relationship between  $V_{out}$  and  $V_1$  and so the super regenerative oscillator can serve as a sensitive detector of quadrupole resonance signals if  $V_1$  is made as small as possible.

The second action of the super-regenerative oscillator is as an exciter of quadrupole resonance transitions. The efficiency of the instrument for this purpose depends on the gain,  $\frac{V_{out}}{V_s}$ , of the system, where  $V_s$  is the amplitude of that component of the nuclear magnetization which is in phase with the pulse tail. This is given by<sup>(4)</sup>

$$\frac{V_{out}}{V_s} \approx k \frac{2C_t}{G_1} f_q \exp.\left(\frac{G_o t_{off}}{2C_t}\right) \quad 4.2$$

where  $k$  is a constant that represents the efficiency of the detector,  $G_1$  is the effective negative conductance in parallel with the tank circuit during the  $t_{ON}$  period,  $C_t$  is the total tank circuit capacitance and  $G_o$  is the effective conductance in parallel with the tank circuit during the  $t_{off}$  period. It follows from equation 4.2 that the gain of the circuit depends strongly on  $C_t$  and hence on the operating frequency, i.e. the efficiency of the system in exciting resonance transitions varies with frequency. Thus, in order to scan over a wide range of frequency,

when searching for resonance signals in a new compound, incorporation of some sort of automatic gain control is necessary to maintain the stability of the gain of the system. This can be done via the exponential term in equation 4.2 since it has the most effect on the gain. Provided  $t_{\text{off}} < \frac{1}{f_q}$ , both  $G_o$  and  $t_{\text{off}}$  can be varied without affecting  $f_q$  and can therefore serve as an automatic gain control which is unaffected by the process of the sideband suppression.

The sidebands in the power spectrum mentioned earlier, sometimes confuse the assignment of the correct quadrupole resonance frequency since any of the strong sidebands can also induce a resonance transition. The accurate identification of the quadrupole resonance frequencies can be made when the sidebands are all suppressed. This can be done simply by varying the quench frequency at a rate which is faster than the recording time constant but slower than the quench frequency itself. This has the effect of shifting the frequencies of the sidebands in and out from the carrier frequency and they are no longer detectable. (1,4)

The information outlined above represents the basis of the Decca Radar N.Q.R. spectrometer, used in this work, in a summarized form. Automatic gain control, sideband suppression and automatic frequency calibration facilities are all incorporated in this spectrometer. The frequency sweep is carried out via a variable capacitor in the tank circuit, by means of a motor drive. A block diagram of the Decca spectrometer is shown in figure 4.2. (2)

Both frequency modulation and Zeeman modulation techniques can be used in the Decca Radar spectrometer in detecting quadrupole resonance signals. The latter technique is more often used since only quadrupole

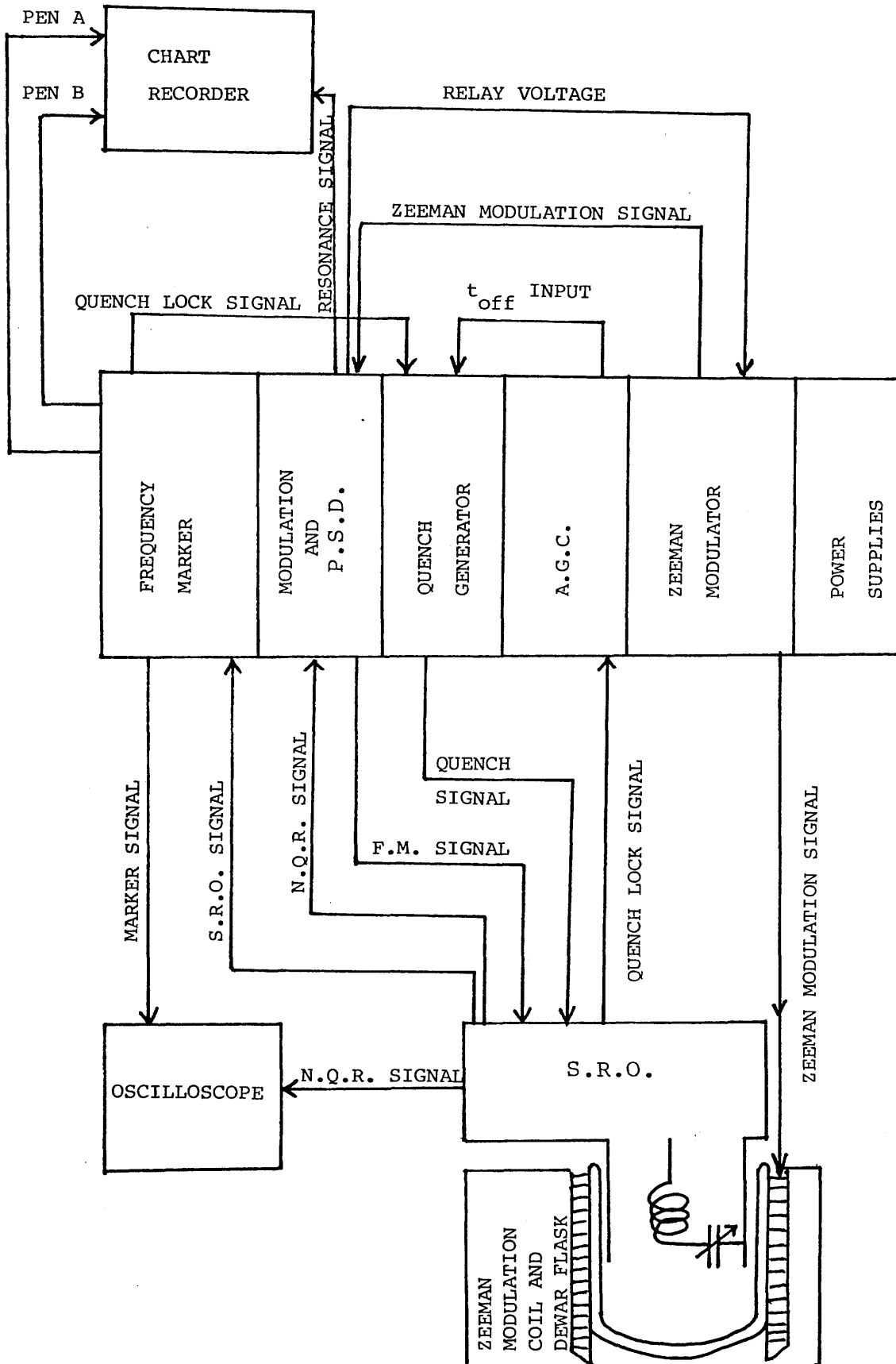


Figure 4.2 Block diagram for Decca Radar N.Q.R. Spectrometer.

resonance signals are then detectable whereas in the frequency modulation method, signals other than resonance absorptions, e.g. radio transmitters or piezoelectric responses, may also be detected.

In addition to quadrupole frequencies, more detailed information about nuclear relaxation processes and molecular motions in solids can be obtained by using pulsed techniques to detect quadrupole resonance transitions. These methods enable the relaxation times of the nuclear spin system to be obtained more accurately.

In pulsed spectrometers, the nuclear spin system in the sample under investigation is subjected to some kind of sequence of pulses of radio-frequency power, and then the decay of the nuclear magnetization in the time between sequences is examined.

In this context, the effective nuclear magnetization vector,  $M$ , is considered initially to be along the direction of the maximum component of the electric field gradient tensor, i.e. along the Z-principal axis of the field gradient, since the quadrupolar nuclei precess only about this direction in zero magnetic field. This situation is similar to the nuclear magnetic polarization encountered in N.M.R. when a magnetic field,  $H_0$ , is applied along the Z-axis. An intense pulse of radio-frequency power is now applied to the sample coil to generate a magnetic field,  $H_1$ , rotating in the XY plane, in the same sense as, and in resonance with the precession of the nuclear moments. Under these conditions, the nuclear magnetization vector now also precesses about the direction of  $H_1$  at a frequency given by  $\gamma H_1/2\pi$ , where  $\gamma$  is the nuclear magnetogyric ratio.<sup>(8)</sup> If a frame of reference,  $x'y'z'$ , is now imagined to rotate in the XY plane in the same direction and

frequency as  $H_1$  then the nuclear magnetization now appears to rotate about the direction of  $H_1$ . The angle of rotation,  $\theta$ , of the macroscopic nuclear magnetization vector,  $M$ , with respect to the  $Z'$ -axis is controlled by the length of the time for which  $H_1$  is applied. The spectrometer arrangement is such that it detects the magnetization in the  $x'y'$  plane. This arrangement is shown schematically in the following figure.

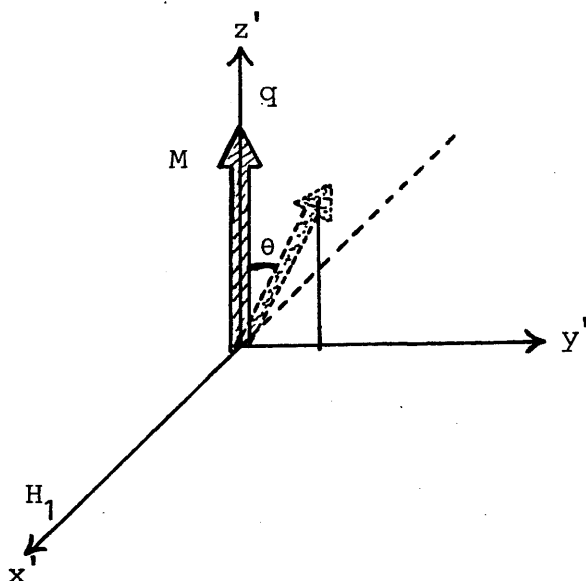


Figure 4.3 The precession of  $M$  about  $H_1$  in a rotating frame of reference,  $x'y'z'$ .

The intensity of the observed signal is therefore proportional to  $\sin\theta$ . Thus the maximum intensity is obtained if a  $90^\circ$  pulse is applied. However, when the pulse is turned off, the spin-spin relaxation processes and the inhomogeneities in the electric field gradient at the quadrupolar

nuclei cause the nuclear moments to fan out in the  $x'y'$  plane at different frequencies introducing a rapid reduction of the signal intensity and eventually it decays exponentially to zero with time constant  $T_2^*$ , the spin-spin relaxation time. This process is known as the free induction decay.

Another important relaxation process exists in this context; that is the spin-lattice relaxation, in which the energy gained by the nuclear spin system, from the radio frequency pulses, is dissipated to the lattice or surrounding medium as thermal energy. This case can be studied if the sample under investigation is subjected to a  $180^\circ$  pulse followed by a  $90^\circ$  pulse after a period  $\tau$  so that the observed signal decays with time constant  $T_1$ , the spin-lattice relaxation time. It should be noticed that,  $T_1$  represents the time constant of the restoration of  $M_z$ , the magnetization component along the  $z'$  axis, to its equilibrium value,  $M$ , while  $T_2^*$  governs the relaxation process in the  $x'y'$  plane. Furthermore,  $T_1$  is extremely important since the spin-lattice relaxation process tends to restore the Boltzmann distribution of the nuclei among the spin states after an intense radio-frequency pulse, at the quadrupole resonance frequency, has been applied, which tends to equalize the population between these states.

Pulse techniques have been found to be more sensitive in detecting quadrupole resonance signals since accumulation of pulse responses leads to a better signal to noise ratio<sup>(9,10)</sup> in comparison with the super-regenerative method.

These techniques have recently been modified to produce highly sensitive methods for detecting quadrupole resonance transitions, the

so-called "double resonance with level crossing" techniques developed by Hahn and co-workers. (11)

In order to apply these methods for a set of quadrupolar nuclei, Q, the sample under investigation must contain, also, the so-called indicator set of nuclei, P. For example P could be any species such as  $^1\text{H}$ , that give strong and easily detectable nuclear magnetic resonance signals, usually observed in the form of a free induction decay after conventional  $90^\circ$  pulses have been applied. (12-14) Furthermore, both sets of nuclei P and Q must have a low-field spin-lattice relaxation time,  $T_1$ , of the order of a few seconds at least. The optimum relaxation time can usually be obtained at an appropriately low temperature. (13)

The level crossing, in this context, can simply be explained in terms of the energy differences between the adjacent spin states in both P and Q nuclei. The energy splitting between the two spin states of a proton,  $\Delta E_P$ , is directly proportional to the strength of the applied magnetic field,  $H_0$ , while in the case of the quadrupolar nucleus, Q, the energy differences,  $\Delta E_{Q_i}$ , between any two adjacent spin states are mainly determined by the quadrupolar interactions of these nuclei. (12) Thus  $\Delta E_P$  can be made to coincide, in turn, with each value of  $\Delta E_{Q_i}$  at appropriate values of the field,  $H_0$ , and hence "level crossings" will occur. The resultant energy changes between the two systems equalizes the spin temperatures, rapidly, for the two pairs of the spin energy levels involved. The level crossing is shown schematically in the figure below. (14)

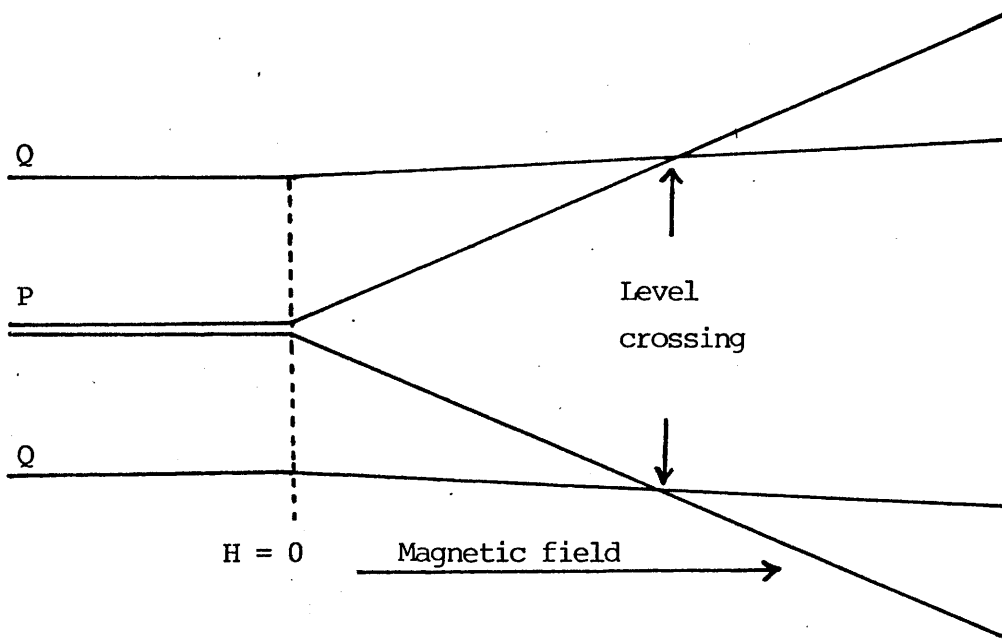


Figure 4.4 The level crossing representation between the spin states in Q and P systems.

In the experimental layout, the apparatus is arranged such that, in one area a homogeneous magnetic field,  $H_0$ , is applied horizontally to the sample when it is in the tank coil of a pulsed proton spectrometer, at constant temperature. This device enables the proton magnetization to be measured from the free induction decay signals obtained after  $90^\circ$  pulses have been applied. <sup>(12,13)</sup> A compressed air piston then enables the sample to be transferred rapidly to a second region of the apparatus containing another radio-frequency transmitting coil in zero magnetic field. This allows the sample to be irradiated at a fixed frequency,

$\nu_i$ , which can then easily be swept by a fixed amount between the successive cycles repeated during the experiment.

The search for pure quadrupole resonance signals is performed by a series of cycles each of which can be described as follows. The sample is subjected to a homogeneous magnetic field,  $H_0$ , until the protons come into equilibrium with the field. This polarizes the P set of nuclei, along the direction of  $H_0$ , more than it does the Q set since the latter have a smaller magnetogyric ratio. The first cycle of the experiment now starts by moving the sample to the second, Q, coil in a very short time, during which an adiabatic demagnetization occurs in the protons, reducing the energy splitting between the two spin states in the protons without affecting their populations. The energy levels of the quadrupolar nucleus, in the Q set, change also, returning to the characteristic quadrupolar spin states in zero magnetic field. A level crossing occurs between the two systems, P and Q, during the demagnetization of the protons and then the two systems become thermally isolated from each other. The sample is irradiated for a short time in the Q coil at a fixed frequency,  $\nu_i$ , chosen to be in the expected region of frequencies for the quadrupolar nuclei in the Q system.

Then, the sample is again subjected to  $H_0$  in the first, P, coil and a  $90^\circ$  radio-frequency pulse is applied. A free induction decay signal is then recorded in order to measure the remaining polarization in the protons. An additional level crossing occurs during this step. Thus if any energy has been absorbed by Q from the irradiation process, some of this energy will be transferred to the P system, reducing its remaining magnetization.

The cycle is repeated several times sweeping  $\nu_i$  by a fixed amount between the successive cycles until the expected range, of quadrupole resonance frequencies, is scanned and the remaining polarizations of the P system are measured at the end of each cycle as described above. The considerable reductions, observed in the remaining magnetizations of the P system, as  $\nu_i$  approaches the pure quadrupole resonance frequencies of the nuclei in Q, give rise to the required quadrupole resonance spectrum.

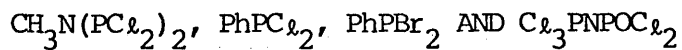
Double resonance techniques are highly sensitive and so they are particularly useful in detecting quadrupole resonance absorptions for nuclei that have very low natural abundances, such as  $^{17}\text{O}$  and  $^2\text{D}$ , (12-15) where these signals are undetectable by means of super-regenerative or other spectrometers. Double irradiation techniques have also been used very successfully in studies of  $^{14}\text{N}$  quadrupole resonance frequencies in a number of compounds (16,17) using  $^1\text{H}$  as an indicator, P, system.

In principle, the indicator nucleus, could also be a quadrupolar nucleus that gives a strong signal. (18)

CHAPTER 5

HALOGEN NUCLEAR QUADRUPOLE RESONANCE STUDIES OF SOME

ACYCLIC COMPOUNDS OF PHOSPHORUS:



5.1 INTRODUCTION

Nuclear quadrupole resonance spectroscopy has turned out to be a fruitful technique in studying chlorine-35 resonance spectra for a number of compounds that contain phosphorus-chlorine bonds. (1-11)

The majority of these studies are concerned with phosphorus(V) but only a very small number involve phosphorus(III) derivatives. Hence, it is worthwhile studying halogen quadrupole resonance spectra in phosphorus-(III) compounds.

In this work, chlorine-35 quadrupole resonance spectra of methyl-aminobisdichlorophosphine,  $\text{CH}_3\text{N}(\text{PCl}_2)_2$ , and dichlorophenylphosphine,  $\text{PhPCl}_2$ , have been examined over the temperature ranges  $85 \leq T \leq 255$  and  $77 \leq T \leq 183\text{K}$  respectively, since signals were only detectable within these ranges.

Bromine nuclear quadrupole resonance data, in general, are quite rare in the literature, particularly for phosphorus(III) derivatives, and hence bromine-79 quadrupole spectra in dibromophenylphosphine,  $\text{PhPBr}_2$ , have also been investigated in this work over the temperature range  $77 \leq T \leq 244\text{K}$  where signals are detectable.

A compound of phosphorus(V) has also been involved in this study. Chlorine-35 quadrupole resonance spectra in trichlorophosphazophosphoryl chloride,  $\text{Cl}_3\text{P}=\text{N}-\text{POCl}_2$ , have been investigated over the temperature range  $77 \leq T \leq 307\text{K}$ .

The quadrupole resonance data obtained for these compounds will be discussed in turn in the following section.

5.2 THE EFFECTS OF TEMPERATURE VARIATION ON HALOGEN N.Q.R. SPECTRA OF  
CH<sub>3</sub>N(PCl<sub>2</sub>)<sub>2</sub>, PhPCl<sub>2</sub>, PhPBr<sub>2</sub> AND Cl<sub>3</sub>PNPOCl<sub>2</sub>

All compounds studied in this work were prepared by methods described in the literature, (12-14) except in the case of PhPCl<sub>2</sub> which was obtained commercially. These preparations are described in detail in Appendix-5A.

The Decca Radar, super-regenerative nuclear quadrupole resonance spectrometer was used to detect N.Q.R. spectra. Signals were detected using Zeeman modulation and accurate frequency measurements were made by interpolation between the frequency calibration markers automatically printed on the chart. These frequencies are accurate to  $\pm 1$  K.Hz.

The sample under investigation was sealed in a thin-walled glass ampoule which fits the coil assembly of the super-regenerative oscillator, and the temperature of the sample and the coil assembly was varied by means of a nitrogen gas flow system which is described, in detail, in Appendix-5B. Each temperature was held fixed for 30-40 minutes, to ensure a uniform temperature over the whole sample, before recording each spectrum. The temperature dependence of the quadrupole resonance frequencies in CH<sub>3</sub>N(PCl<sub>2</sub>)<sub>2</sub>, PhPCl<sub>2</sub>, PhPBr<sub>2</sub> and Cl<sub>3</sub>PNPOCl<sub>2</sub> are plotted in figures 5.1, 5.2, 5.3 and 5.4 respectively. The observed variations of these frequencies with temperature have been fitted to polynomials of the form

$$\nu = a + b'T + \frac{c'}{T} \quad 5.1$$

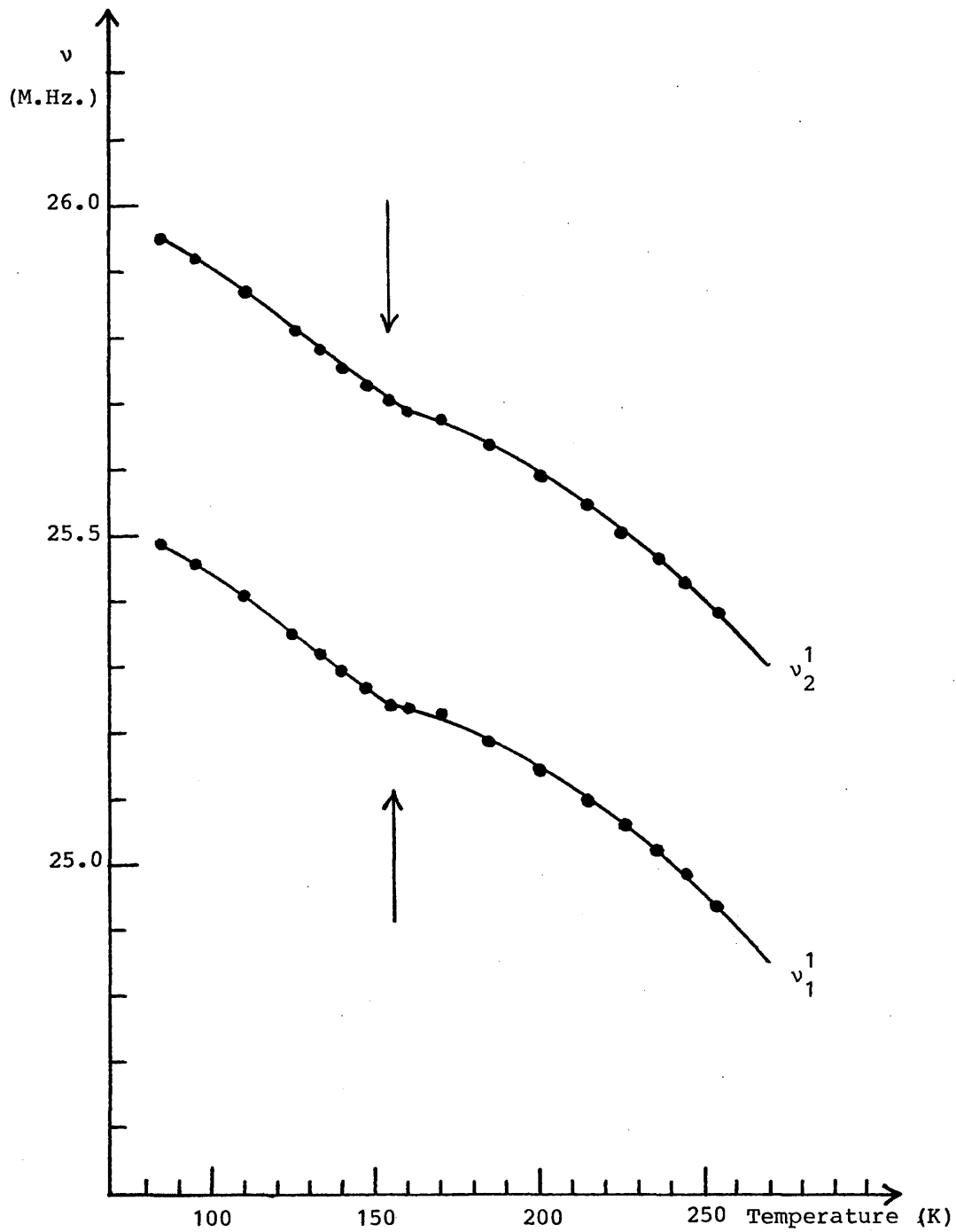


Figure 5.1 Chlorine-35 N.Q.R. frequencies,  $\nu$  (M.Hz.), for  $\text{CH}_3\text{N}(\text{PCl}_2)_2$  vs. temperature (K).

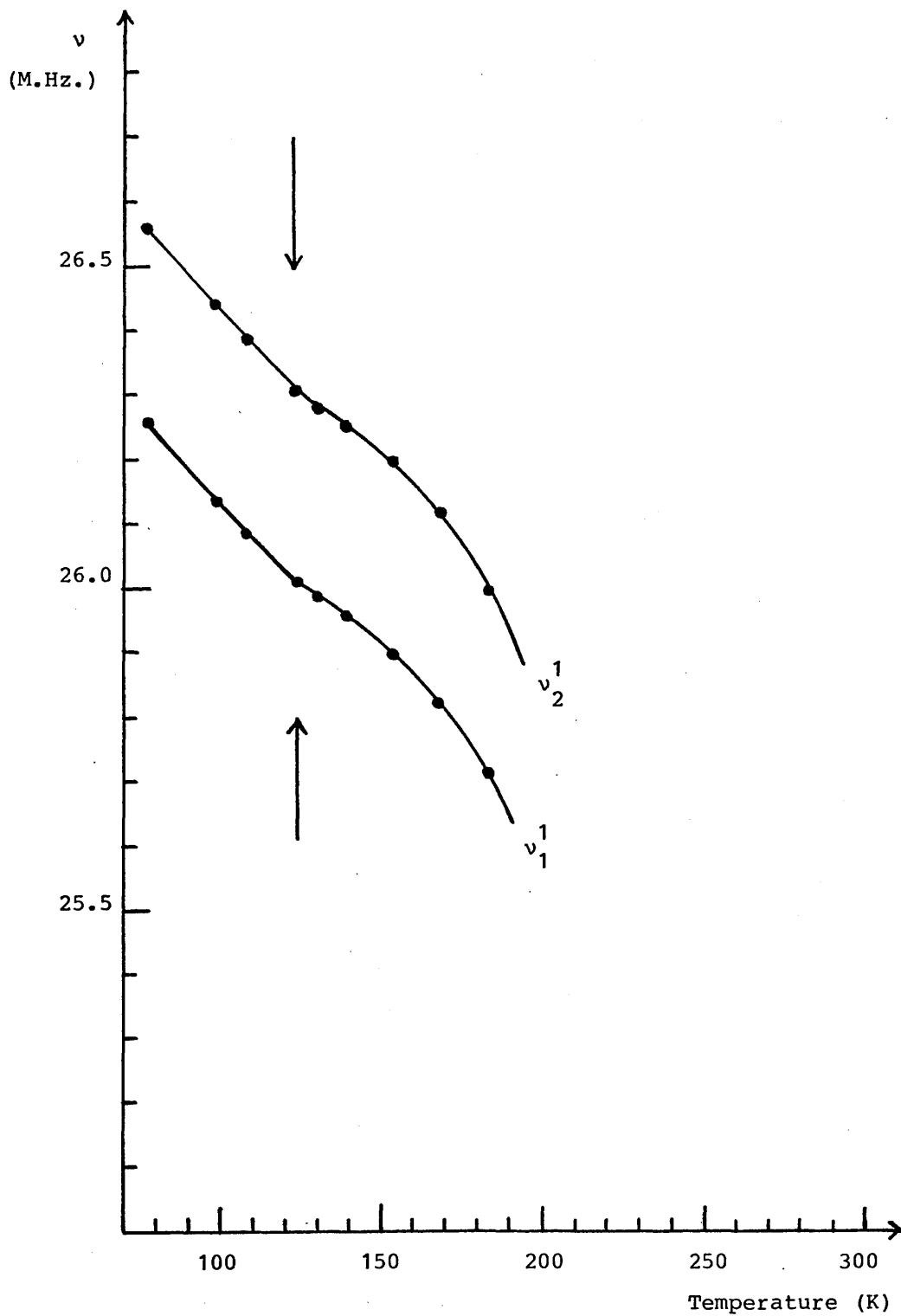


Figure 5.2 Chlorine-35 N.Q.R. frequencies,  $\nu$  (M.Hz.), for  $\text{PhPCl}_2$  vs. temperature (K)

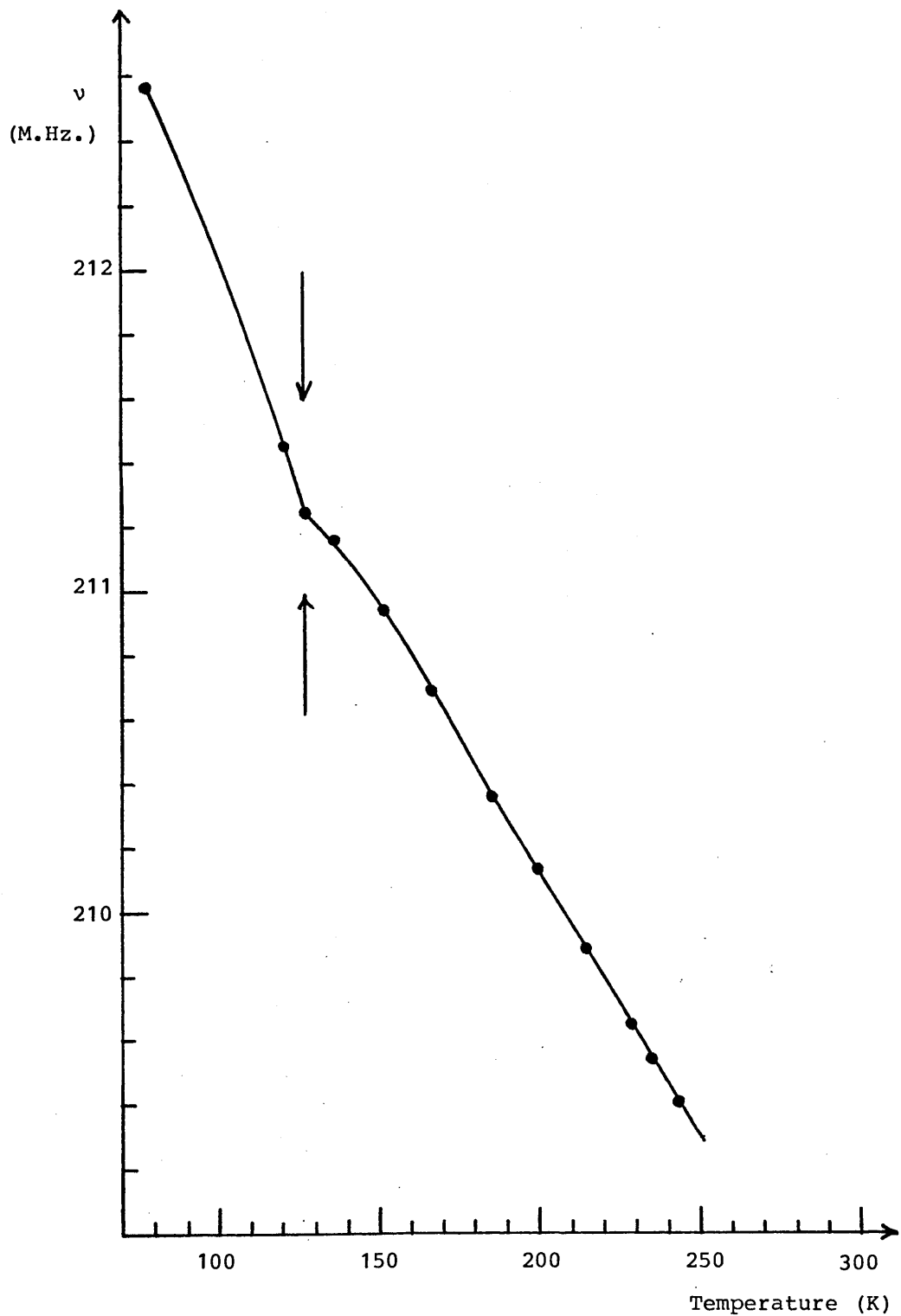


Figure 5.3 Bromine-79 N.Q.R. frequencies,  $\nu$  (M.Hz.), for  $\text{PhPBr}_2$  vs. temperature (K).

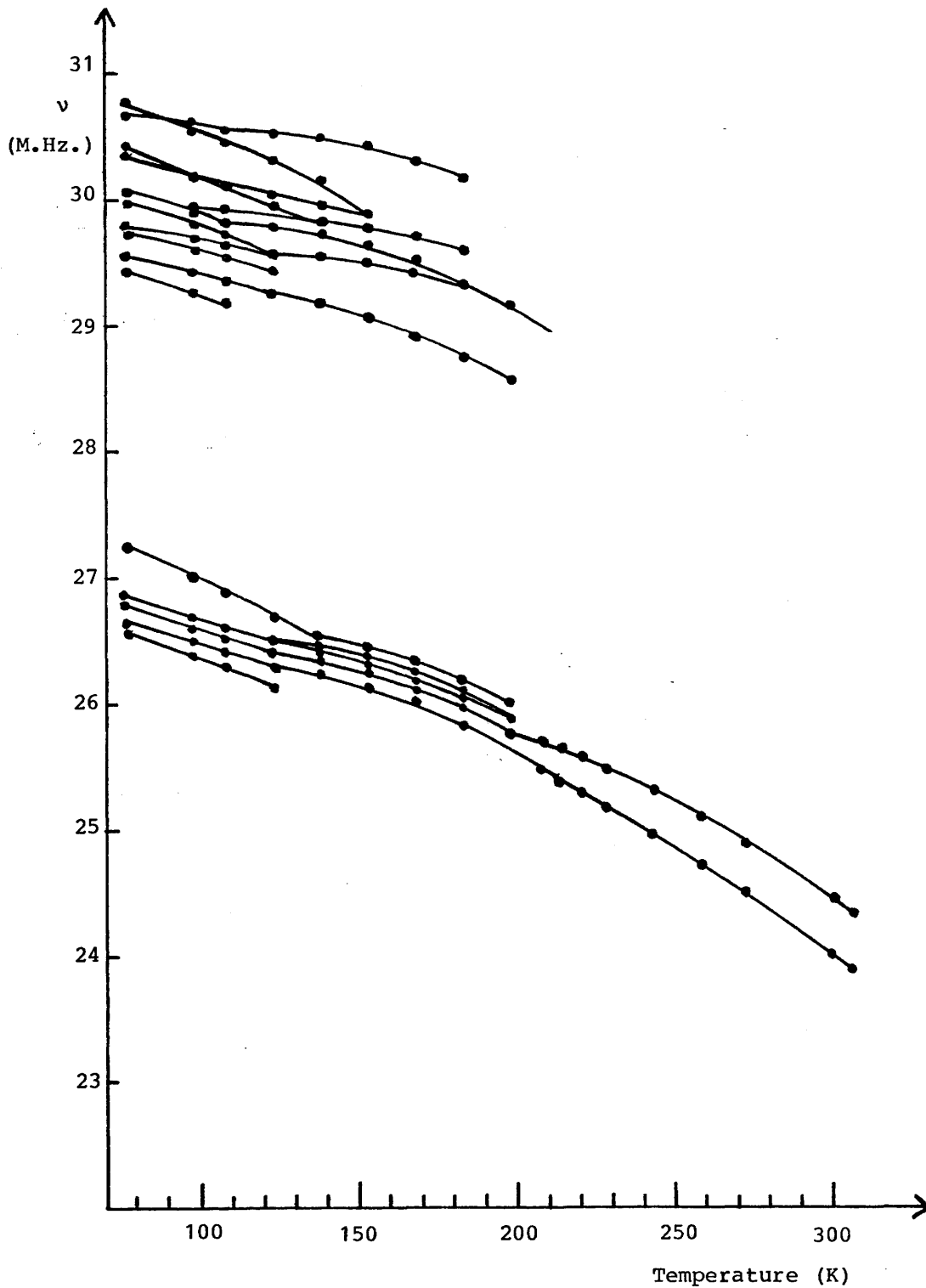


Figure 5.4 Chlorine-35 N.Q.R. frequencies,  $\nu$  (M.Hz.), for  $\text{Cl}_3\text{PNPOCl}_2$  vs. temperature (K).

as required by Bayer-Kushida's theory presented in chapter 2. The best curves have been fitted to the experimental variations of frequencies with temperature and the coefficients,  $a$ ,  $b'$  and  $c'$  obtained. The temperature coefficients,  $(\frac{\partial \nu}{\partial T})_{\substack{P=1 \text{ Kg.cm}^{-2} \\ T=295\text{K}}}$  have then been calculated

for all quadrupole resonance lines observed in this work. These data are all given in Table 5.1.

Tables 5.2 and 5.3 list chlorine-35 and bromine-79 quadrupole resonance frequencies for acyclic phosphine and phosphoryl derivatives and include the present results together with other data obtained from the literature quoted<sup>(15,16,1,17)</sup> for comparison purposes.

Figure 5.1 and Table 5.1 show that only two quadrupole signals, designated as  $\nu_1$  and  $\nu_2$ , with relative intensities of 1:1 were observed for  $\text{CH}_3\text{N}(\text{PCl}_2)_2$  over the temperature range  $85 \leq T \leq 255\text{K}$ . This indicates that this molecule is bisected by a plane of symmetry that is retained over the temperature range investigated. This must be the plane containing the C-N bond and bisecting the angle PNP in figure 5.5.

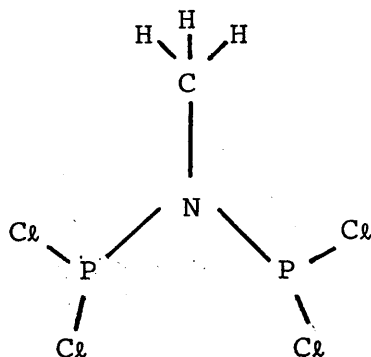


Figure 5.5 Projection of the structure of  $\text{CH}_3\text{N}(\text{PCl}_2)_2$

Table 5.1

Polynomials, and temperature coefficients of resonance frequencies obtained by fitting the best curves of the form

$$\nu = a + b'T + \frac{c'}{T}$$

to the experimental variation of frequencies with temperature.

Compound	Resonance <sup>I</sup>	a	b'	c'	$\left(\frac{\partial \nu}{\partial T}\right)$ P=1Kg.cm <sup>-2</sup> T=295K
CH <sub>3</sub> N(PCl <sub>2</sub> ) <sub>2</sub>	$\nu_1^1$	27.403x10 <sup>6</sup>	- 6935	-175.164x10 <sup>6</sup>	- 4922
	$\nu_2^1$	27.075x10 <sup>6</sup>	- 5360	- 81.678x10 <sup>6</sup>	- 4421
PhPCl <sub>2</sub>	$\nu_1^1$	28.840x10 <sup>6</sup>	-11998	-168.433x10 <sup>6</sup>	-10063
	$\nu_2^1$	29.248x10 <sup>6</sup>	-12583	-171.798x10 <sup>6</sup>	-10609
PhPBr <sub>2</sub>	$\nu$	211.752x10 <sup>6</sup>	-12944	+200.094x10 <sup>6</sup>	-15243
Cl <sub>3</sub> PNPOCl <sub>2</sub>	$\nu_1^1$	31.291x10 <sup>6</sup>	-20625	-316.085x10 <sup>6</sup>	-16993
	$\nu_2^1$	34.127x10 <sup>6</sup>	-24387	-695.817x10 <sup>6</sup>	-16391

a values are in Hz, b' in Hz.K<sup>-1</sup>, c' in Hz.K and  $\left(\frac{\partial \nu}{\partial T}\right)$  in Hz.K<sup>-1</sup>.

<sup>I</sup> Superscript to resonances indicates relative intensities.

Table 5.2

Chlorine-35 N.Q.R. frequencies for some acyclic phosphine and phosphoryl compounds with P-Cl bonds

Compound	N.Q.R. frequency (M.Hz.)	Temperature (K)	Reference
<u>Phosphorus(III) derivatives</u>			
PhPCl <sub>2</sub>	26.261;26.557	77	A
PCl <sub>3</sub>	26.107;26.202	77	15
CH <sub>3</sub> N(PCl <sub>2</sub> ) <sub>2</sub>	25.492;25.956	85	A
Bu <sup>t</sup> N(PCl <sub>2</sub> ) <sub>2</sub>	24.428;24.851 25.123;25.136	293	16
<u>Phosphorus(V) derivatives</u>			
POCl <sub>3</sub>	28.938;28.986	77	1
Cl <sub>3</sub> PNPOCl <sub>2</sub>	26.837;30.079	77	A
Ph <sub>3</sub> PNPOCl <sub>2</sub>	25.088;25.463	293	16

A is the present work.

Table 5.3

Bromine-79 N.Q.R. frequencies in phosphorustribromide and  
dibromophenylphosphine

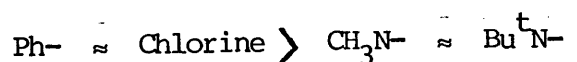
Compound	N.Q.R. frequency (M.Hz.)	Temperature (K)	Reference
$\text{PBr}_3$	219.605	83	17
$\text{PhPBr}_2$	212.581	77	A

A is the present work.

A liquid crystal proton { phosphorus-31 } nuclear magnetic double resonance analysis of this compound shows that the atoms, C, N, P and P all lie in the same plane with a PNP interbond angle of  $117 \pm 0.5^\circ$  and P-N bond lengths of  $1.66_4 \pm 0.01 \text{ \AA}$ .<sup>(18)</sup> The  $\text{CH}_3\text{N}(\text{PCl}_2)_2$  molecule is believed to possess two planes of symmetry and that the P-N bonds in this molecule have significant  $d_\pi - p_\pi$  character,<sup>(18)</sup> since the PNP interbond angle is considerably greater than tetrahedral, and the P-N bond lengths are significantly shorter than  $1.769 \pm 0.019 \text{ \AA}$ , expected for a P-N single bond.<sup>(19)</sup> The N.Q.R. data imply that only one of these molecular planes of symmetry is used in the crystal structure. Tables 5.1 and 5.2 show that the differences between the two pairs of the chlorine atoms in  $\text{CH}_3\text{N}(\text{PCl}_2)_2$  molecule are minute and are well within the range expected as a result of packing effects in the solid. The N.Q.R. data are consistent with those obtained from the liquid crystal N.M.R. study.

Figure 5.1 shows explicitly that this molecule undergoes a single phase transition at about 160K as indicated by the small discontinuity in the curve at that temperature.

The data in Table 5.2 enable conclusions to be drawn about the relative electronegativities of the functional groups in these molecules. The table shows that, in the phosphorus(III) compounds listed, the effective relative electronegativities of the functional groups involved decrease in the following order



if allowances are made for the different temperatures used in these quadrupole resonance measurements. Replacing a chlorine atom in  $\text{PCl}_3$  by an amino residue therefore pushes the electron density on to the remaining chlorine atoms increasing the polarities of P-Cl bonds. The P-Cl bond lengths therefore increase, the electron densities on the chlorine atoms increase and thus the chlorine nuclear quadrupole resonance frequencies decrease. However, on going from  $\text{PCl}_3$  to  $\text{PhPCl}_2$  the frequency variations are well within the range expected as a result of the difference in the packing effects of Ph- and Cl in these solids.

Figure 5.2 and Tables 5.1 and 5.2 show that two quadrupole resonance signals,  $\nu_1$  and  $\nu_2$ , with relative intensities 1:1 were detected for  $\text{PhPCl}_2$ , over the temperature range  $77 \leq T \leq 183\text{K}$ . Typical spectra of these signals are shown in figures 5.6 and 5.7 respectively, at 138K. The quadrupole resonance spectrum together with Tables 5.1 and 5.2 show that there are two structurally different chlorine atoms in this solid. Chlorine-35 quadrupole resonance data for  $\text{PhPCl}_2$  have already been described, at 77K, by Lucken and Whitehead<sup>(4)</sup> and by Zakirov et al.<sup>(6)</sup> A single line is described in each case. Lucken and Whitehead<sup>(4)</sup> observed a signal at 26.557 M.Hz. while the frequency obtained by Zakirov et al.<sup>(6)</sup> is 26.390 M.Hz. A comparison between these frequencies and that given in Table 5.2 shows that the former frequency corresponds, exactly, to  $\nu_2$  and the latter is very nearly  $\nu_1$ , in our case.

It is shown in figure 5.2 that  $\text{PhPCl}_2$  undergoes a single phase transition at about 123K.

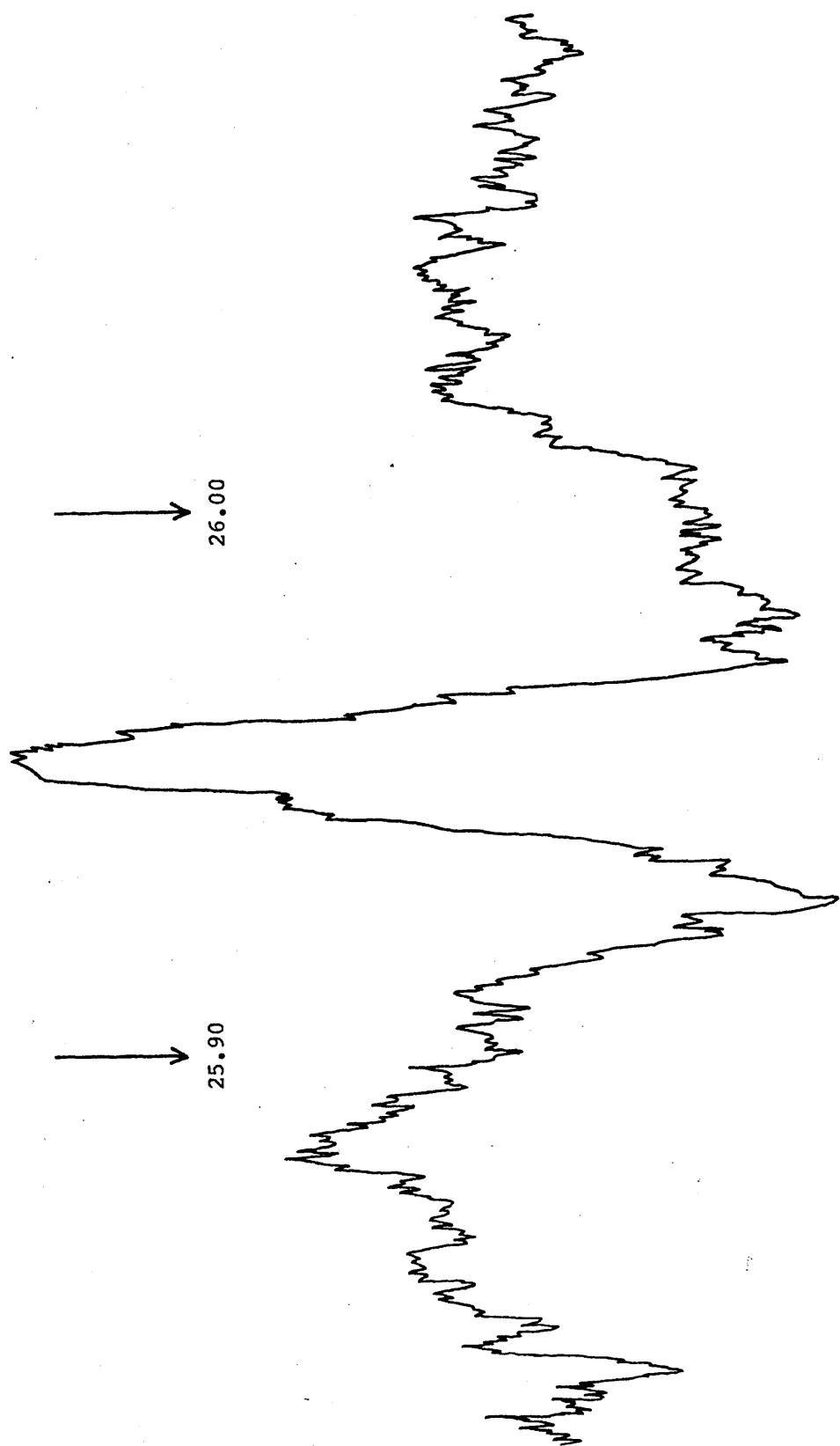


Figure 5.6 Chlorine-35 N.Q.R. spectrum,  $\nu_1$ , for PhPCl<sub>2</sub> at 138K.

Frequencies are given in M.Hz.

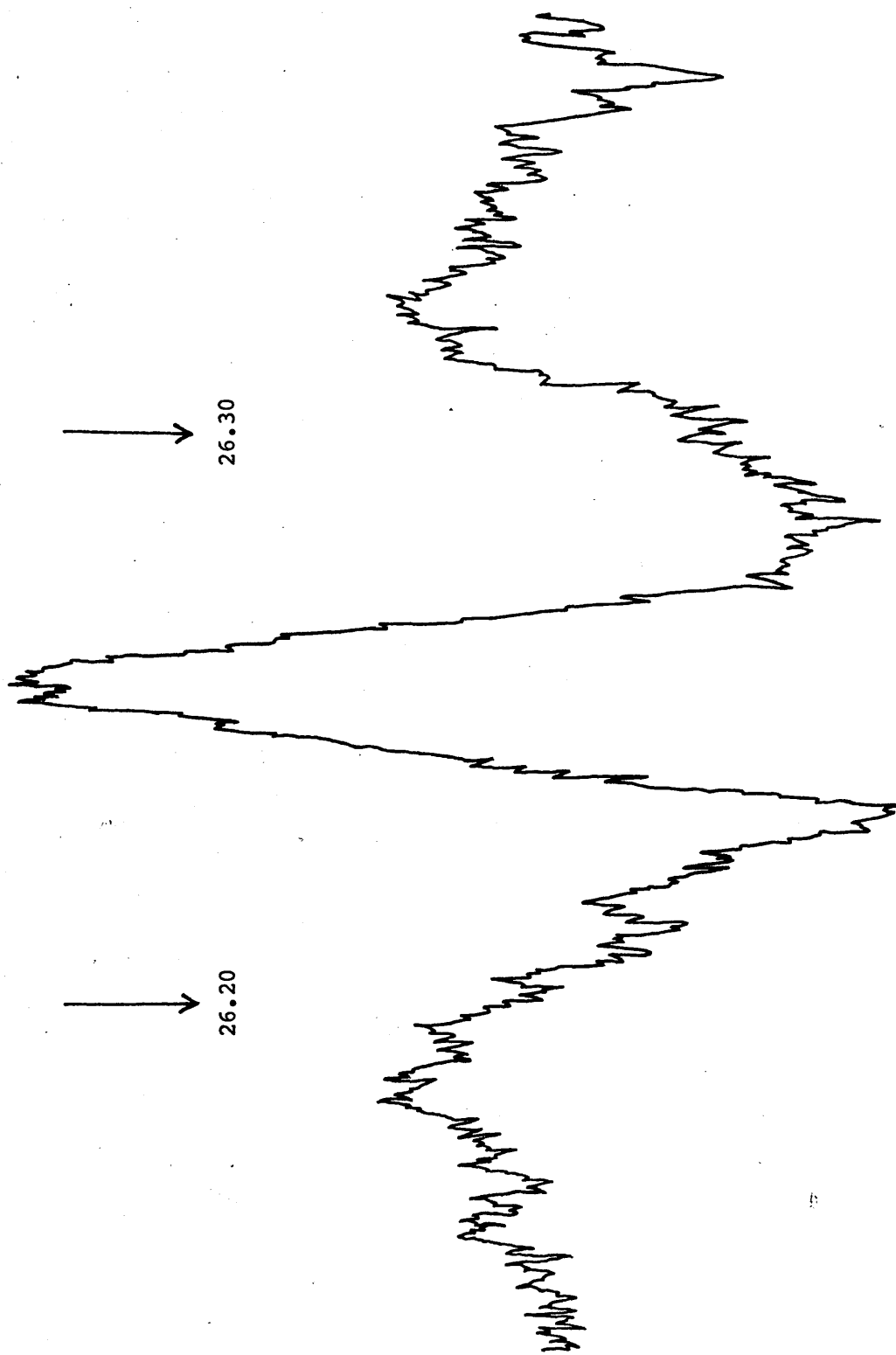


Figure 5.7 Chlorine-35 N.O.R. spectrum,  $\nu_2$ , of  $\text{PhPCl}_2$  at 138K.

Frequencies are given in M.Hz.

Tables 5.1 and 5.3 together with figure 5.3 show that only a single quadrupole resonance line is observed for  $\text{PhPBr}_2$  over the temperature range  $77 \leq T \leq 244\text{K}$ . This shows quite definitely that the  $\text{PhPBr}_2$  molecule is bisected by a plane of symmetry that is retained over the temperature range examined. A typical bromine-79 quadrupole resonance spectrum in  $\text{PhPBr}_2$ , at 229K, is shown in figure 5.8.

Figure 5.3 shows that  $\text{PhPBr}_2$  experiences a single phase transition, at about 125K, similar to that encountered in the case of  $\text{PhPCl}_2$ .

Table 5.3 shows that the bromine atom is effectively more electro-negative than the phenyl, Ph-, group. Replacing a bromine atom in  $\text{PBr}_3$  by a phenyl group pushes the electron density towards the remaining bromine atoms thereby increasing the polarities of the P-Br bonds. These bonds become longer, the electron densities on the bromine atoms increase and the bromine quadrupole resonance frequency then decreases.

Tables 5.1-5.3 and figures 5.1-5.3 show that the bromine-79 nucleus is a more sensitive monitor of both physical and chemical changes than the chlorine-35 nucleus in these phosphorus(III) derivatives. Table 5.1 shows clearly that the bromine-79 nucleus is more sensitive to changes in temperature than the chlorine-35 nucleus attached to the phosphorus-(III) atom.

$\text{Cl}_3\text{PNPOCl}_2$  was the last acyclic compound studied in this work. Figure 5.4 and Table 5.1 show that only two signals, relative intensities 1:1, were detectable in the temperature range  $200 \leq T \leq 307\text{K}$ . However these lines split and many more quadrupole signals are observed in the range  $77 \leq T \leq 200\text{K}$ . Furthermore, the additional line splitting on lowering the temperature below 200K, shown on figure 5.4, clearly shows

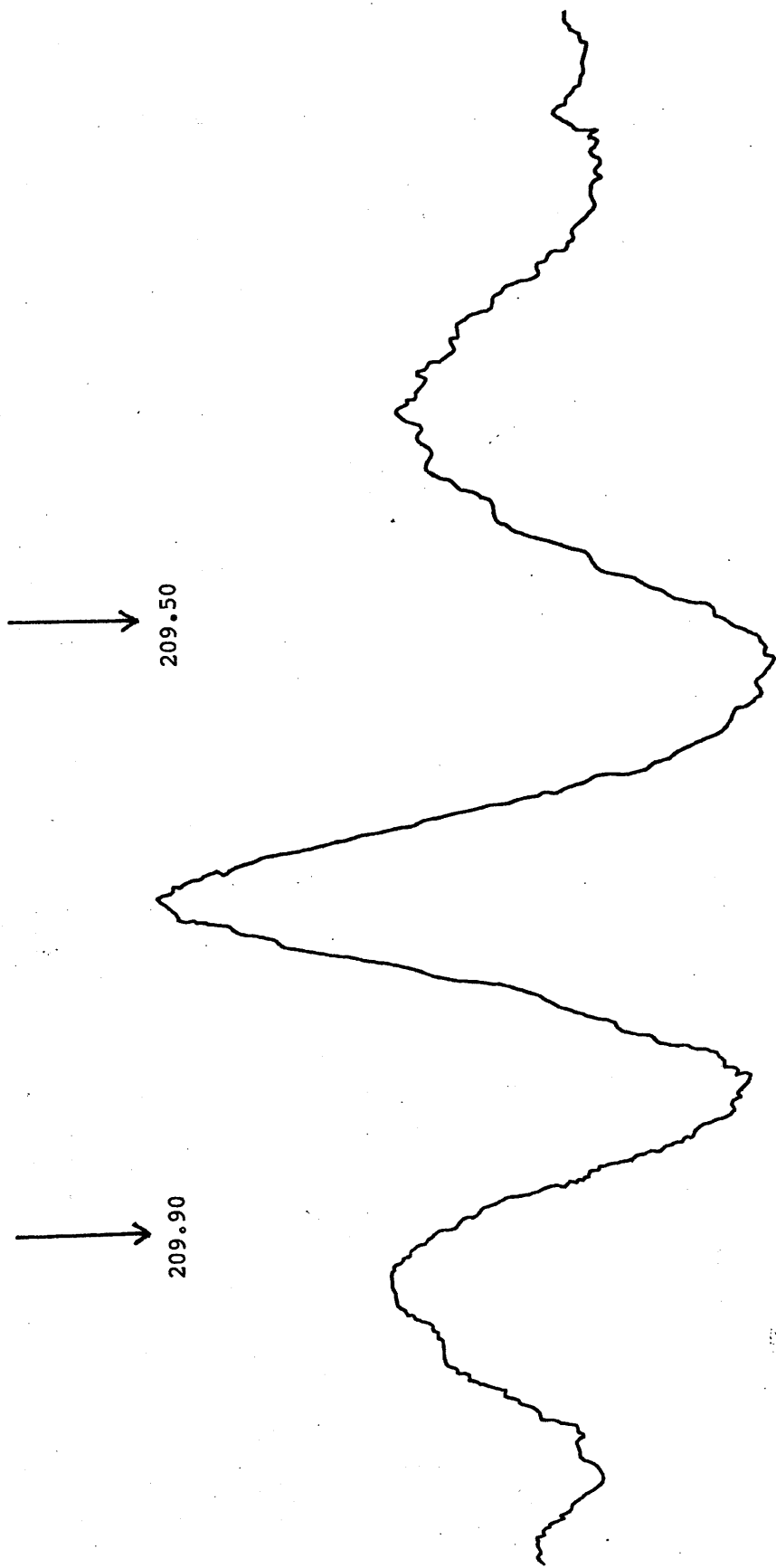
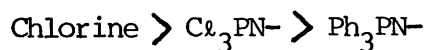


Figure 5.8 Bromine-79 N.Q.R. spectrum of PhPBr<sub>2</sub> at 229K.  
Frequencies are given in M.Hz.

that at least two phase transitions take place in this compound when the temperature is reduced. Fifteen quadrupole signals are detected at 77K. They separate into two groups, in two distinct frequency ranges indicating the presence of two chemically inequivalent groups of chlorine atoms in this molecule. At 77K, the average frequency of the first five signals is 26.837 M.Hz. and that for the other ten peaks is 30.079 M.Hz. as shown in Table 5.2. The former frequency has been assigned to the chlorine atoms in the  $-\text{POCl}_2$  group since this frequency is typical of those found for chlorine atoms in the same type of environment.<sup>(4,20)</sup> The higher resonance frequencies, whose average is 30.079 M.Hz., are therefore associated with chlorine atoms in  $\text{Cl}_3\text{P}=\text{N}-$  group.

These results, at 77K, and the assignments discussed above confirm the chlorine-35 quadrupole resonance data obtained by Kaplansky et al<sup>(5)</sup> at the same temperature. The qualitative description of the chemical structure of  $\text{Cl}_3\text{PNPOCl}_2$  presented by these authors<sup>(5)</sup> implies that the two chlorine atoms in  $-\text{POCl}_2$  group are equivalent to each other as are the three chlorine atoms in  $\text{Cl}_3\text{PN}-$  group. This description is consistent with quadrupole resonance data obtained in the present work.

Table 5.2 shows that the effective electronegativities of the functional groups, in these phosphorus(V) derivatives, decrease in the following order



decreasing electronegativity →

Replacing a chlorine atom in  $\text{POCl}_3$  by  $\text{Cl}_3\text{PN-}$  or  $\text{Ph}_3\text{PN-}$  therefore pushes the electron density on to the other two chlorines, in the  $-\text{POCl}_2$  group, the P-Cl bonds become more polar and the bond lengths increase, the chlorine atoms therefore become more ionic and their quadrupole frequencies decrease.

Table 5.2 shows that chlorine-35 quadrupole resonance frequencies are not very characteristic for either phosphorus(III) or phosphorus(V) derivatives. Phosphorus(III) derivatives cannot safely be distinguished from phosphorus(V) on the basis of chlorine-35 quadrupole frequencies.

However, Table 5.1 shows that the temperature coefficients  $\left(\frac{\partial \nu}{\partial T}\right)_{\substack{P=1\text{Kg.cm}^{-2} \\ T=295\text{K}}}$

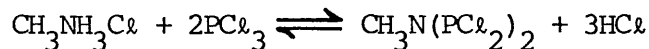
of quadrupole resonance frequencies in  $\text{Cl}_3\text{PNPOCl}_2$  are considerably greater than the corresponding coefficients in the phosphorus(III) chloro derivatives given in this Table. Thus this fact might be used to discriminate between phosphorus(III) and phosphorus(V) derivatives, provided chlorine-35 quadrupole spectra are available in each case over a wide range of temperature.

APPENDIX - 5A

PREPARATION OF THE ACYCLIC COMPOUNDS (12-14)

5A.1 Preparation of  $\text{CH}_3\text{N}(\text{PCl}_2)_2$

Methylaminobisdichlorophosphine can readily be synthesised from the reaction of excess  $\text{PCl}_3$  with methylamine hydrochloride in sym-tetrachloroethane. The reaction takes place according to the following equation (12)



when the reaction mixture is heated under reflux for 7-10 days.

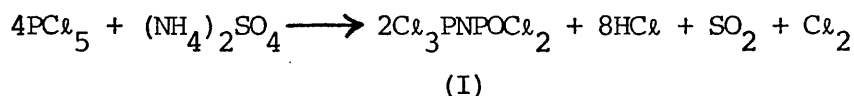
33.75g, (0.5 mole) of  $\text{CH}_3\text{NH}_3\text{Cl}$  and 275g, (2.0 mole) of  $\text{PCl}_3$  was mixed with about 200 cm<sup>3</sup> of sym-tetrachloroethane. The mixture was then refluxed for about 9 days, until only a small amount of the solid methylamine hydrochloride remained. The reaction mixture was then cooled and filtered and the excess sym-tetrachloroethane and  $\text{PCl}_3$  removed under vacuum. The pure colourless liquid methylaminobisdichlorophosphine,  $\text{CH}_3\text{N}(\text{PCl}_2)_2$ , was obtained by fractional distillation of the product mixture under vacuum. Pure  $\text{CH}_3\text{N}(\text{PCl}_2)_2$  boils at 47-52°C (0.5 mm Hg). The yield obtained was about 40g.

### 5A.2 Preparation of PhPBr<sub>2</sub>

Dibromophenylphosphine was obtained<sup>(13)</sup> by heating a mixture of 50g of PhPCl<sub>2</sub> with about 100g of PBr<sub>3</sub> at 100-200°C, using a normal distillation apparatus in which the flask is fitted with an air condenser. The side products, PCl<sub>3</sub> and PBr<sub>3-n</sub> Cl<sub>n</sub> (n=1 or 2), are continuously distilled out of the reaction mixture until the pure product of liquid PhPBr<sub>2</sub>, which has a boiling point of 124-126°C at 11 mm Hg, is obtained.

### 5A.3 Preparation of $\text{Cl}_3\text{P=N-POCl}_2$

The title compound, trichlorophosphazophosphoryl chloride, (I), can be obtained in almost quantitative yield from the reaction of  $\text{PCl}_5$  with  $(\text{NH}_4)_2\text{SO}_4$  in sym-tetrachloroethane.<sup>(14)</sup> Reaction takes place, when this mixture is heated to 146°C for an hour under a reflux condenser. The reaction can be expressed by the following equation



In this work the reaction was carried out using 93.5g (0.45 mole) of  $\text{PCl}_5$  and 13.2g (0.10 mole) of  $(\text{NH}_4)_2\text{SO}_4$  in 200 cm<sup>3</sup> of refluxing sym-tetrachloroethane for an hour. The best yield, about 50g (~0.2 mole) of (I) is obtained when the reaction mixture is cooled, filtered, and the solvent is removed using a rotary evaporator. The colourless oily product is recrystallized below 0°C. The final product can be purified either by very slow recrystallization from sym-tetrachloroethane at room temperature, more rapidly below 0°C, or by distillation of the colourless oily product under reduced pressure (b.p. 110-115°C at 0.1mm Hg). The pure  $\text{Cl}_3\text{PNPOCl}_2$  forms colourless crystals, melting point = 35°C.

APPENDIX - 5B

THE NITROGEN GAS-FLOW SYSTEM

The nuclear quadrupole resonance spectra, presented in this thesis, were usually studied over the temperature range  $77 \leq T \leq 300\text{K}$  at intervals of 10-15K. These studies were started by recording the nuclear quadrupole resonance spectra of the samples being investigated at room temperature and following the resonance frequencies as a function of temperature down to 77K.

Recording the spectra at room temperature was performed by normal manipulation of the Decca-Radar N.Q.R. spectrometer. The spectra at 77K were recorded by immersing the entire coil assembly of the super-regenerative oscillator, including the sample under investigation, in a Dewar flask filled with liquid nitrogen for 30-40 minutes before recording the spectra. The N.Q.R. spectrometer was modified so that any temperature in the range  $77 \leq T \leq 300\text{K}$  can easily be obtained and held fixed for the fairly long period of time required to record the nuclear quadrupole resonance spectrum. The nitrogen gas-flow system is an easy and reliable device which can be coupled to the spectrometer as a temperature controlling system. Figure 5B.1 shows the coupling of this type of cooling system with the Decca spectrometer used in this work.

The entire tank coil of the super-regenerative oscillator is placed in a special Dewar flask which is fitted with an inlet at its base and closed with an appropriate lid at the top. A steady stream of dry

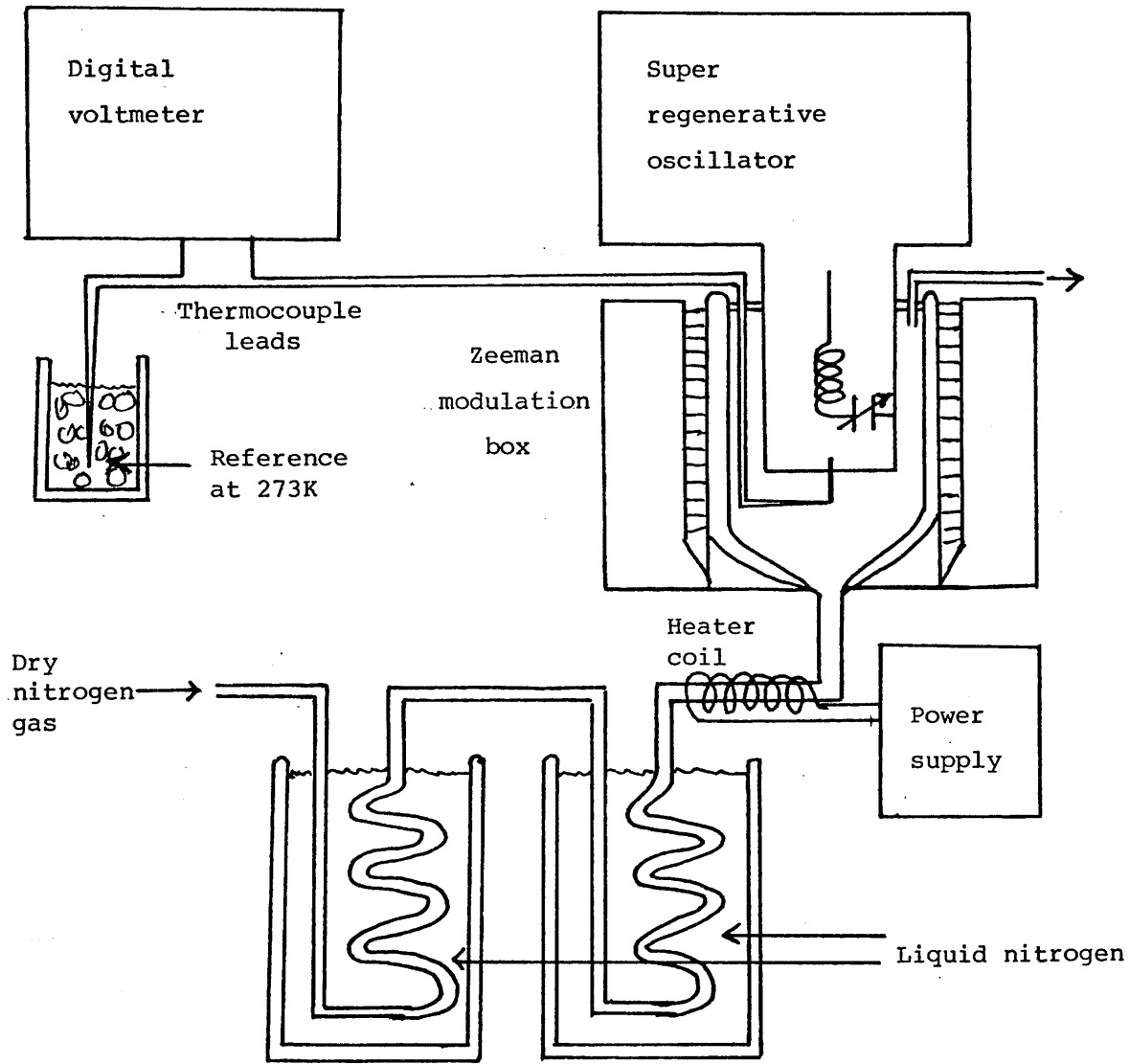


Figure 5B-1 The nitrogen gas-flow system. All other connections are made as for normal spectrometer operation

nitrogen gas is pre-chilled by passing it through two coils of a copper tube each of which is immersed in a Dewar flask of liquid nitrogen and then the desired temperature is obtained by controlling the nitrogen gas flow rates and by making use of a small heating coil. The nitrogen gas at the required temperature is then directly passed through the system until thermal equilibrium is reached.

The temperature measurements were made by means of a copper-constantan thermocouple which is accurate to  $\pm 1K$ . The reference junction of the thermocouple was maintained at 273K by dipping it in an ice-water bath. Each temperature was kept fixed for 30-40 minutes before recording the spectra.

CHAPTER 6

HALOGEN QUADRUPOLE RESONANCE STUDIES OF SOME

CYCLOPHOSPH(III)AZANE DERIVATIVES

6.1 INTRODUCTION

Chlorine-35 quadrupole resonance studies have been carried out for a number of phosphorus(V) derivatives in which chlorine atoms are bonded to phosphorus in a trigonal bipyramidal environment. (1-7) These include chloro derivatives of the cyclotriphosphazatrienes, (1-5) and the cyclodiphosphazanes (5-7) of the form  $(Cl_3PNR)_2$ , where  $R = CH_3-$ ,  $C_2H_5-$ , or  $Ph-$ .

However, very little halogen quadrupole resonance data is available in the literature for cyclophosph(III)azane derivatives. Chlorine-35 quadrupole resonance frequencies have been reported (8) for the trivalent phosphorus compound  $(ClPNBu^t)_2$  at 295K but no studies have so far been carried out on the corresponding bromocyclophosph(III)-azane.

In this chapter, chlorine-35 quadrupole resonance spectra are investigated for 2,4,6-trichloro-1,3,5-triethylcyclotriphosph(III)azane,  $(Cl_3PNET)_3$ , 2,4-dichloro-1,3-diphenyldiazadiphosphetidine,  $(Cl_2PNPh)_2$ , and 2,4-dichloro-1,3-di(tert-butyl)diazadiphosphetidine,  $(Cl_2PNBu^t)_2$ , over the temperature ranges  $103 \leq T \leq 270K$ ,  $217 \leq T \leq 301K$ , and  $77 \leq T \leq 300K$  respectively; signals were only detectable within these ranges of temperature.

Furthermore, bromine-79 quadrupole resonance spectra are examined for 2,4-dibromo-1,3-di(tert-butyl)diazadiphosphetidine,  $(\text{BrPNBu}^t)_2$ , whilst this compound is subjected to, first, pressure variations within the range  $1 \leq P \leq 352 \text{ Kg.cm}^{-2}$  and second, to temperature changes, within the range  $77 \leq T \leq 300\text{K}$ , at  $P = 1 \text{ Kg.cm}^{-2}$ .

This study is also extended to include the effects of weak magnetic fields, within the range  $0 \leq H_0 \leq 40 \text{ Gauss}$ , on the chlorine-35 and the bromine-79 quadrupole resonance spectra of  $(\text{ClPNBu}^t)_2$  and  $(\text{BrPNBu}^t)_2$  respectively. The N.Q.R. data enable the asymmetry parameters and hence the  $\pi$  characters in the P-Cl and P-Br bonds in these compounds to be approximately estimated.

Detailed analysis and discussion of these data are made in the following sections.

6.2 TEMPERATURE DEPENDENCE OF CHLORINE-35 N.Q.R. FREQUENCIES IN

(ClPNET)<sub>3</sub>, (ClPNPh)<sub>2</sub> AND (ClPNBu<sup>t</sup>)<sub>2</sub>

The chlorocyclotriposphazane (ClPNET)<sub>3</sub> was prepared<sup>(9)</sup> by allowing PCl<sub>3</sub> and EtNH<sub>3</sub>Cl to react in sym-tetrachloroethane. (ClPNPh)<sub>2</sub> and (ClPNBu<sup>t</sup>)<sub>2</sub> were synthesised by literature methods.<sup>(10,11)</sup> The detailed procedures for preparing these derivatives are described in Appendix 6A. The identities and purities of the compounds were established by means of melting points, <sup>1</sup>H and <sup>31</sup>P nuclear magnetic resonance spectroscopy. The halogen quadrupole resonance spectra were all recorded using the Decca nuclear quadrupole resonance spectrometer, and the temperature variations were made by means of the nitrogen gas-flow system, described earlier.

The observed variations of the chlorine-35 quadrupole resonance frequencies in (ClPNET)<sub>3</sub>, (ClPNPh)<sub>2</sub> and (ClPNBu<sup>t</sup>)<sub>2</sub> with temperature, under constant atmospheric pressure, are shown in figures 6.1, 6.2 and 6.3 respectively, and the highest quadrupole frequencies observed for these chlorocyclophosph(III)azane derivatives are given in Table 6.1

Table 6.2 lists the coefficients a, b' and c' obtained from least squares fits of the halogen quadrupole frequencies to polynomials of the form of equation 5.1. The temperature coefficients,

$\left(\frac{\partial \nu}{\partial T}\right)_{P=1\text{Kg.cm}^{-2}; T=295\text{K}}$ , of these resonance frequencies are also

included in Table 6.2

Figure 6.1 and Tables 6.1 and 6.2 indicate the presence of three structurally different chlorine atoms in the solid (ClPNET)<sub>3</sub>. The

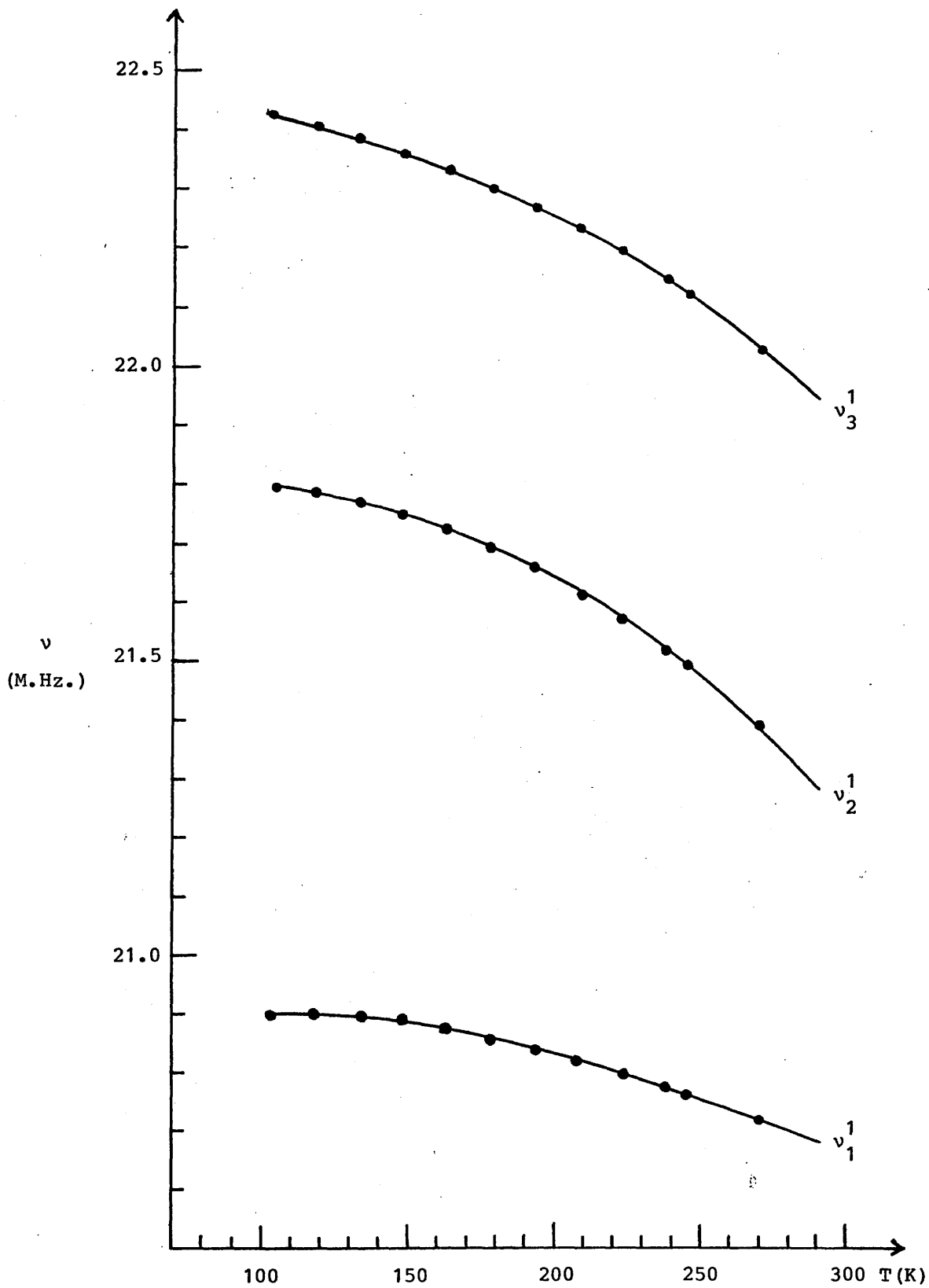


Figure 6.1 Chlorine-35 N.Q.R. frequencies,  $\nu$ (M.Hz.), for  $(ClPNET)_3$  vs. temperature (K).

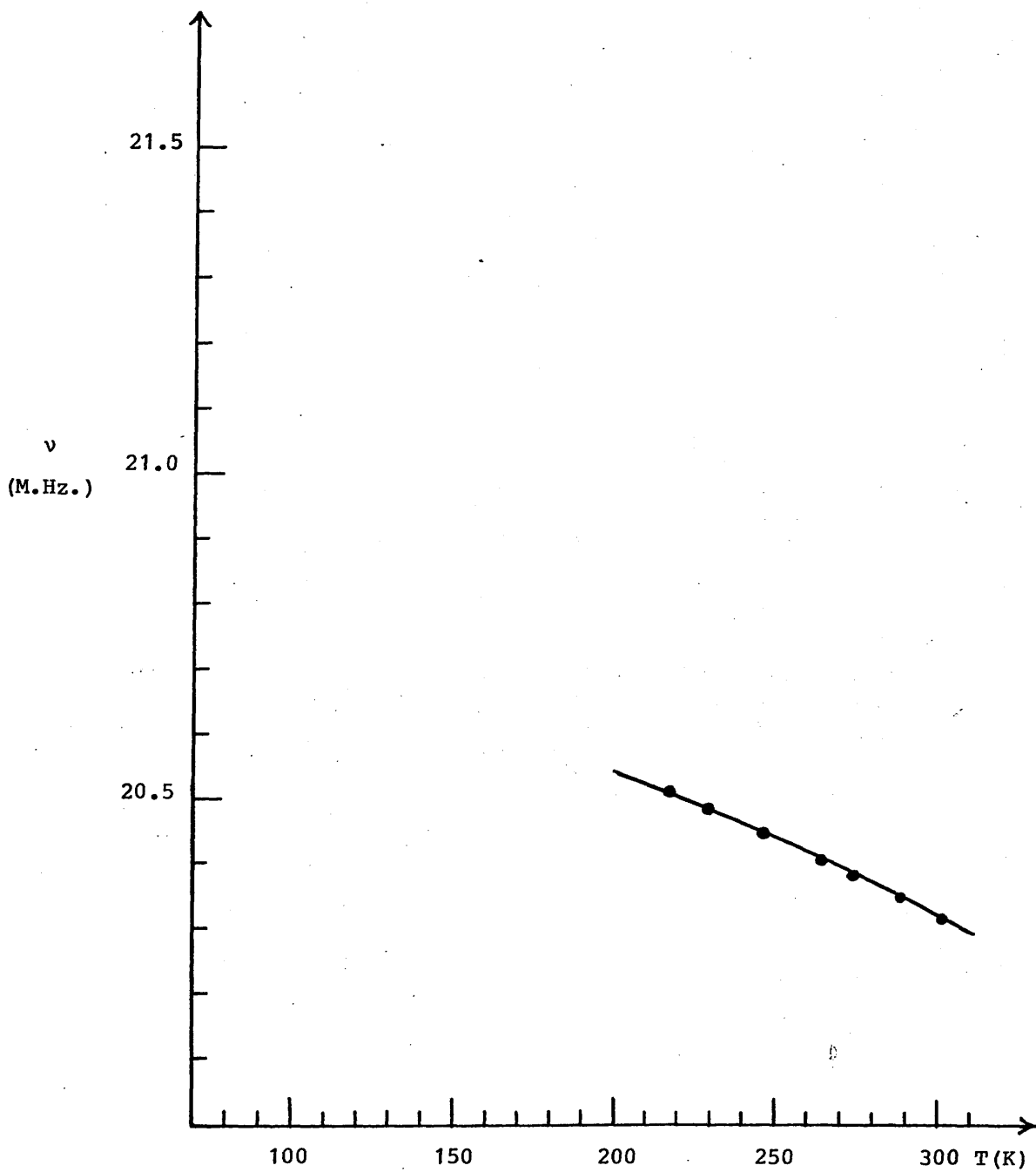


Figure 6.2 Chlorine-35 N.Q.R. frequencies,  $\nu$ (M.Hz.), for  $(ClPNPh)_2$  vs. temperature (K).

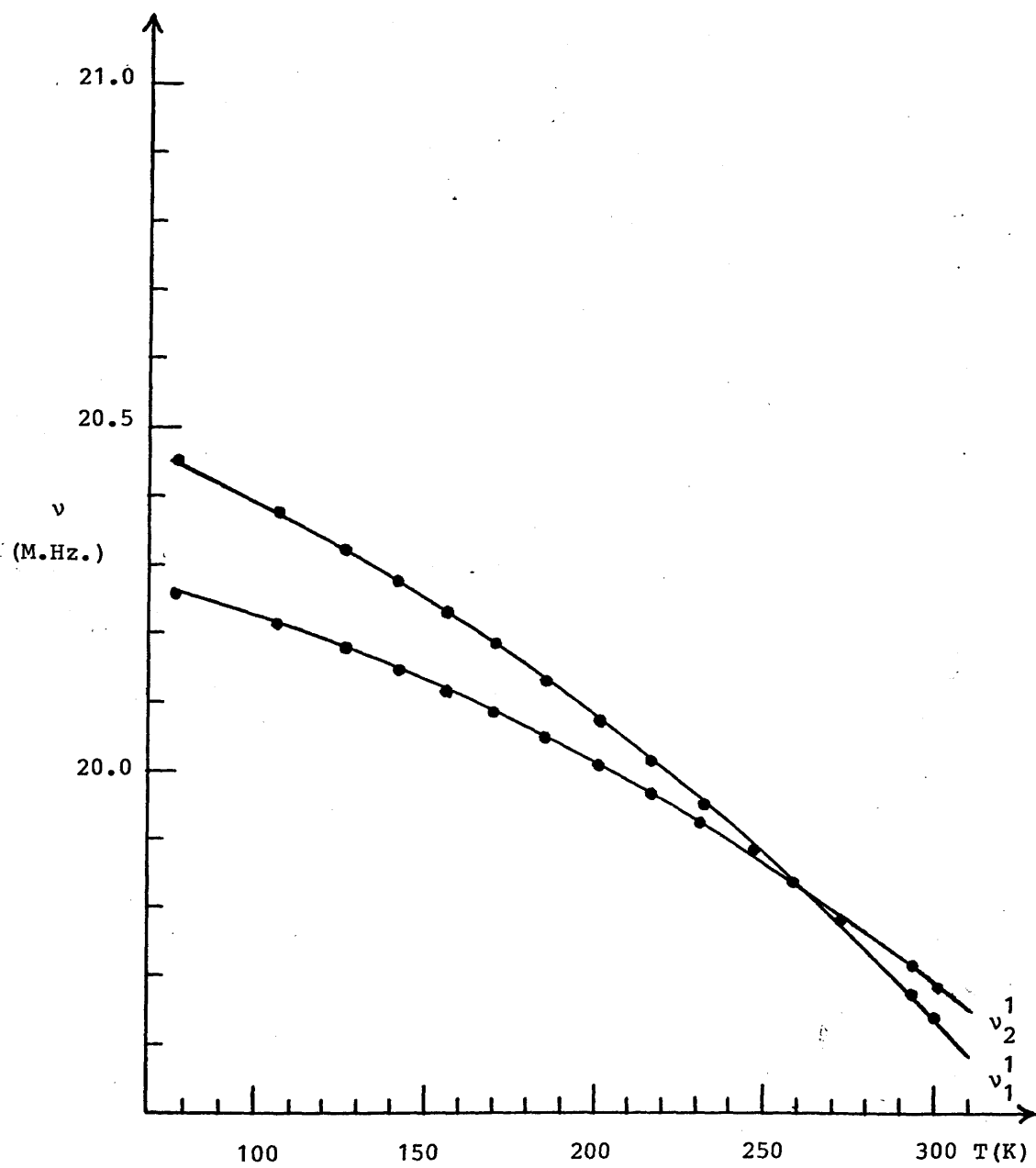


Figure 6.3 Chlorine-35 N.Q.R. frequencies,  $\nu$ (M.Hz.), for  $(C_2PNBu^t)_2$  vs. temperature (K).

Table 6.1

Chlorine-35 nuclear quadrupole resonance frequencies in  
chlorocyclophosph(III)azane derivatives

Compound	m.pt (°C)	Resonance <sup>I</sup>	Frequencies (M.Hz.)	Temperature (K)
(ClPNEt) <sub>3</sub>	32	v <sub>1</sub> <sup>1</sup>	20.900	103
		v <sub>2</sub> <sup>1</sup>	21.793	
		v <sub>3</sub> <sup>1</sup>	22.425	
(ClPNPh) <sub>2</sub>	153-155	v	20.525	217
(ClPNBu <sup>t</sup> ) <sub>2</sub>	42-44	v <sub>1</sub> <sup>1</sup>	20.260	77
		v <sub>2</sub> <sup>1</sup>	20.447	

<sup>I</sup> Superscripts to resonances represent relative intensities.

Table 6.2

Coefficients obtained by fitting the best curves of the form

$$\nu = a + b'T + \frac{c'}{T}$$

to the experimental variation of frequencies with temperature

Compound	Resonance <sup>I</sup>	a	b'	c'	$\left(\frac{\partial \nu}{\partial T}\right)_{P,T}$ P=1Kg.cm <sup>-2</sup> T=295K
(C&PNEt) <sub>3</sub>	$\nu_1^1$	21.124x10 <sup>6</sup>	-1532	+ 2.614x10 <sup>6</sup>	-1562
	$\nu_2^1$	24.091x10 <sup>6</sup>	-7270	-197.419x10 <sup>6</sup>	-5002
	$\nu_3^1$	24.441x10 <sup>6</sup>	-6496	-176.228x10 <sup>6</sup>	-4471
(C&PNPh) <sub>2</sub>	$\nu$	20.370x10 <sup>6</sup>	-1076	+ 83.582x10 <sup>6</sup>	-2037
(C&PNBu <sup>t</sup> ) <sub>2</sub>	$\nu_1^1$	22.215x10 <sup>6</sup>	-6871	-155.390x10 <sup>6</sup>	-5085
	$\nu_2^1$	21.904x10 <sup>6</sup>	-5681	-152.710x10 <sup>6</sup>	-3926

(a Values are in Hz., b' in Hz.K<sup>-1</sup>, c' in Hz.K, and  $\left(\frac{\partial \nu}{\partial T}\right)_{P,T}$  in Hz.K<sup>-1</sup>)

(<sup>I</sup> Superscripts to resonances indicate relative intensities)

(These values are valid for temperatures greater than 200K)

markedly different  $\left(\frac{\partial v}{\partial T}\right)_P$  values given in Table 6.2 indicate that the (N-P)<sub>3</sub> ring cannot be planar; it must be slightly puckered. Two conformations can account for these data depending on whether the (ClPNET)<sub>3</sub> molecule adopts a cis- or a trans-configuration with respect to the chlorine atoms. In the former case the molecule must have a slight twist-boat conformation exaggerated in figure 6.4 in which N<sub>1</sub>, N<sub>3</sub> and P<sub>6</sub> are very nearly coplanar, P<sub>4</sub> is displaced slightly below the plane, P<sub>2</sub> and N<sub>5</sub> are displaced further above the plane.

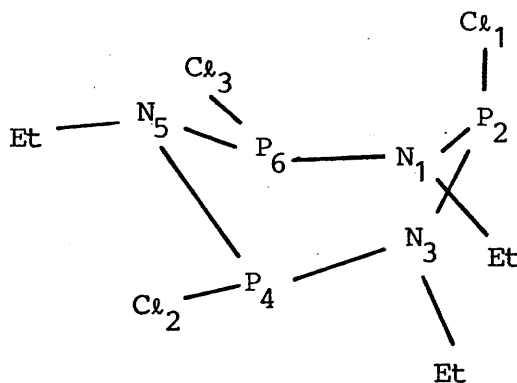


Figure 6.4 Projection of the structure of cis-(ClPNET)<sub>3</sub>

A distorted slight-chair conformation can also account for the data given in Table 6.2 if the trans-configuration is assumed for the (ClPNET)<sub>3</sub> molecule. In this case, the  $\left(\frac{\partial v}{\partial T}\right)_P$  values indicate that the atoms N<sub>1</sub>, N<sub>3</sub> and P<sub>6</sub> lie essentially in one plane, P<sub>4</sub> lies slightly above the plane, P<sub>2</sub> is displaced further above and N<sub>5</sub> moves down below this plane as shown in figure 6.5.

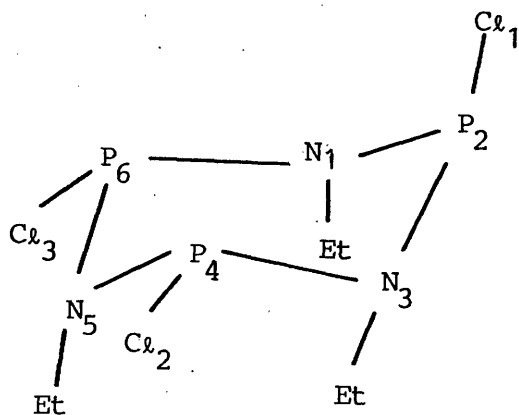


Figure 6.5 Projection of the structure of  $\text{trans}-(\text{ClPNEt})_3$

It should be noted that the quadrupole resonance signals obtained for  $(\text{ClPNEt})_3$  are assigned to the correspondingly numbered atoms as in figures 6.4 and 6.5. Furthermore, it is shown in these figures that the molecule has an axial and two pseudo-equatorial P-Cl bonds. The axial chlorine atoms are known<sup>(5)</sup> to have slightly lower quadrupole resonance frequencies than the equatorial and so  $\nu_1$  is assigned to the axial chlorine atom,  $\text{Cl}_1$ , in  $(\text{ClPNEt})_3$ .

The plots in figure 6.1 show that no phase transitions take place in  $(\text{ClPNEt})_3$  within the temperature range  $103 \leq T \leq 270\text{K}$ , however the spectrum of this solid fades out at 103K.

Two chlorocyclodiphosph(III)azane derivatives were involved in this work. Figure 6.2 and Tables 6.1 and 6.2 show that only a single

quadrupole resonance line was detected for  $(C\&PNPh)_2$  over the temperature range  $217 \leq T \leq 301K$ . This indicates that this molecule possesses a centre of symmetry or else it is bisected by a mirror plane which contains both nitrogen atoms and which is perpendicular to the  $(P-N)_2$  ring. The latter case can be true only if the molecule adopts a cis-configuration with respect to the halogen atoms.

It should be noted that the cis-configuration for  $(C\&PNPh)_2$  might have some priority since it is consistent with the phosphorus-31 N.M.R. analysis<sup>(12)</sup> carried out on this compound.

Figure 6.2 shows that the chlorine-35 quadrupole resonance spectrum for  $(C\&PNPh)_2$  disappears in the temperature range  $77 \leq T \leq 217K$ .

As shown in Tables 6.1 and 6.2 and in figure 6.3 two quadrupole resonance signals with relative intensities 1:1 are observed for the cyclodiphosph(III)azane  $(C\&PNBu^t)_2$ . Figure 6.3 shows clearly that these signals are resolved over the entire temperature range investigated except between 247 to 272K where they overlap to give a single line spectrum. These data indicate that the chlorine atoms in  $(C\&PNBu^t)_2$  are crystallographically equivalent only within the temperature range  $247 \leq T \leq 272K$ , where the molecule possesses a centre of symmetry, or it is bisected by a plane of symmetry if the chlorine atoms in the  $(C\&PNBu^t)_2$  molecule adopt a cis-configuration with respect to the  $(P-N)_2$  ring. The latter conclusion, based on quadrupole resonance data, are quite consistent with data obtained from X-ray analysis<sup>(13,14)</sup> carried out on  $(C\&PNBu^t)_2$ . The latter studies show that this molecule is bisected by a non-crystallographic plane of symmetry. This is the plane normal to the, slightly puckered,  $(P-N)_2$

ring and containing both nitrogen atoms. Furthermore, it is found that the chlorine atoms in this molecule adopt a cis-configuration with respect to the ring<sup>(13,14)</sup> as shown in figure 6.6.

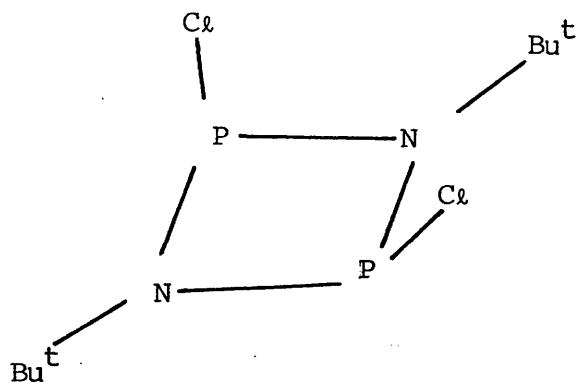
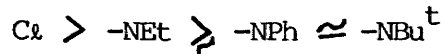


Figure 6.6 Projection of the structure of cis-(ClPNBu<sup>t</sup>)<sub>2</sub>

Figure 6.3 shows no phase transition to occur in (ClPNBu<sup>t</sup>)<sub>2</sub> over the temperature range  $77 \leq T \leq 300\text{K}$ .

Furthermore, a comparison between the chlorine-35 quadrupole resonance frequencies given in Table 6.1 and those obtained<sup>(15)</sup> in the case of PCl<sub>3</sub>, 26.107 and 26.202 M.Hz. at 77K, shows explicitly that the electronegativity of the chlorine atom is considerably greater than the electronegativities of the -NEt, -NPh, and -NBu<sup>t</sup> groups, even when allowance is made for the different temperatures used in these measurements. The effective relative electronegativities of these functional groups can be ordered as follows



decreasing electronegativity  
→

Replacement of a chlorine atom in  $\text{PCl}_3$  by any of these amino residues, therefore, pushes the electron density on to the other chlorine atoms leading to the substantial lengthening of the remaining P-Cl bonds in the cyclophosph(III)azane molecules. The P-Cl bonds become more polar, the electron densities on the chlorine atoms increase and hence the quadrupole resonance frequencies decrease.

These conclusions are supported by the fact that<sup>(13,14)</sup> the P-Cl bond length,  $2.105(9)\text{\AA}$ , in  $(\text{ClPNBu}^t)_2$  is significantly longer than  $2.039(2)\text{\AA}$  found<sup>(16)</sup> in  $\text{PCl}_3$ .

### 6.3 PRESSURE DEPENDENCE OF BROMINE-79 QUADRUPOLE RESONANCE FREQUENCIES

#### IN $(\text{BrPNBu}^t)_2$

Pressure measurements have been carried out on chlorine-35 quadrupole resonance frequencies in some chlorocyclotriposphazatriene<sup>(3,4)</sup> and chlorocyclodiphosphazane<sup>(17)</sup> derivatives. However, similar measurements have not been reported for corresponding bromine quadrupole resonance frequencies and hence it was of interest to investigate the bromine-79 quadrupole spectra of  $(\text{BrPNBu}^t)_2$  while this compound is subjected to hydrostatic pressure.

$(\text{BrPNBu}^t)_2$  was prepared<sup>(18)</sup> by reacting  $\text{PBr}_3$  with  $\text{NH}_2\text{Bu}^t$  using experimental conditions similar to that<sup>(11)</sup> adopted in preparation of  $(\text{C}\&\text{PNBu}^t)_2$ . The procedure used in preparing this compound is also described in Appendix 6A.

Bromine-79 quadrupole resonance transitions occur at high frequencies, where the oscillating system is extremely sensitive to small changes in its geometry and hence the pressure vessel required to investigate these frequencies at high pressures must be very carefully designed. The experimental aspects of this work and designing the pressure vessel are described, in detail, in Appendix 6B.

In this section, the effects of pressure variations on bromine-79 quadrupole resonance spectra of  $(\text{BrPNBu}^t)_2$  are examined within the range  $1 \leq P \leq 352 \text{ Kg.cm}^{-2}$  at 295K. The pressure dependence of quadrupole resonance frequencies in this compound is shown in figure 6.7. This figure shows explicitly that the quadrupole frequencies are

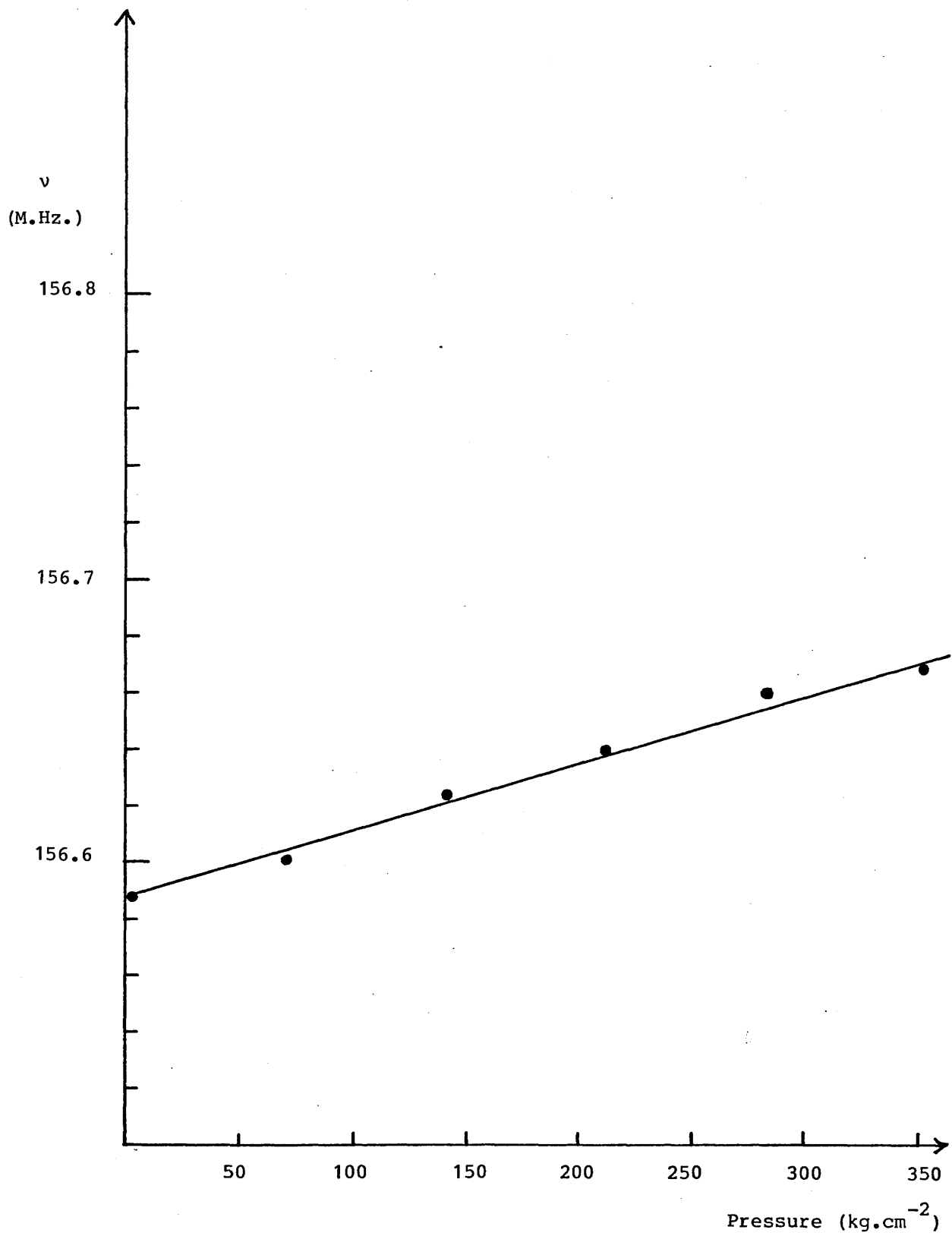


Figure 6.7 Plot of bromine-79 N.Q.R. frequencies vs. pressure for  $(\text{BrPNBu}^t)_2$  at 295K.

linearly related to the applied pressure and so the pressure coefficient,  $\left(\frac{\partial \nu}{\partial P}\right)_{T=295K}$ , is independent of pressure within the range  $1 \leq P \leq 352 \text{ Kg.cm}^{-2}$ .

The gradient of the straight line plot in figure 6.7 gives

$$\left(\frac{\partial \nu}{\partial P}\right)_{T=295K} = 237.1 \text{ Hz.Kg.}^{-1} \text{cm}^2.$$

The observed variations of quadrupole resonance frequencies with the applied pressure can be explained in terms of several effects. (4) The "dynamic" influence, arising from isotropic application of pressure to a molecular solid, makes positive contributions to the pressure coefficients,  $\left(\frac{\partial \nu}{\partial P}\right)_T$ ; this compression reduces the amplitudes of the vibrational motions of the quadrupolar nuclei and hence it increases quadrupole resonance frequencies.

The hydrostatic pressure also causes "static" distortions of the electric field gradients and hence changes the quadrupole resonance frequencies, since shearing movements of the electric dipoles take place in an anisotropic solid; the static effects may therefore make either positive or negative contributions to  $\left(\frac{\partial \nu}{\partial P}\right)_T$  depending on the nature of the solid under investigation. Figure 6.7 shows clearly that positive contributions to  $\left(\frac{\partial \nu}{\partial P}\right)_T$  effectively dominate the behaviour of quadrupole resonance frequencies with pressure in  $(\text{BrPNBu}^t)_2$  within the pressure range examined.

The figure also shows that  $(\text{BrPNBu}^t)_2$  displays only a single line quadrupole spectrum within the pressure range  $1 \leq P \leq 352 \text{ Kg.cm}^{-2}$ . This implies that the  $(\text{BrPNBu}^t)_2$  molecule is either centrosymmetric or it is bisected by a plane of symmetry that is retained over the pressure range examined. Furthermore, figure 6.7 shows that no phase transitions take place in this solid within the pressure range investigated.

A typical spectrum obtained for  $(\text{BrPNBu}^t)_2$  subjected to a pressure of  $141 \text{ Kg.cm}^{-2}$  at 295K is illustrated in figure 6.8

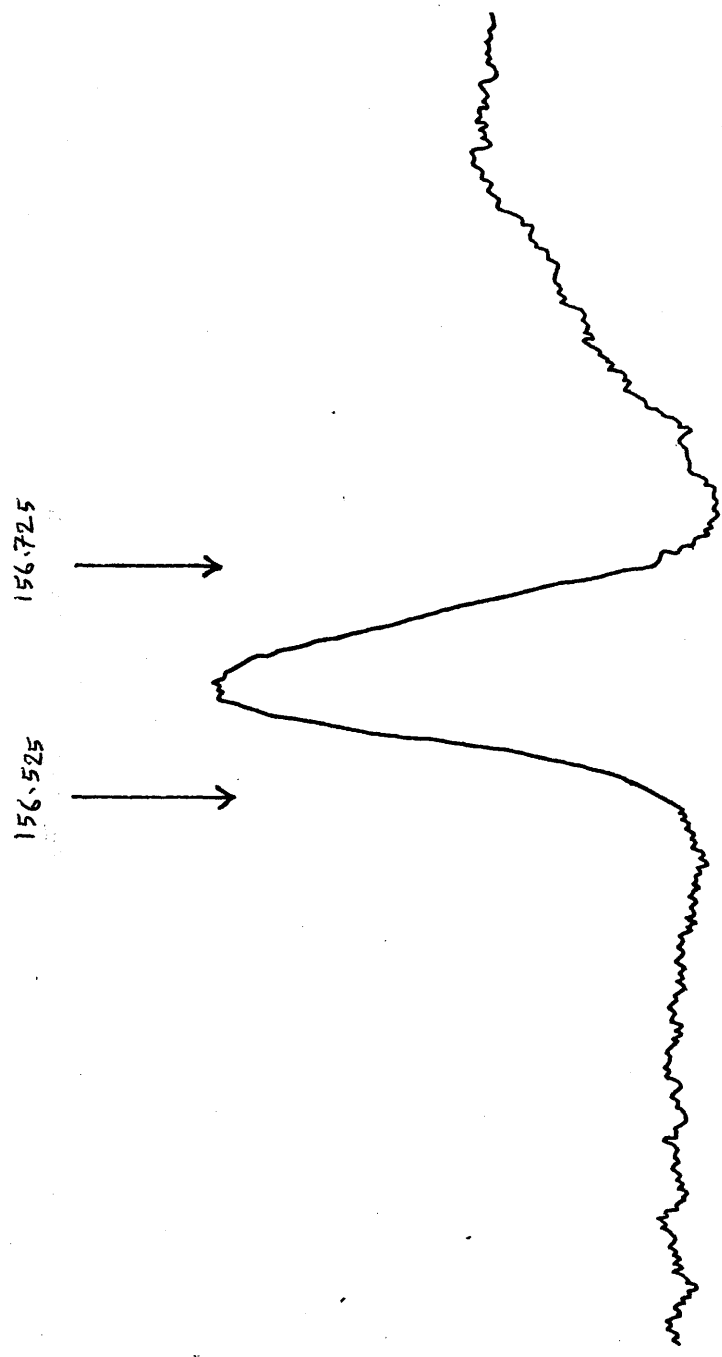


Figure 6.8 Bromine-79 N.Q.R. spectrum for  $(\text{BrPNBu}^t)_2$  at a pressure of  $141 \text{ Kg.cm}^{-2}$ , at 295K.  
Frequencies are given in M.Hz.

6.4 TEMPERATURE DEPENDENCE OF BROMINE-79 QUADRUPOLE RESONANCE

FREQUENCIES IN  $(\text{BrPNBu}^t)_2$

(i) Constant pressure conditions

The effects of temperature variations on bromine-79 quadrupole resonance frequencies in  $(\text{BrPNBu}^t)_2$  have been investigated over the temperature range  $77 \leq T \leq 300\text{K}$  under constant atmospheric pressure. The resonance frequencies are, surprisingly, very nearly linear functions of temperature as shown in figure 6.9.

Table 6.3 gives the bromine-79 quadrupole resonance frequencies, at 300 and 77K, obtained for  $(\text{BrPNBu}^t)_2$ . The table includes also the coefficients,  $a$ ,  $b'$  and  $c'$  obtained from least square fits to polynomials of the form of equation 5.1, valid over the temperature range  $200 \leq T \leq 300\text{K}$ . Values of the differential coefficients,  $(\frac{\partial \nu}{\partial T})_{P,T}$ ,  $(\frac{\partial \nu}{\partial P})_T$  and  $(\frac{\partial \nu}{\partial T})_{V,T}$  are listed in Table 6.4

Figure 6.9 and Table 6.3 again show that the  $(\text{BrPNBu}^t)_2$  molecule possesses a centre of symmetry or it is bisected by a mirror plane. The latter case is possible only if the molecule has a cis-configuration with respect to the bromine atoms.

The last conclusion might be more justified by the fact that the phosphorus-31 N.M.R. analysis indicates<sup>(19)</sup> that the bromine atoms in the  $(\text{BrPNBu}^t)_2$  molecule adopt a cis-configuration with respect to the  $(\text{P-N})_2$  ring.

Figure 6.9 shows almost a straight line graph indicating that no phase transition takes place in this solid within the temperature range investigated.

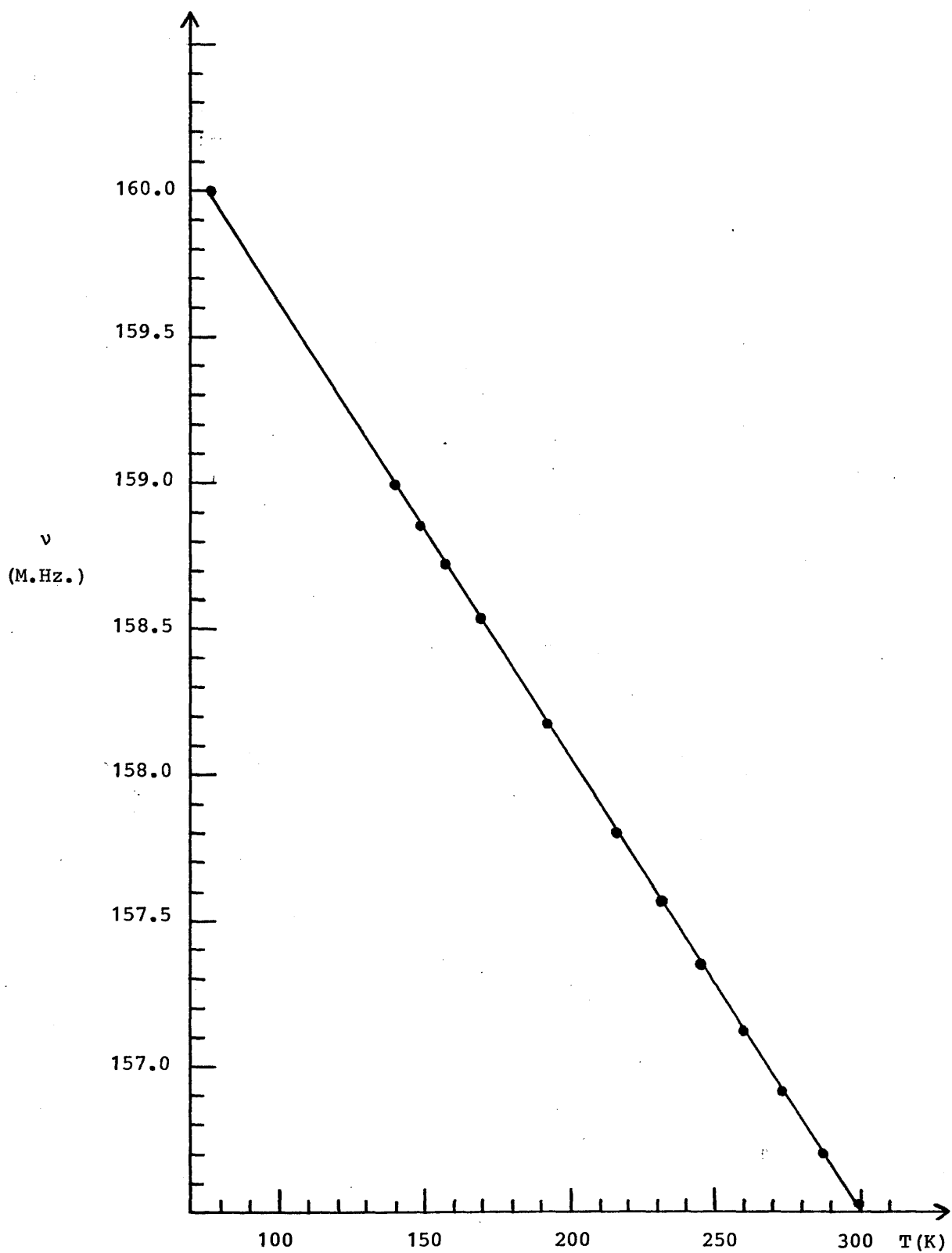


Figure 6.9 Bromine-79 N.Q.R. frequencies,  $\nu$ (M.Hz.), for  $(\text{BrPNBu}^t)_2$  vs. temperature (K).

Table 6.3

Coefficients obtained by fitting the best curves of the form

$$\nu = a + b'T + \frac{c'}{T}$$

to the experimental variation of frequencies in  $(\text{BrPNBu}^t)_2$  with temperature.

---

<u>Frequencies (M.Hz.)</u>		a	b'	c'
at 300K	at 77K			
156.531	160.000	$161.059 \times 10^6$	-14977	$-10.925 \times 10^6$

---

Values of a are in Hz., b' in  $\text{Hz.K}^{-1}$ , and c' in  $\text{Hz.K}$ .

Table 6.4

Differential coefficients obtained for  $(\text{BrPNBu}^t)_2$

$\left(\frac{\partial \nu}{\partial T}\right)_{P=1\text{Kg.cm}^{-2}, T=295\text{K}}$	$\left(\frac{\partial \nu}{\partial P}\right)_{T=295\text{K}}$	$\left(\frac{\partial \nu}{\partial T}\right)_V, T=295\text{K}$
-14851	237.1	-9398

Values of  $\left(\frac{\partial \nu}{\partial T}\right)_{P,T}$  are in  $\text{Hz.K}^{-1}$ ,  $\left(\frac{\partial \nu}{\partial P}\right)_T$  in  $\text{Hz.Kg.}^{-1}\text{cm}^2$ . and

$\left(\frac{\partial \nu}{\partial T}\right)_{V,T}$  in  $\text{Hz.K}^{-1}$ .

The bromine-79 quadrupole resonance frequency obtained for  $(\text{BrPNBu}^t)_2$  at 77K, given in Table 6.3, is considerably less than the corresponding frequency, 219.605 M.Hz., found<sup>(20)</sup> in the case of  $\text{PBr}_3$  at 83K. This implicitly shows that the bromine atom is effectively more electronegative than  $-\text{NBu}^t$  residue. Replacing the former by the latter pushes the electron density on to the remaining bromine atoms in the molecule, the P-Br bonds become more polar, P-Br bond lengths increase, the bromine atoms become more negative and hence their quadrupole resonance frequencies decrease.

It should be noted that the quadrupole spectrum obtained for  $(\text{BrPNBu}^t)_2$  was surprisingly broad, line width, maximum slope, was about 100K.Hz. A typical spectrum observed at 216K is shown in figure 6.10

#### (ii) Constant volume conditions

The origin of the effects of temperature variations on halogen quadrupole resonance spectra are considered and discussed in detail in chapter 2.

Values of  $\left(\frac{\partial \nu}{\partial T}\right)_{P,T}$  and  $\left(\frac{\partial \nu}{\partial P}\right)_T$  obtained in the previous sections and given in Table 6.4 can now be substituted in equation 2.48 in order to obtain the temperature coefficient,  $\left(\frac{\partial \nu}{\partial T}\right)_V$ , under constant volume conditions. The volume coefficients of thermal expansion,  $\alpha$ , and the isothermal volume compressibility coefficients,  $\chi$ , required for this calculation are in general very rare for covalent phosphorus compounds and are not available for any of the bromo derivatives considered in this thesis. Thus it was necessary to use approximate values of  $\alpha$  and  $\chi$  measured for other molecular solids available in the

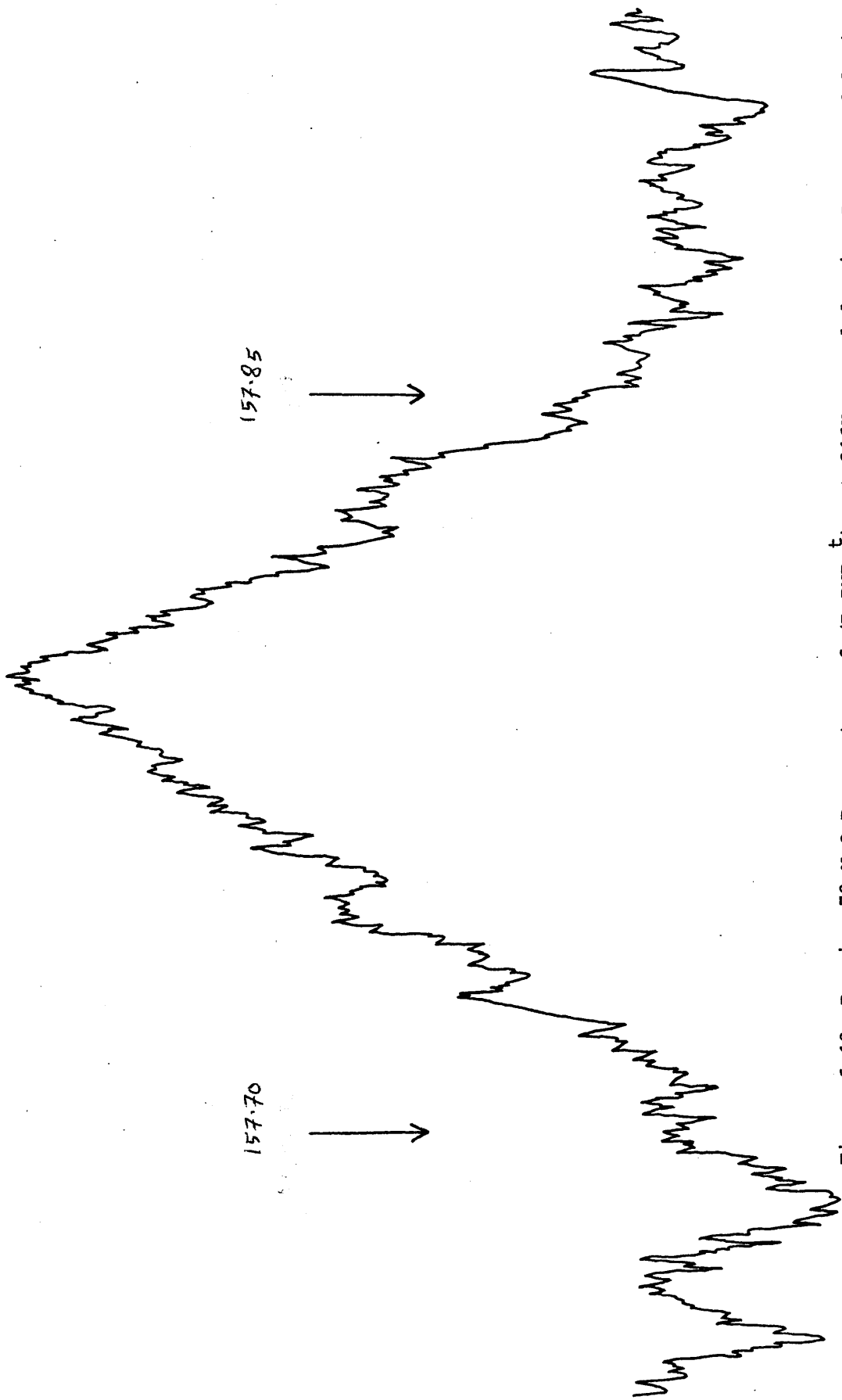


Figure 6.10 Bromine-79 N.Q.R. spectrum of (BrPNBu<sup>t</sup>)<sub>2</sub> at 216K recorded using Zeeman modulation.

Frequencies are given in M.Hz.

literature. We have used therefore typical values of  $\alpha$  and  $\chi$  of the order of  $260 \times 10^{-6} \text{ K}^{-1}$  and  $11 \times 10^{-6} \text{ Kg.}^{-1} \text{ cm}^2$ , respectively, obtained<sup>(4,5)</sup> for molecular species  $\text{PBr}_3$ ,  $\text{POBr}_3$  and  $\text{POCl}_3$ . The ratio  $(\frac{\alpha}{\chi})$  in equation 2.48 has therefore been approximated to  $23 \text{ Kg.cm}^{-2} \text{ K}^{-1}$  for  $(\text{BrPNBu}^t)_2$  and the data obtained from this treatment are given in Table 6.4.

In principle it should now be possible, by means of equation 2.35, to account for the values of  $(\frac{\partial v}{\partial T})_V$  given in the last table using librational data obtained from Raman and infra-red spectra. Unfortunately the librational data does not seem to have been documented and therefore the correlation was not possible in this case.

6.5 THE HALOGEN QUADRUPOLE RESONANCE SPECTRA OF  $(C\&PNBu^t)_2$  AND  $(BrPNBu^t)_2$  IN APPLIED MAGNETIC FIELDS

Zeeman studies, in this work, were based essentially on the technique developed by Morino and Toyama<sup>(21)</sup> to obtain the asymmetry parameters in polycrystalline samples, since it has not been possible to grow sufficiently large single crystals of any of the cyclodiphosph(III)azane derivatives to enable the asymmetry parameters to be measured using the frequency-field<sup>(22)</sup> or the zero-splitting locus<sup>(23)</sup> methods. These methods are described in chapter 3.

Chlorine-35 and bromine-79 quadrupole resonance spectra of  $(C\&PNBu^t)_2$  and  $(BrPNBu^t)_2$ , respectively, were examined in weak magnetic fields, within the range  $0 \leq H_0 \leq 40$  Gauss, applied parallel to the radio-frequency field used to induce the transitions. The desired magnetic field was generated by passing appropriate direct current through a pair of Helmholtz coils.

The spectra of  $(C\&PNBu^t)_2$  were recorded by a straightforward manipulation of the Decca spectrometer using the frequency modulation technique. However, in the case of  $(BrPNBu^t)_2$  the signal was too broad and it was necessary to couple the spectrometer output to a computer of average transients, C.A.T., and hence accumulated signals were recorded. The experimental arrangement for this work is described in more detail in Appendix 6C.

The peaks at  $\pm 2\nu_L$ , predicted by Morino and Toyama,<sup>(21)</sup> were never clearly identified in the spectra because of overlapping with neighbouring sidebands and noise problems; however the characteristic peaks at

$\pm \nu_L$  were quite easily observed. The latter peaks are shown clearly in figure 6.11 which represents a typical spectrum obtained for the chlorine-35 quadrupole signal,  $\nu_2$ , of  $(C\ell PNBu^t)_2$  when  $H_0 = 16.05$  Gauss. The linewidth parameters,  $\delta$ , were measured in each case from the appropriate spectra and then the asymmetry parameters were obtained from the plots of  $\delta(2\nu_L)^{-1}$  against  $H_0^{-1}$ .

Tables 6.5 and 6.6 list the values of  $\delta$  obtained for the  $\nu_1$  and  $\nu_2$  resonances, respectively, in  $(C\ell PNBu^t)_2$  and the corresponding graphs of  $\delta(2\nu_L)^{-1}$  versus  $H_0^{-1}$  are plotted in figures 6.12 and 6.13. The asymmetry parameters,  $\eta$ , obtained from these graphs together with the observed frequencies, at 300K, then enable the quadrupole coupling constants,  $\frac{eqQ}{h}$ , to be derived from equation 1.32. The data obtained for  $(C\ell PNBu^t)_2$  are given in Table 6.7.

Similarly, the  $\delta$  values obtained in the case of  $(BrPNBu^t)_2$  are listed in Table 6.8 and the graph of  $\delta(2\nu_L)^{-1}$  against  $H_0^{-1}$  is shown in figure 6.14. The values of  $\eta$  and  $\frac{eqQ}{h}$  obtained for  $(BrPNBu^t)_2$  are given in Table 6.9.

The N.Q.R. data now enable an approximate Townes and Dailey<sup>(24)</sup> type of analysis to be made for the P-Cl and P-Br bonds in these molecules. The asymmetry parameter,  $\eta$ , is related to the  $\pi$ -character and the quadrupole coupling constant by the following expression<sup>(25)</sup>

$$\eta = \frac{3}{2} \pi \frac{(\frac{eqQ}{h})_{\text{atom}}}{(\frac{eqQ}{h})_{\text{molecule}}} \quad 6.1$$

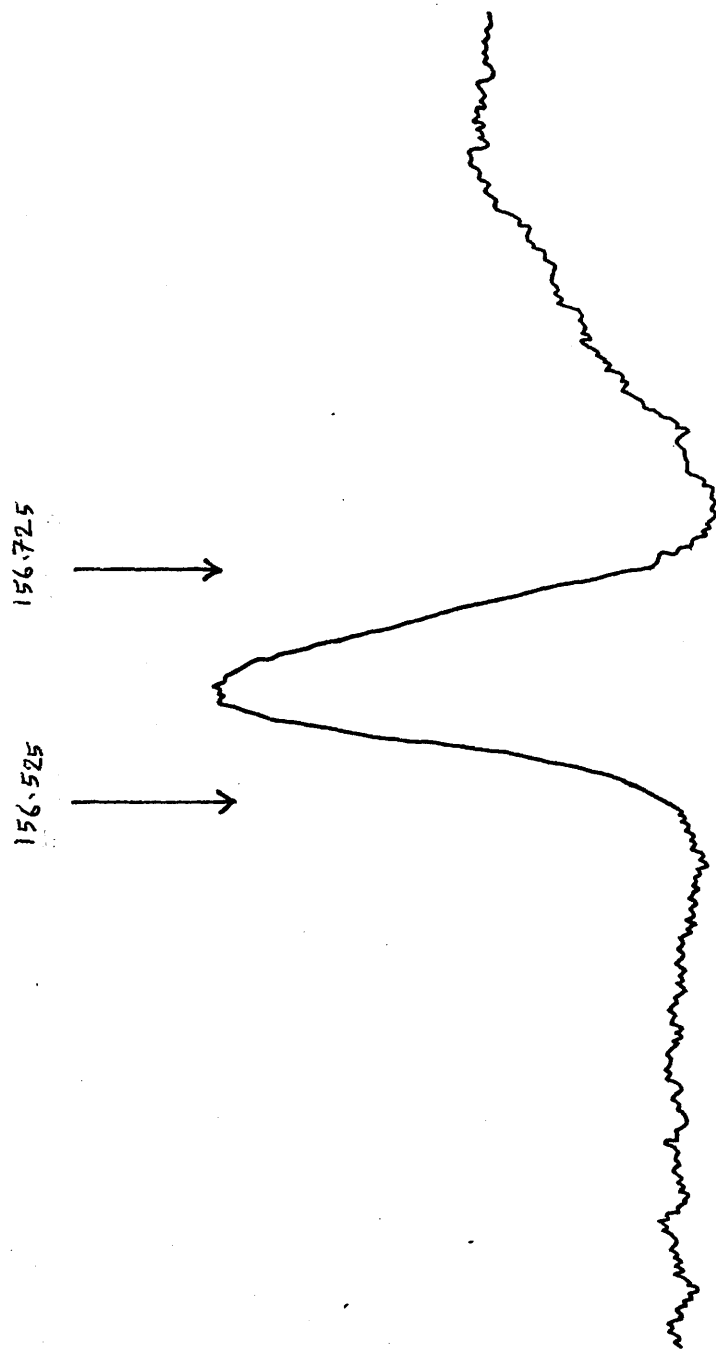


Figure 6.8 Bromine-79 N.Q.R. spectrum for  $(\text{BrPNBu}^t)_2$  at a pressure of  $141 \text{ Kg.cm}^{-2}$ , at 295K.  
Frequencies are given in M.Hz.

Table 6.5

Linewidth parameters,  $\delta$ , and  $\delta(2\nu_L)^{-1}$  measured from the analysis of the  $\nu_1$  quadrupole signal of  $(C\&PNBu^t)_2$  in weak magnetic fields.

Magnetic field (Gauss)	Larmor frequency for chlorine-35 (K.Hz.)	$\delta$ (K.Hz.)	$\frac{\delta}{2\nu_L}$
16.05	6.696	1.352	0.101
20.00	8.344	1.500	0.090
23.85	9.950	1.418	0.071
27.75	11.577	1.718	0.074
35.50	14.811	1.833	0.062
39.40	16.438	1.952	0.059

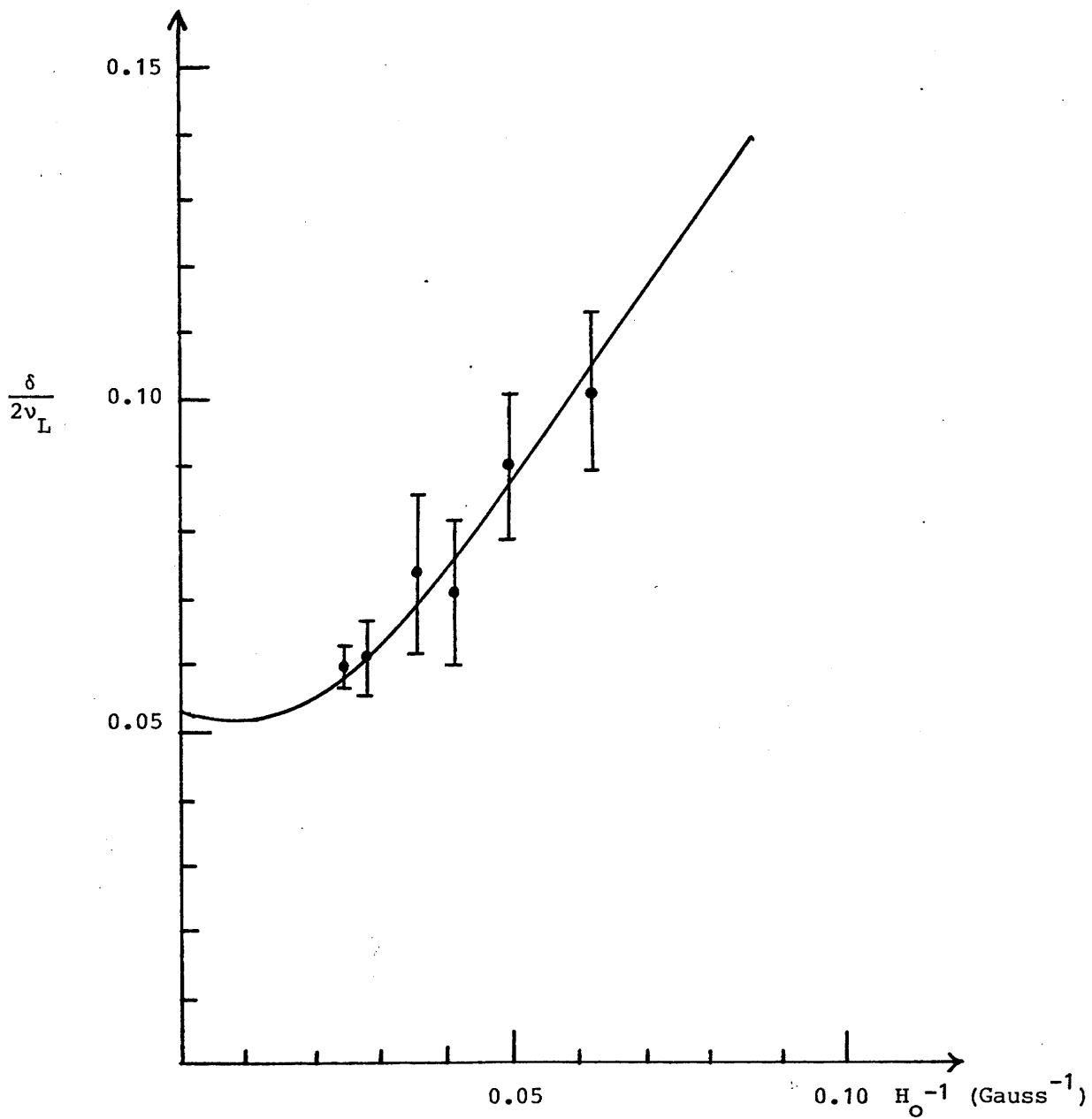


Figure 6.12 Plot of  $\delta(2\nu_L)^{-1}$  vs.  $H_0^{-1}$  for the  $\nu_1$  resonance in  $(C_2PNBu^t)_2$  at 295K.

Table 6.6

Linewidth parameters,  $\delta$ , and  $\delta(2\nu_L)^{-1}$  measured from the analysis of the  $\nu_2$  quadrupole signal of  $(\text{C}\&\text{PNBu}^t)_2$  in weak magnetic fields.

Magnetic field (Gauss)	Larmor frequency for chlorine-35 (K.Hz.)	$\delta$ (K.Hz.)	$\frac{\delta}{2\nu_L}$
16.05	6.696	1.394	0.104
20.00	8.344	1.548	0.093
27.75	11.577	1.770	0.076
31.65	13.204	1.820	0.069
35.50	14.811	1.705	0.058
39.40	16.438	1.840	0.056

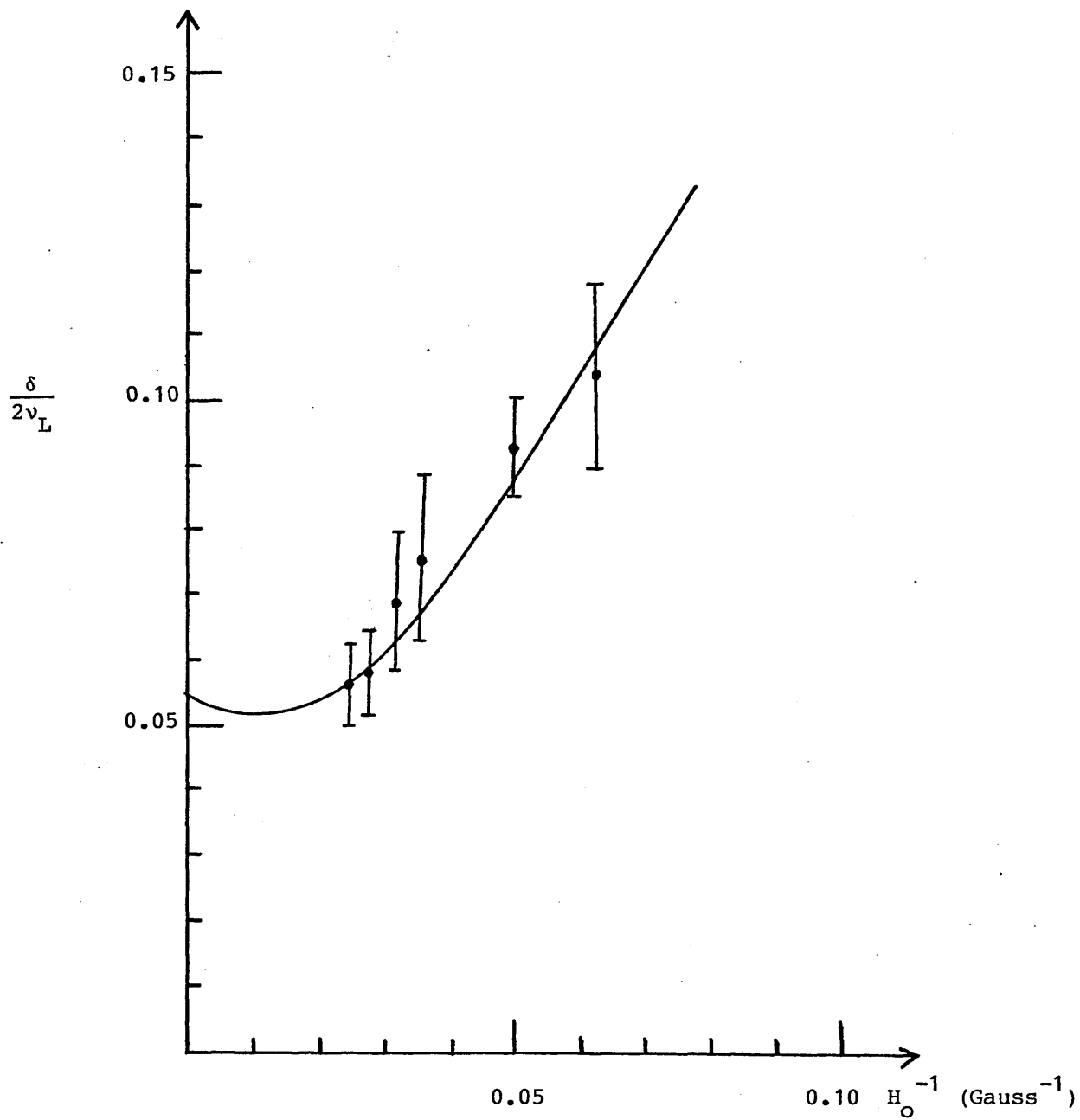


Figure 6.13 Plot of  $\delta(2\nu_L)^{-1}$  vs.  $H_0^{-1}$  for the  $\nu_2$  resonance in  $(C\&PNBu^t)_2$  at 295K.

Table 6.7

Chlorine-35 quadrupole resonance frequencies, asymmetry parameters and quadrupole coupling constants obtained for  $(C\ell PNBu^t)_2$  at 300K

Resonance	N.Q.R. frequency at 300K (M.Hz.)	$\eta$	$eqQ/h$ (M.Hz.)
$\nu_1$	$19.694 \pm 0.001$	$0.05 \pm 0.01$	$39.372 \pm 0.008$
$\nu_2$	$19.642 \pm 0.001$	$0.05 \pm 0.01$	$39.268 \pm 0.008$

Table 6.8

Linewidth parameters,  $\delta$ , and  $\delta(2\nu_L)^{-1}$  measured from the analysis of the bromine-79 quadrupole signal of  $(\text{BrPNBu}^t)_2$  in weak magnetic fields.

Magnetic field (Gauss)	Larmor frequency for bromine-79 (K.Hz.)	$\delta$ (K.Hz.)	$\frac{\delta}{2\nu_L}$
16.05	17.121	3.788	0.111
20.00	21.334	4.040	0.095
23.85	25.441	4.293	0.084
27.75	29.601	4.293	0.073
31.65	33.761	4.546	0.067
39.40	42.028	4.546	0.054

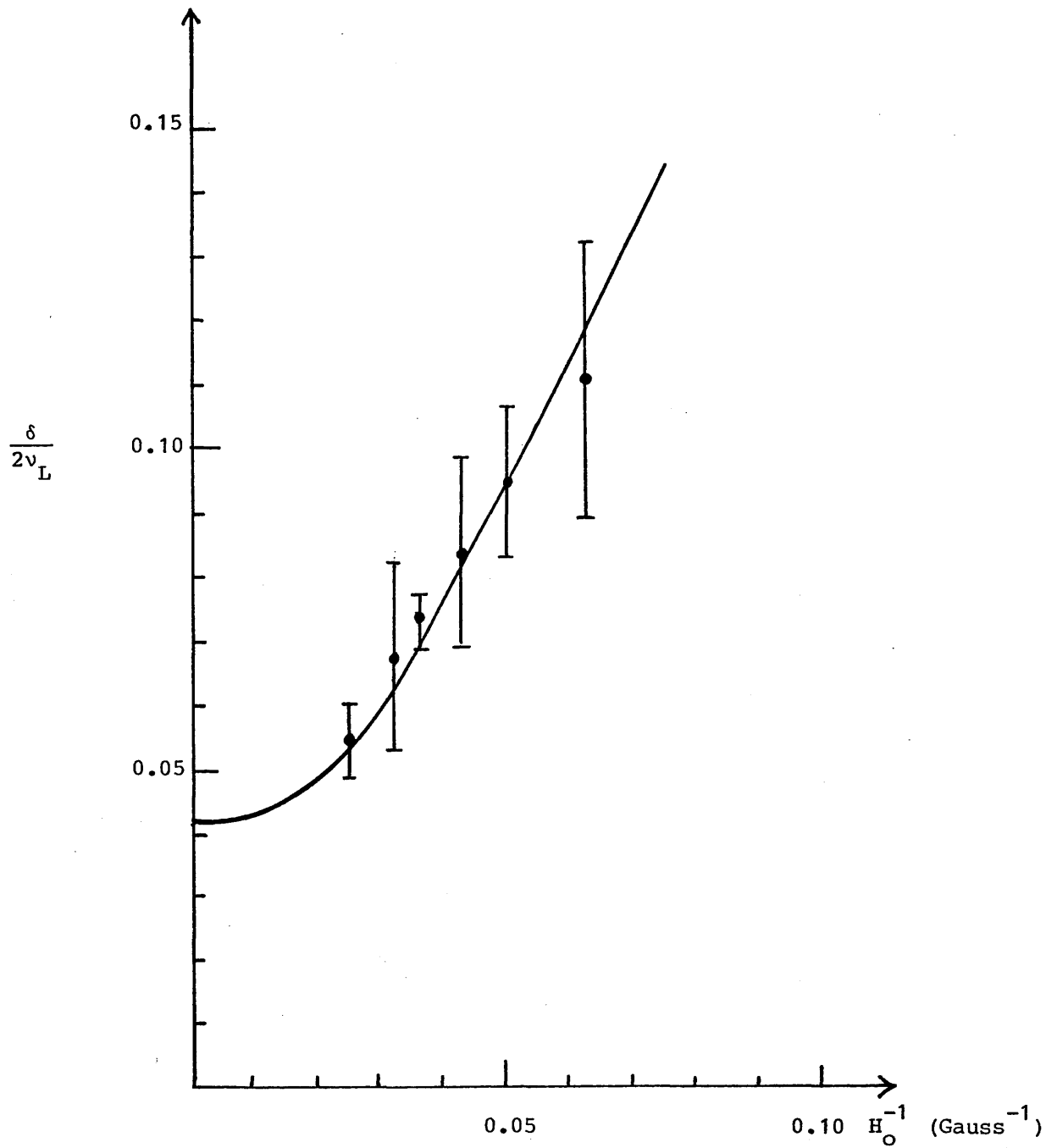


Figure 6.14 Plot of  $\delta(2\nu_L)^{-1}$  vs.  $H_0^{-1}$  for the bromine-79 resonance in  $(\text{BrPNBu}^t)_2$  at 295K.

Table 6.9

Bromine-79 quadrupole resonance frequency, the asymmetry parameter and quadrupole coupling constants obtained for  $(\text{BrPNBu}^t)_2$  at 300K

Resonance	N.Q.R. frequency at 300K (M.Hz.)	$\eta$	$eqQ/h$ (M.Hz.)
v	$156.531 \pm 0.001$	$0.04 \pm 0.01$	$312.98 \pm 0.05$

This equation and the data given in Tables 6.7 and 6.9 enable the  $\pi$ -character to be approximately estimated in the P-Cl and P-Br bonds, since the atomic quadrupole coupling constants,  $(eQ/h)_{\text{atom}}$ , for chlorine-35 and bromine-79 nuclei are known<sup>(26,27)</sup> to be 109.7 and 769.8 M.Hz. respectively. As it turns out, the  $\pi$ -character cannot contribute any more than about 1% to the nature of the P-Cl and P-Br bonds in these molecules.

Thus, the N.Q.R. data obtained in this work imply that the  $\pi$ -bonding, in these cyclodiphosph(III)azane derivatives, has only a very minute importance.

APPENDIX - 6A

PREPARATION OF CYCLOPHOSPH(III)AZANE DERIVATIVES

6A.1 Preparation of (C<sub>2</sub>H<sub>5</sub>PNHCl)<sub>3</sub>

The title compound was prepared<sup>(9)</sup> by mixing 93 g (0.67 mol) phosphorus trichloride, 50 g (0.61 mol) ethylamine hydrochloride, and 500 ml sym-tetrachloroethane in a 1ℓ flask fitted with a 100 cm air condenser and a paraffin oil bubbler which allows the evolution of the hydrogen chloride gas as a side product of the reaction. The mixture was boiled under reflux for 6 days, cooled to ambient temperature, filtered and the solvent removed. The oily brown residue was then distilled under reduced pressure, boiling point 135°C (0.005 mm Hg), and the distillate recrystallized from light petroleum ether (b.p. 40-60°C) to give 50.7 g (67.3%) of 2,4,6-trichloro-1,3,5-triethyl-cyclotriphosph(III)azane, melting point 32°C.

6A.2 Preparation of  $(C\ell PNPh)_2$

This derivative was prepared by<sup>(10)</sup> mixing 200 g (1.55 mol) of finely divided aniline hydrochloride, 600 g (4.37 mol) of  $PC\ell_3$ , and 1ℓ sym-tetrachloroethane. The mixture was boiled under reflux for 24 hours, the hot solution was filtered through a glass wool plug, and evaporated to dryness at about 110°C under reduced pressure. The white residue was dissolved in 100 ml of hot  $PC\ell_3$  and chilled to -20°C for 5 hours to give long needle crystals of 2,4-dichloro-1,3-diphenyl-diazadiphosphetidine after several recrystallizations. The product has a melting point of 153-155°C.

6A.3 Preparation of  $(\text{ClPNBu}^t)_2$

This compound was prepared by adding <sup>(11)</sup> 62.8 g (0.860 mol) of t-butylamine dropwise to a stirred solution of 39.5 g (0.287 mol) of  $\text{PCl}_3$  in 600 ml ether at  $-78^\circ\text{C}$ . The reaction mixture was then warmed up to room temperature, filtered and the filtrate evaporated until about 100 ml was left. More t-butylamine hydrochloride was deposited and filtered off and the ether then evaporated from the filtrate. The colourless oil was distilled under reduced pressure, 0.1 mm Hg, to give 38% of the 2,4-dichloro-1,3-di(tert-butyl)diazadiphosphetidine, melting point  $40-42^\circ\text{C}$ .

6A.4 Preparation of  $(\text{BrPNBu}^t)_2$

$(\text{BrPNBu}^t)_2$  was prepared from the <sup>(18)</sup> reaction of t-butylamine and phosphorus tribromide,  $\text{PBr}_3$ , using an experimental procedure similar to that described in 6A.3. The product obtained in this reaction was 2,4-dibromo-1,3-di(tert-butyl)diazadiphosphetidine, melting point 98-100°C.

APPENDIX - 6B

BROMINE QUADRUPOLE SPECTRA AT HIGH PRESSURES

Several pressure vessels have been designed and used for studying chlorine-35 quadrupole spectra<sup>(5)</sup> at frequencies below 35 M.Hz., as well as other magnetic resonance phenomena,<sup>(28,29)</sup> at high pressures. But surprisingly, the pressure vessels suitable for investigation of the quadrupole resonance phenomena that occur at high frequencies have not yet been described in the literature and so it was necessary to design a special pressure device which enables the bromine quadrupole resonance spectra to be examined at elevated pressures.

At high frequencies, the oscillating system becomes extremely sensitive to small changes in the geometry of the coil assembly of the spectrometer and so a great number of difficulties have been faced in designing the pressure vessel used in the present work. Electrical difficulties were overcome by trial and error. The size and the geometry of the pressure vessel were made to be very similar to the original Decca coil assembly. The pressure vessel described in this section can be used over a relatively small range of pressure since the Teflon plug, which will be described later, represents a weak point in the vessel. The device has been routinely used quite safely within the range  $1 \ll P \ll 352 \text{ Kg.cm}^{-2}$ .

Figure 6B.1 shows a block diagram of the pressure system used in experiments described in this thesis.

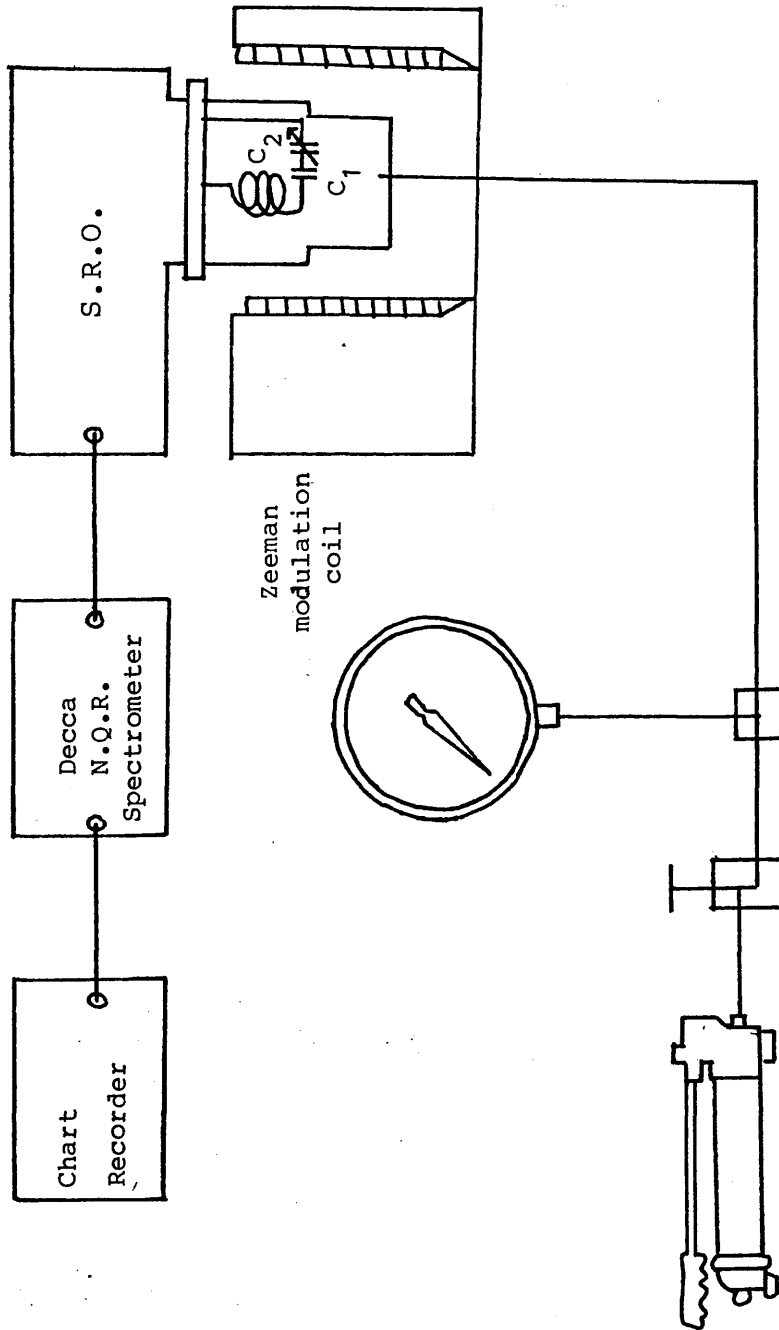


Figure 6B.1 Block diagram of the pressure system.

All connections to the spectrometer are normal.

The body of the pressure vessel is constructed of copper-beryllium alloy which is a non-magnetic metal and so all spectra were recorded very successfully using the Zeeman modulation technique. The alloy contains 1.7 to 1.9% beryllium and a heat treatment is required to harden the material. Therefore the pressure vessel is first designed carefully, machined and then subjected to the so-called precipitation hardening process which is performed by heating the vessel to  $335 \pm 5^{\circ}\text{C}$  for two hours in a suitable muffle furnace. The pressure vessel, at room temperature, is then treated with dilute hydrochloric acid to remove the toxic beryllium oxide produced on the surface and finally washed with water.

A view of the whole pressure vessel is displayed in figure 6B.2, and the individual parts of the system are drawn in figures 6B.3, 6B.4, 6B.5, and 6B.6. The dimensions of each part are also indicated in these figures. Figure 6B.2 shows clearly that the pressure vessel consists of two parts each of which is now described separately.

The upper part of the system is the more critical one since it includes all the electrical components required to complete the oscillating circuit of the spectrometer. Figure 6B.3 shows the shape and the dimensions of this part in detail. The outside diameters of the frame and of the body are made exactly as for the normal Decca coil assembly so that it can be attached to its normal position on the super-regenerative oscillator using slightly longer screws. Figure 6B.3 shows that this part is internally threaded and a conical hole is made in the centre of the frame.

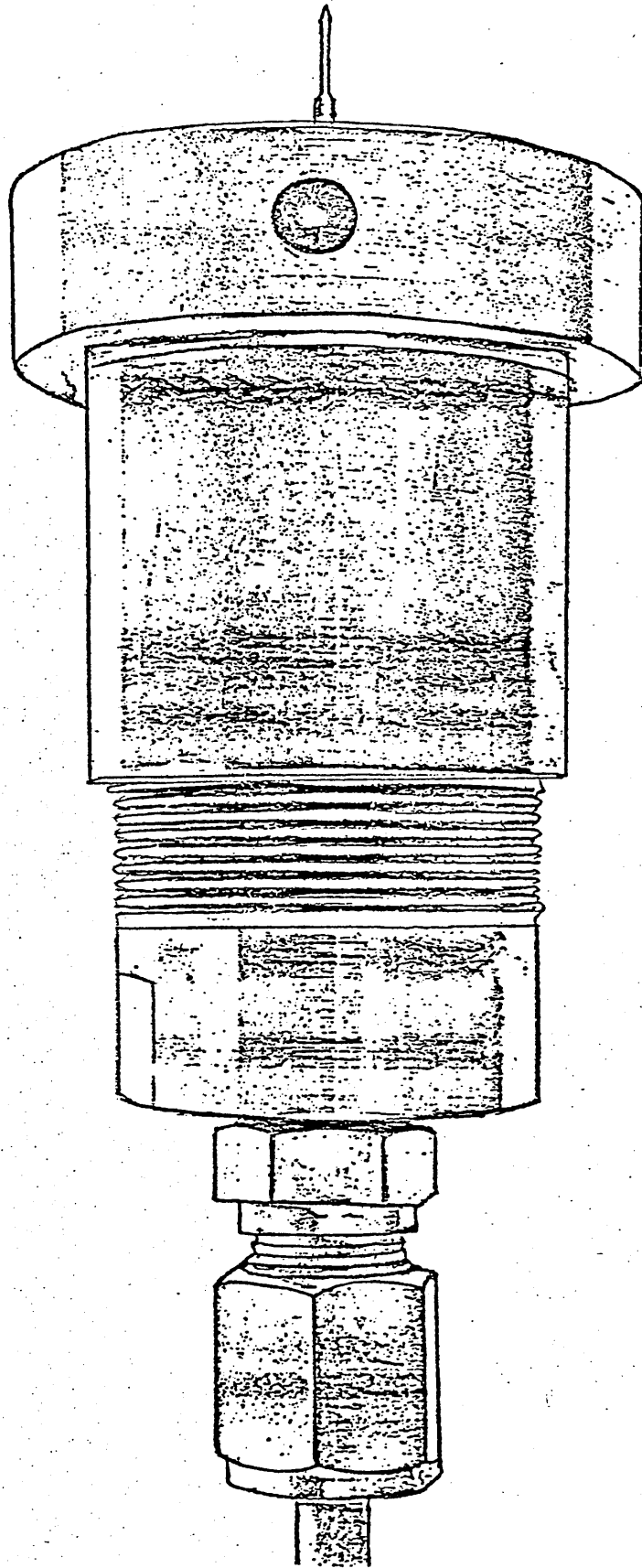


Figure 6B.2 The pressure vessel

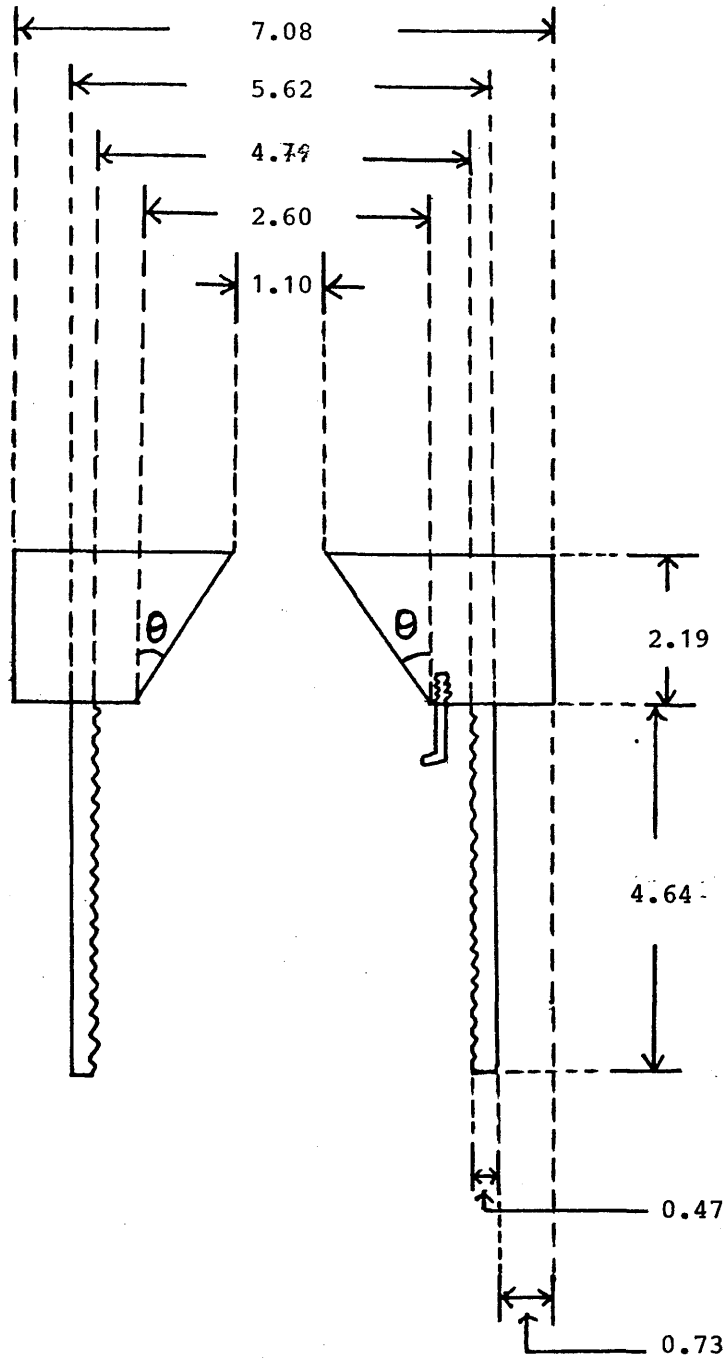


Figure 6B.3 The upper part of the pressure vessel.

All dimensions are given in cm.  $\theta = 20^\circ$ .

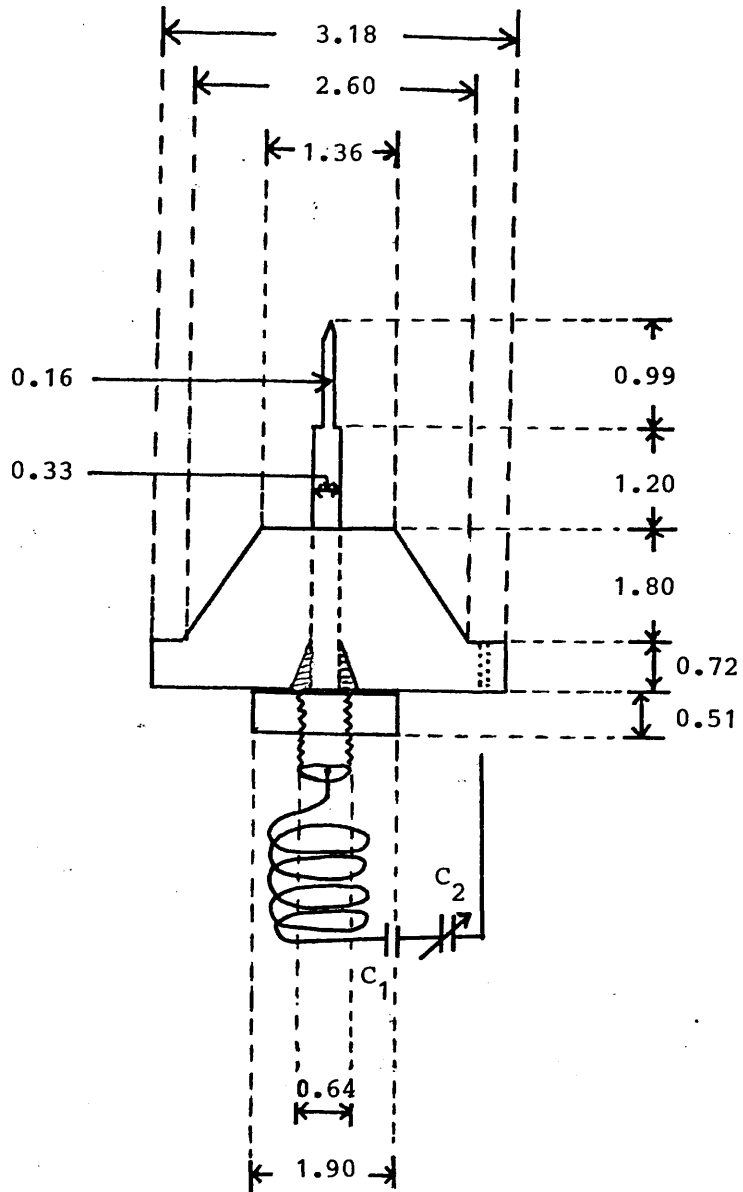


Figure 6B.4 The Teflon plug and all electrical components present inside the pressure vessel.

All dimensions are given in cm.

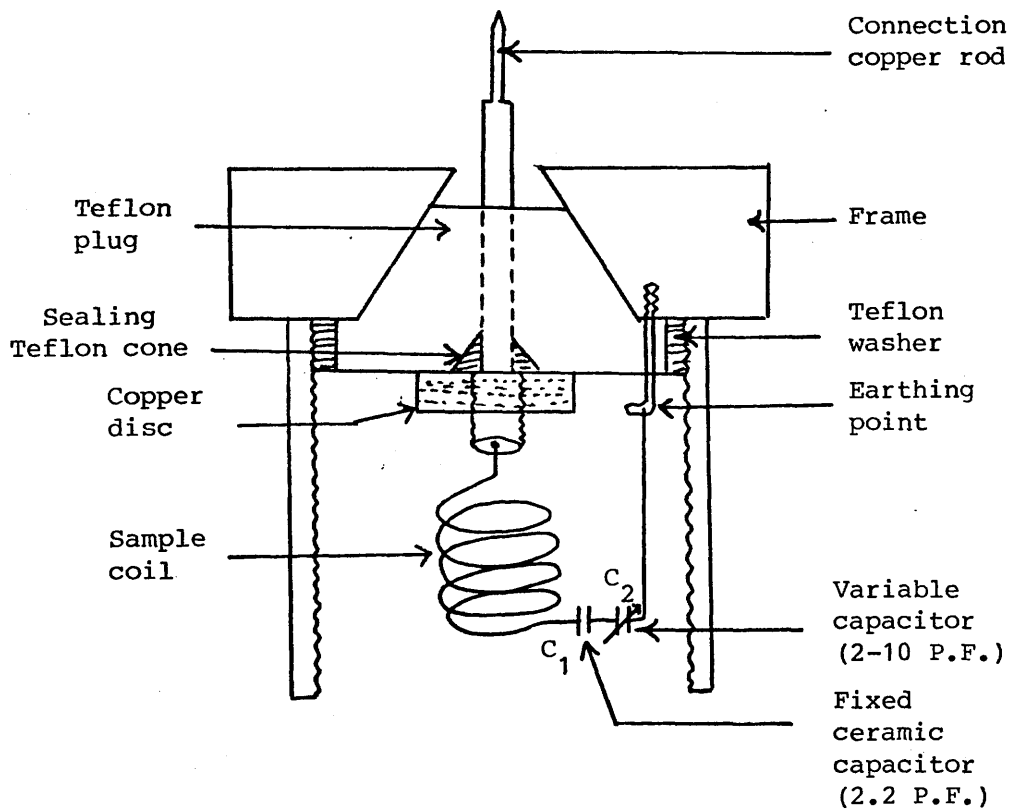


Figure 6B.5 The upper half of the pressure vessel complete with its electrical components.

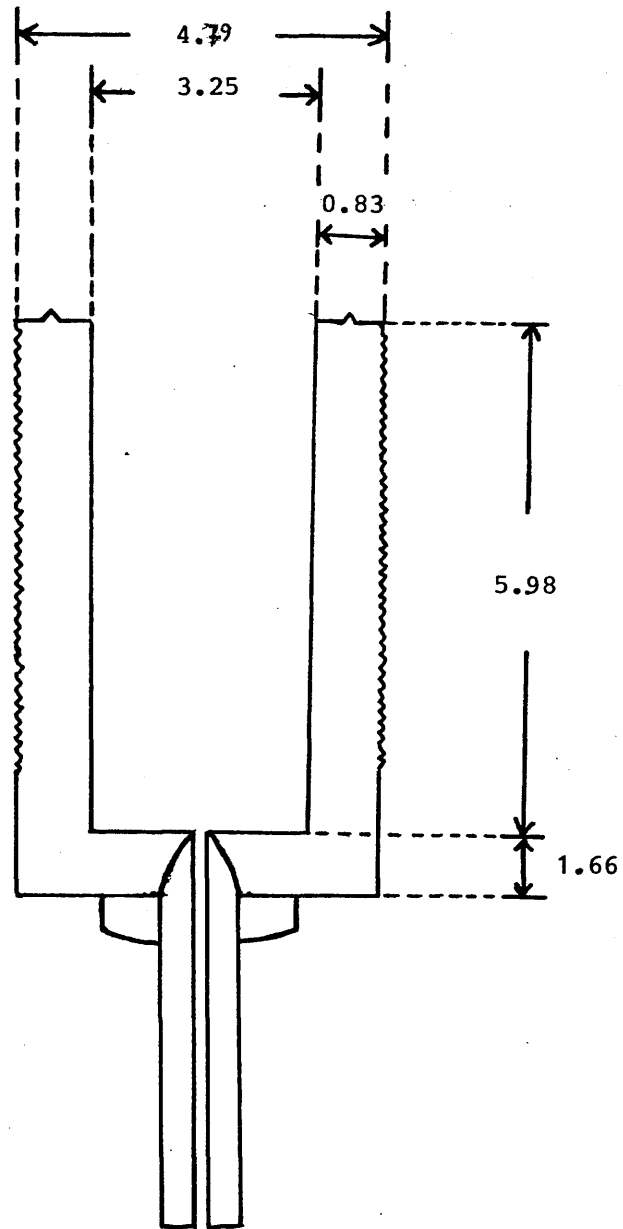


Figure 6B.6 The lower part of the pressure vessel.

All dimensions are given in cm.

The latter hole contains a similar shaped Teflon plug, shown in figures 6B.4 and 6B.5, which prevents direct earthing of the high frequency oscillating fields supplied from the oscillator to the sample coil. Connection with the oscillator circuit is made via a connecting copper rod which is held tightly, by the cone-to-cone self sealing system, in a small hole made in the centre of the Teflon plug. The upper part of this copper rod is shaped exactly as its analogue in the Decca assembly and so it makes the normal connection to the oscillator. Just below the Teflon plug, the connecting rod is threaded into a small copper disc to prevent "firing out" of the rod under pressure.

The electrical circuit inside the pressure vessel involves the copper rod, mentioned above, the sample coil, the ceramic fixed capacitor,  $C_1$ , and a variable capacitor,  $C_2$ , all connected in series and then earthed to the body of the pressure vessel from the other end of the latter capacitor, see figure 6B.5. All capacitors used for this purpose were obtained commercially. The ceramic capacitor  $C_1$  has a fixed capacitance of 2.2 P.F. while the capacitor  $C_2$  was the "ITT miniature film dielectric trimmer type 808 11109" minimum capacitance 2 P.F., capacitance swing 10 P.F. Figures 6B.4 and 6B.5 show the components of the electrical circuit in the pressure vessel used in this work.

The lower part of the pressure vessel is very simple. It consists of a cylindrical container, externally threaded, and fitted with an inlet high pressure tubing at its base. This part is shown in figure 6B.6.

When this part is screwed into the upper half of the pressure vessel and tightened down by means of normal torque wrench tools, the knife-edges shown in figure 6B.6 bite quite deeply into the Teflon washers providing an efficient seal. The plugs and washers were made of Teflon since it flows very slowly under pressure and so it ensures a good self sealing mechanism. Each Teflon component can be used for several weeks before needing replacement since it flows extremely slowly under pressure.

The polycrystalline sample was contained in a small plastic container which fits the sample coil inside the pressure vessel. Several small holes were made in the body and in the lids of this container to allow the pressure transmitting fluid to mix with the sample ensuring the application of the hydrostatic pressure on the sample. All compounds studied under pressure were unaffected by the hydraulic fluid used in the pressure system.

An "Enerpac" hydraulic handpump was used to generate the desired pressure in each experiment. This pump can produce pressures of up to  $2800 \text{ Kg.cm}^{-2}$ . A normal "Enerpac" hydraulic oil was used as a pressure transmitting fluid; and "Novaswiss" pressure tubing, valves, elbows and tee-pieces were used in connecting the pump with the pressure vessel. The stainless steel tubing used in this work has outside and inside diameters of  $3/8$ " (0.95 cm) and  $1/8$ " (0.32 cm), respectively, and a pressure rating of  $4000 \text{ Kg.cm}^{-2}$ . Conventional cone-to-cone sealing systems were used in all connections in the pressure system. The pressure measurements were made using a normal Budenberg pressure gauge

which is accurate to  $\pm 2 \text{ Kg.cm}^{-2}$  over the pressure range  $1 \leq P \leq 2800 \text{ Kg.cm}^{-2}$ . The gauge was calibrated by recording the N.Q.R. spectrum of  $\text{Cu}_2\text{O}$  as a function of pressure and the results are compared with the data already documented for this compound.

Each quadrupole resonance experiment, at any pressure within the range examined was performed as follows.

The sample container, including the polycrystalline specimen, is fixed in the sample coil inside the upper part of the pressure vessel attached to the super-regenerative oscillator. The desired frequency was obtained by adjusting the small variable capacitor,  $C_2$ , manually. When the pressure is applied inside the system, the hydraulic oil fills the spaces between the plates of the variable capacitor,  $C_2$ , changing the dielectric constant of the medium and hence the frequency of the oscillator decreases by about 3-6 M.Hz. depending on the operating frequency. Accordingly, allowances had to be made so that the capacitor  $C_2$  was adjusted to the frequency which is higher, by 3-6 M.Hz., than the actual frequency of the bromine quadrupole signal concerned.

The spectrometer is then switched off, and this part of the pressure vessel disconnected from the oscillator. The two halves of the pressure device are screwed and tightened down together properly and the whole pressure vessel is now re-attached to the oscillator. The vessel is then connected to the pressure system and the spectrometer is switched on for one hour. The desired pressure is then applied, the final frequency adjustment is made, by normal manipulations of the Decca oscillator, to frequencies just above the required frequency, and the oscillator is now switched on, using its maximum speed, to sweep down through the quadrupole signal concerned and the

spectrum is recorded in the normal way using Zeeman modulation. It should be noted that the frequency sweeping, under these circumstances, is performed only by means of some variable capacitors inside the oscillator so that only few M.Hz. range can be scanned and therefore accurate manual adjustment of the frequency is necessary before recording each spectrum.

A very good signal-to-noise ratio can be obtained when the system is properly adjusted, as described above, and this advantage has always been clearly observed in all spectra obtained for our compounds.

Figure 6.8 represents an example obtained for  $(\text{BrPNBu}^t)_2$  at  $P = 141$   $\text{Kg.cm}^{-2}$ .

APPENDIX - 6C

EXPERIMENTAL ASPECTS OF ZEEMAN N.Q.R. STUDIES

Application of a weak static magnetic field, required in Zeeman quadrupole resonance experiments, severely decreases the intensity of the quadrupole signal, according to equation 3.30. Therefore in most cases, the N.Q.R. spectrometer output needs to be coupled to a computer of average transients, C.A.T., in order to accumulate the characteristic lineshape predicted by Morino and Toyama for polycrystalline samples. The experimental aspects of the use of Decca-Radar N.Q.R. spectrometer in conjunction with a Technical Measurement Corporation C-1024 Time Averaging Computer, used in this work, are now described in some detail.

The coupled "spectrometer-CAT" system is unable to record the quadrupole signal and the markers simultaneously since the C.A.T. has only a single Y input connected to the phase sensitive detector output from the spectrometer. However, this is not a serious problem since the frequency difference between different points in each Zeeman spectrum is the only necessary measurement to be made in these experiments. These measurements are easily carried out since the adjacent sideband signals can clearly be observed and hence the frequency range scanned can accurately be estimated. Furthermore, the applied magnetic field can also be estimated from the observed Zeeman spectrum since the separation between the characteristic peaks, predicted by Morino and Toyama, is equal to twice the Larmor precession frequency of the halogen nucleus concerned in that particular magnetic field.

The Zeeman spectrum is accumulated by sweeping the frequency of the spectrometer through the quadrupole signal by means of a ramp voltage of up to 25 volts supplied by the CAT to the external F.M. input on the MW312 unit in the Decca spectrometer. The accumulated signal is then fed to the chart recorder from the "analogue output" socket of the CAT through a D.C. output balancing circuit which enables a normal signal to be obtained by adding or subtracting a constant voltage to the CAT output.

The magnetic field required for each Zeeman experiment was generated by passing a suitable current, from a D.C. power supply, through a pair of Helmholtz coils in the centre of which the coil assembly of the super-regenerative oscillator and the sample under investigation were placed. No cancellation of the earth's magnetic field at the sample was attempted.

The experimental arrangement of the use of the N.Q.R. spectrometer with the time averaging computer, CAT, is shown in figure 6C.1. All other connections are made as for the normal manipulation of the Decca spectrometer. Typical operating conditions, for the N.Q.R. spectrometer and the time averaging computer, used in recording Zeeman spectra investigated in this work are summarised in Table 6C.1. After setting the system as in this table, the process of accumulating each spectrum starts by adjusting the spectrometer to the accurate frequency of the quadrupole signal concerned. The function selector switch on the C.A.T. is set to "Internal Trigger" and accumulation of the spectrum starts once the "Trigger Source" knob is switched to "Recur". The signal accumulation automatically continues until the required number

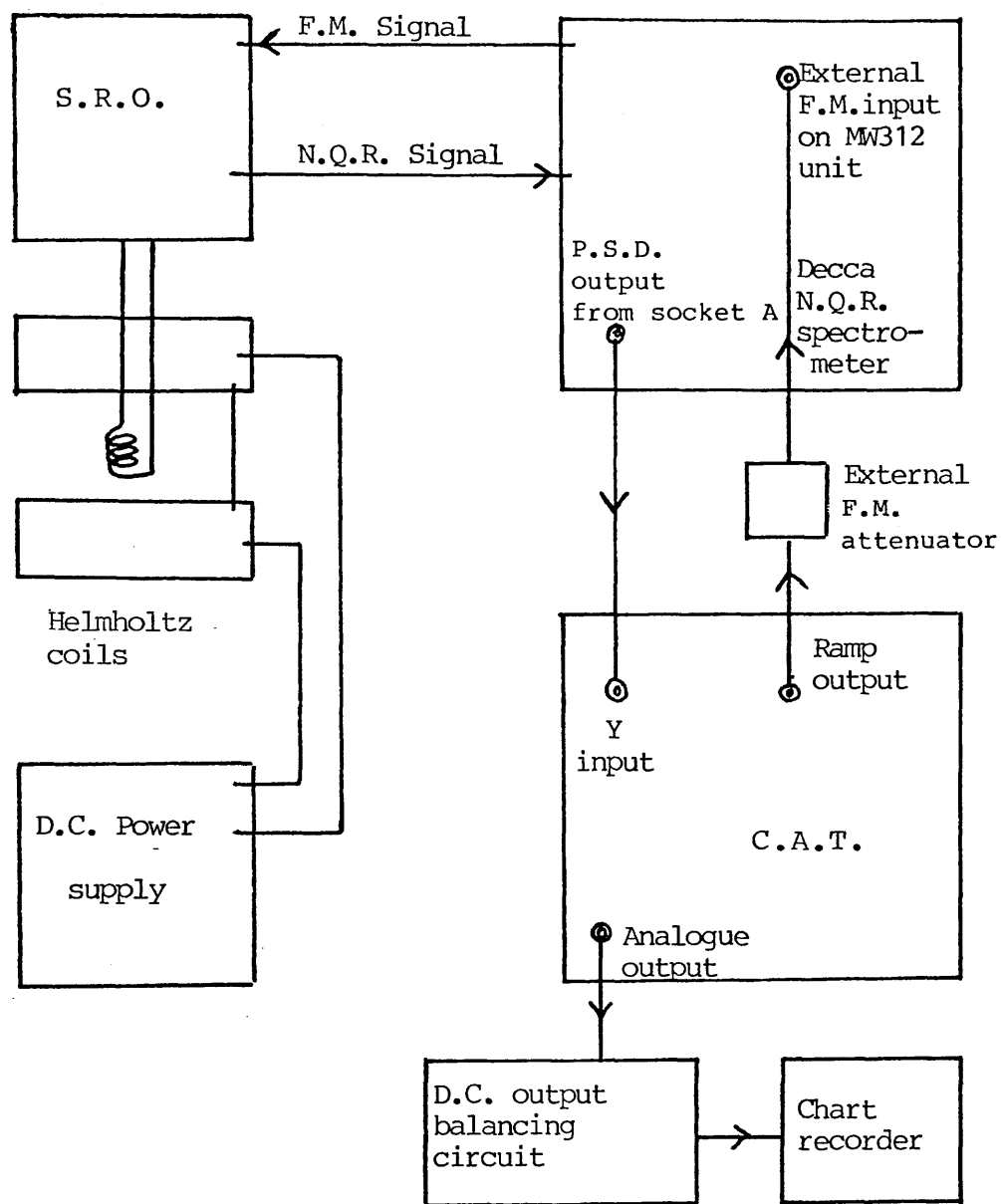


Figure 6C.1 Block diagram of the experimental arrangement when the Time Average Computer is coupled to the Decca N.Q.R. spectrometer in Zeeman N.Q.R. studies. All other connections are made as for normal spectrometer operation.

Table 6C - 1

Typical operating conditions used in recording Zeeman N.Q.R. spectra investigated in the present work.

N.Q.R. Spectrometer Settings		C A T Settings	
R.F. level	6	stand by switch	add
quench p.r.f.	50 K.Hz.	flyback time	0
FM1 amplitude	4x0.1	search rate	min
amplifier	4	sweep width	25 x 10
P.S.D. phase	5 o'clock	sweep time	25 sec
time constant	3 sec.	memory location	1-1024
A.G.C.	4	recording time	25 sec
coherence	4		
sideband suppression	off		
external F.M. attenuator	3 x 1		

of scans have been performed and the final spectrum can then be photographed directly from the CAT oscilloscope or, alternatively, fed to a chart recorder to get a permanent spectrum. A good signal-to-noise ratio can be obtained in zero magnetic field with only 25 scans through the signal.

CHAPTER 7

BROMINE QUADRUPOLE RESONANCE STUDIES OF SOME

BROMOCYCLOTRIPHOSPHAZATRIENE DERIVATIVES

7.1 INTRODUCTION

Several chlorocyclotriphosphazatriene derivatives have been extensively examined using nuclear quadrupole resonance techniques.<sup>(1-6)</sup> Many examples of bromine quadrupole resonance spectra have been documented, but in general very little of this concerns P-Br fragments and none concerns bromocyclotriphosphazatriene species, except for preliminary data that were reported by Indian workers<sup>(7)</sup> for  $N_4P_4Br_8$  and for  $N_3P_3Br_6$  during the course of the work described here.

In this chapter, the effects of pressure variations, within the range  $1 \leq P \leq 352 \text{ Kg.cm}^{-2}$ , and temperature changes, over the range  $77 \leq T \leq 300\text{K}$ , on bromine-79 and/or bromine-81 quadrupole resonance spectra of  $N_3P_3Br_6$ ,  $N_3P_3Br_5NHP_r^i$  where  $Pr^i = -CH(CH_3)_2$ ,  $cis-N_3P_3Br_4(NMe_2)_2$ , and  $cis-N_3P_3Br_3Ph_3$  are examined and discussed in detail.

The effects of weak magnetic fields, within the range  $0 \leq H_0 \leq 40 \text{ Gauss}$ , on the bromine-81 quadrupole resonance spectra of  $N_3P_3Br_6$  are also examined in order to determine the asymmetry parameters,  $\eta$ , and thence obtain information about the  $\pi$ -characters of the P-Br bonds in this solid.

Attempts have also been made to study bromine quadrupole resonance spectra of  $N_3P_3Br_5NMe_2$ , but unfortunately this compound failed to give

any quadrupole signals within the entire temperature range  $77 \leq T \leq 300\text{K}$ .

The nuclear quadrupole resonance data enable conformations to be assigned to these molecules. The data obtained in the present work are extensively discussed in the following sections.

7.2 BROMINE QUADRUPOLE RESONANCE SPECTRA OF  $N_3P_3Br_6$ ,  $N_3P_3Br_5NHPr^i$ ,  
 $cis-N_3P_3Br_4(NMe_2)_2$  AND  $cis-N_3P_3Br_3Ph_3$  SUBJECTED TO HYDROSTATIC  
PRESSURES

$N_3P_3Br_6$ ,  $cis-N_3P_3Br_4(NMe_2)_2$ ,  $cis-N_3P_3Br_3Ph_3$  and  $N_3P_3Br_5NMe_2$  were synthesised by literature methods. (8-11)  $N_3P_3Br_5NHPr^i$  was prepared by reacting an aqueous solution of isopropylamine with  $N_3P_3Br_6$  in ether using a method similar to that (11) adopted in the preparation of  $N_3P_3Br_5NMe_2$ . The detailed procedures used in preparing these compounds are described in Appendix 7.

The identities and purities of these products were established by means of melting points, micro analyses, infra-red spectroscopy and  $^{31}P$ -N.M.R. spectroscopy.

All spectra were recorded using the Decca N.Q.R. spectrometer and the pressure system described earlier. Data within the pressure range of  $1 \leq P \leq 492 \text{ Kg.cm}^{-2}$  were examined in some cases, but this range was reduced later to  $1 \leq P \leq 352 \text{ Kg.cm}^{-2}$ , for safety reasons.

Table 7.1 lists the bromine nuclear quadrupole resonance frequencies obtained for all compounds studied when they were subjected to pressures of 1 and  $352 \text{ Kg.cm}^{-2}$  at 295K.

The effects of pressure variations on bromine-79 and bromine-81 quadrupole resonance frequencies in  $N_3P_3Br_6$  are plotted in figures 7.1 and 7.2 respectively. The pressure dependence of the bromine-81 quadrupole frequencies in  $N_3P_3Br_5NHPr^i$  and in  $cis-N_3P_3Br_4(NMe_2)_2$  are shown in figures 7.3 and 7.4 respectively.

Table 7.1

Bromine quadrupole resonance frequencies and pressure coefficients  
obtained for bromocyclotriphosphazatriene derivatives at 295K.

Compound	Isotope	Resonance <sup>I</sup>	Frequencies (M.Hz.)		$\left(\frac{\partial \nu}{\partial P}\right)_{T=295K}$
			P=1Kg.cm <sup>-2</sup>	P=352Kg.cm <sup>-2</sup>	
N <sub>3</sub> P <sub>3</sub> Br <sub>6</sub>	<sup>79</sup> Br	v <sub>1</sub> <sup>2</sup>	229.29	229.40	243.8
		v <sub>2</sub> <sup>1</sup>	231.51	231.50	0.0
		v <sub>3</sub> <sup>2</sup>	234.46	234.65	538.5
		v <sub>4</sub> <sup>1</sup>	235.51	235.71	568.9
	<sup>81</sup> Br	v <sub>1</sub> <sup>2</sup>	191.73	191.79	170.6
		v <sub>2</sub> <sup>1</sup>	193.51	193.50	0.0
		v <sub>3</sub> <sup>2</sup>	195.95	196.10	418.1
		v <sub>4</sub> <sup>1</sup>	196.96	197.09	440.9
N <sub>3</sub> P <sub>3</sub> Br <sub>5</sub> NHPr <sup>i</sup>	<sup>81</sup> Br	v <sub>1</sub> <sup>1</sup>	168.09	168.16	209.2
		v <sub>2</sub> <sup>1</sup>	185.75	185.80	135.3
		v <sub>3</sub> <sup>1</sup>	189.75	189.78	101.5
		v <sub>4</sub> <sup>1</sup>	191.86	191.98	369.8
		v <sub>5</sub> <sup>1</sup>	193.09	193.24	477.4
cis-N <sub>3</sub> P <sub>3</sub> Br <sub>4</sub> (NMe <sub>2</sub> ) <sub>2</sub>	<sup>81</sup> Br	v <sub>1</sub> <sup>2</sup>	156.46	156.50	153.6
		v <sub>2</sub> <sup>1</sup>	185.90	185.90	0.0
		v <sub>3</sub> <sup>1</sup>	187.30	187.32	56.8
cis-N <sub>3</sub> P <sub>3</sub> Br <sub>3</sub> Ph <sub>3</sub>	<sup>79</sup> Br	v <sub>1</sub> <sup>1</sup>	196.08	195.96	-327.1
		v <sub>2</sub> <sup>2</sup>	196.68	196.56	-355.5

<sup>I</sup> Superscripts to resonances indicate relative intensities.

Values of  $\left(\frac{\partial \nu}{\partial P}\right)_T$  are given in units of Hz.Kg.<sup>-1</sup>cm<sup>2</sup>.

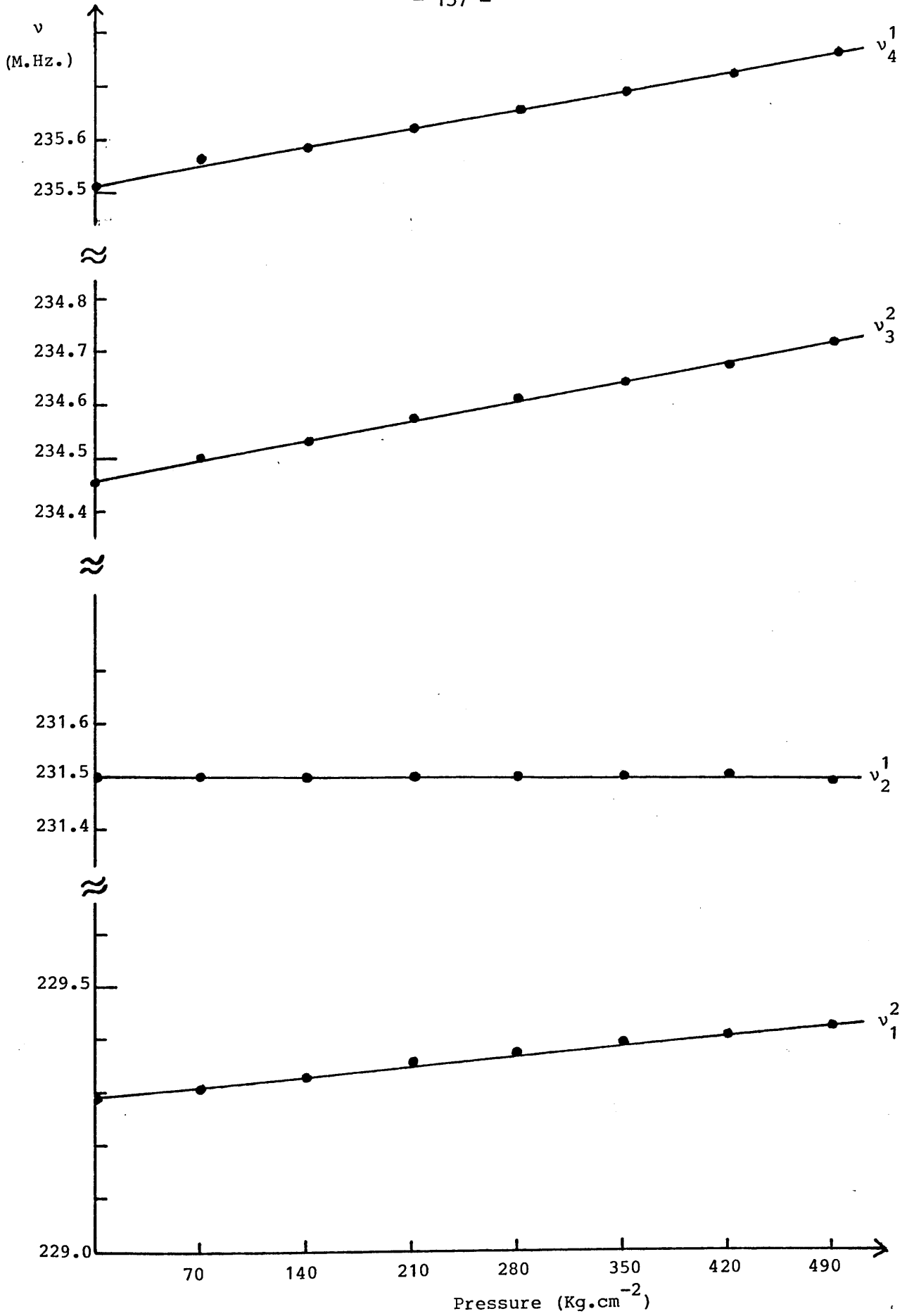


Figure 7.1 Plots of bromine-79 N.Q.R. frequencies vs. pressure for  $N_3P_3Br_6$  at 295K.

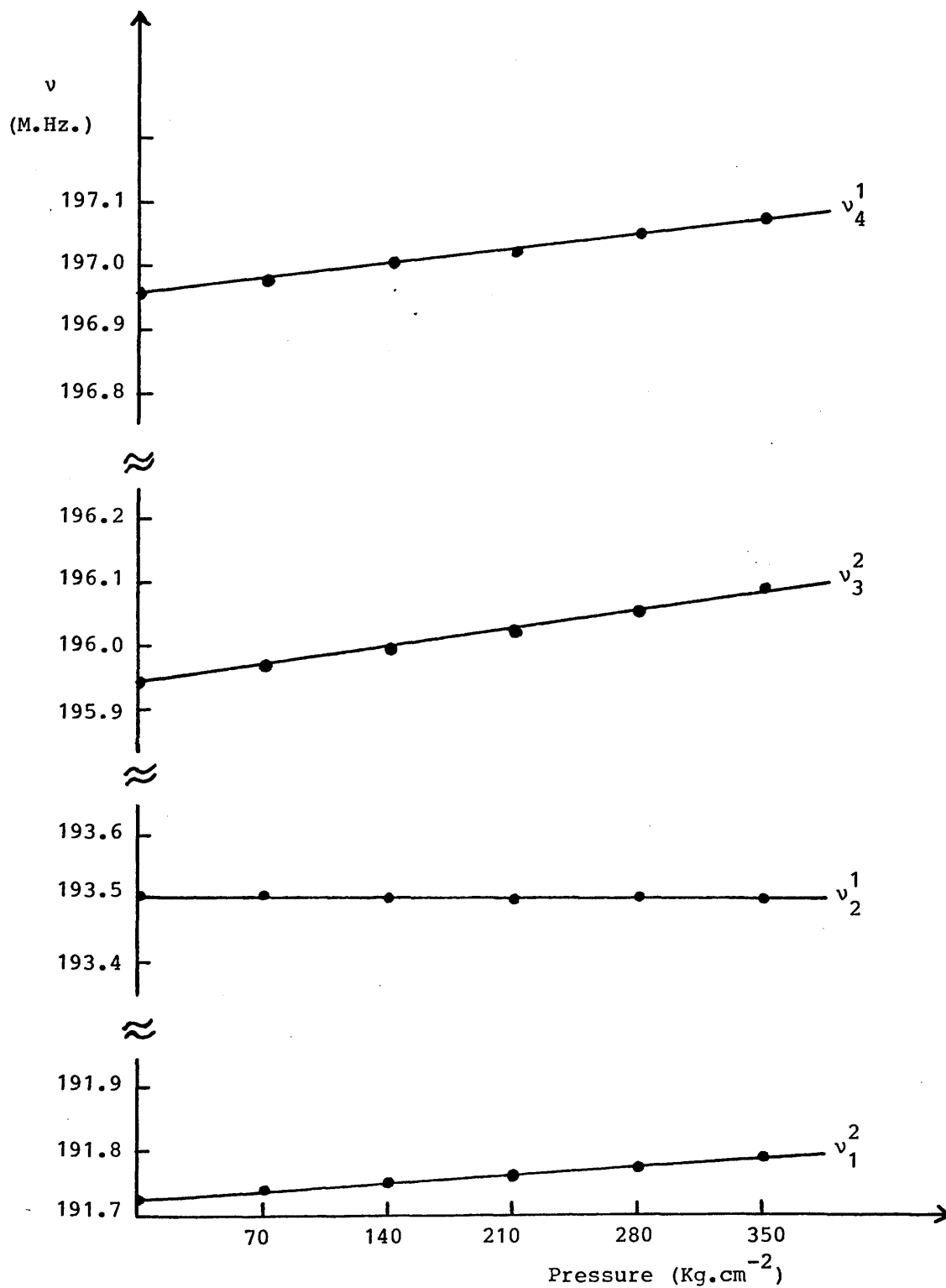


Figure 7.2 Plots of bromine-81 N.Q.R. frequencies vs. pressure for  $N_3P_3Br_6$  at 295K.

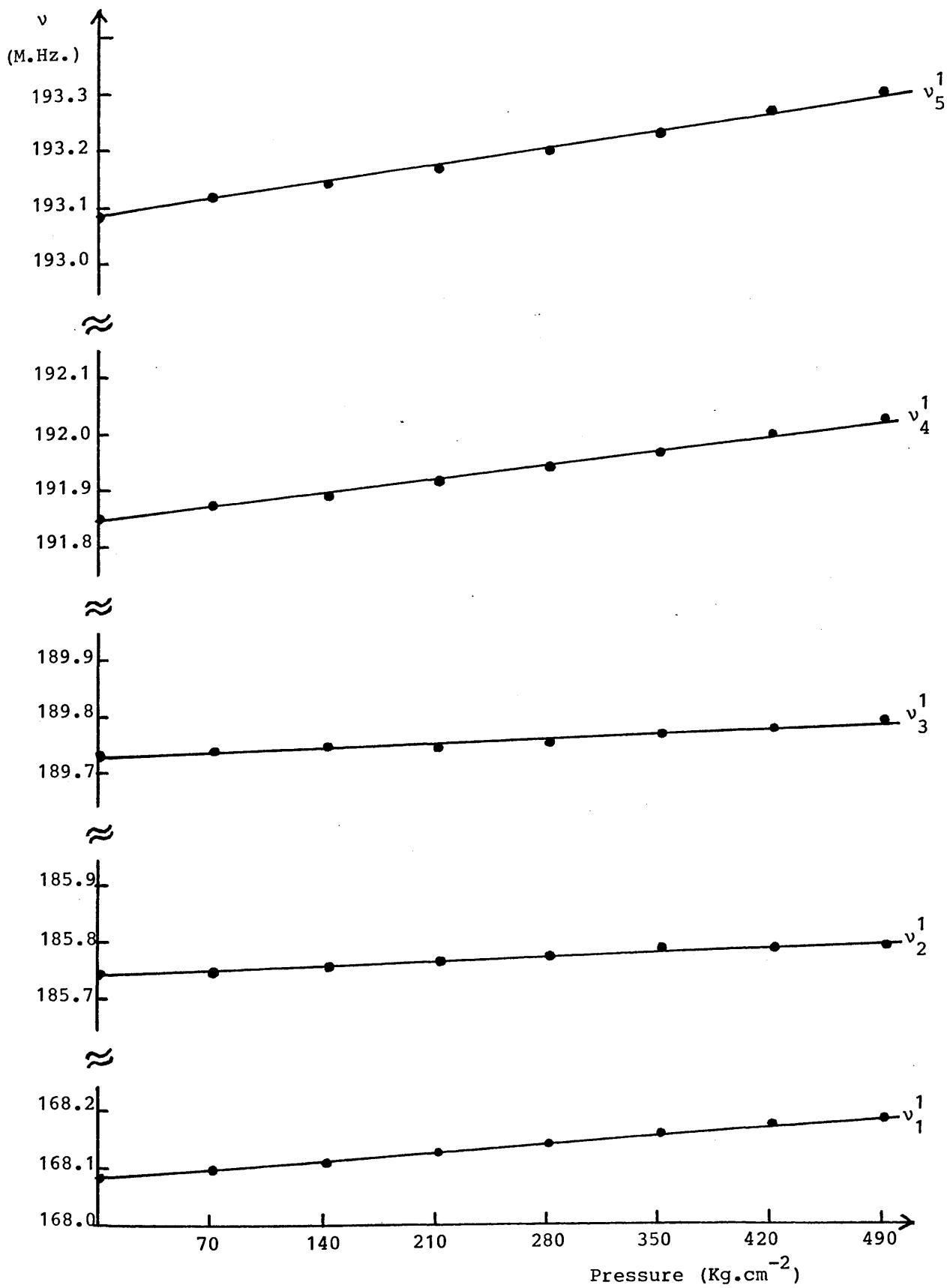


Figure 7.3 Plots of bromine-81 N.Q.R. frequencies vs. pressure for  $\text{N}_3\text{P}_3\text{Br}_5\text{NHPr}^i$  at 295K.

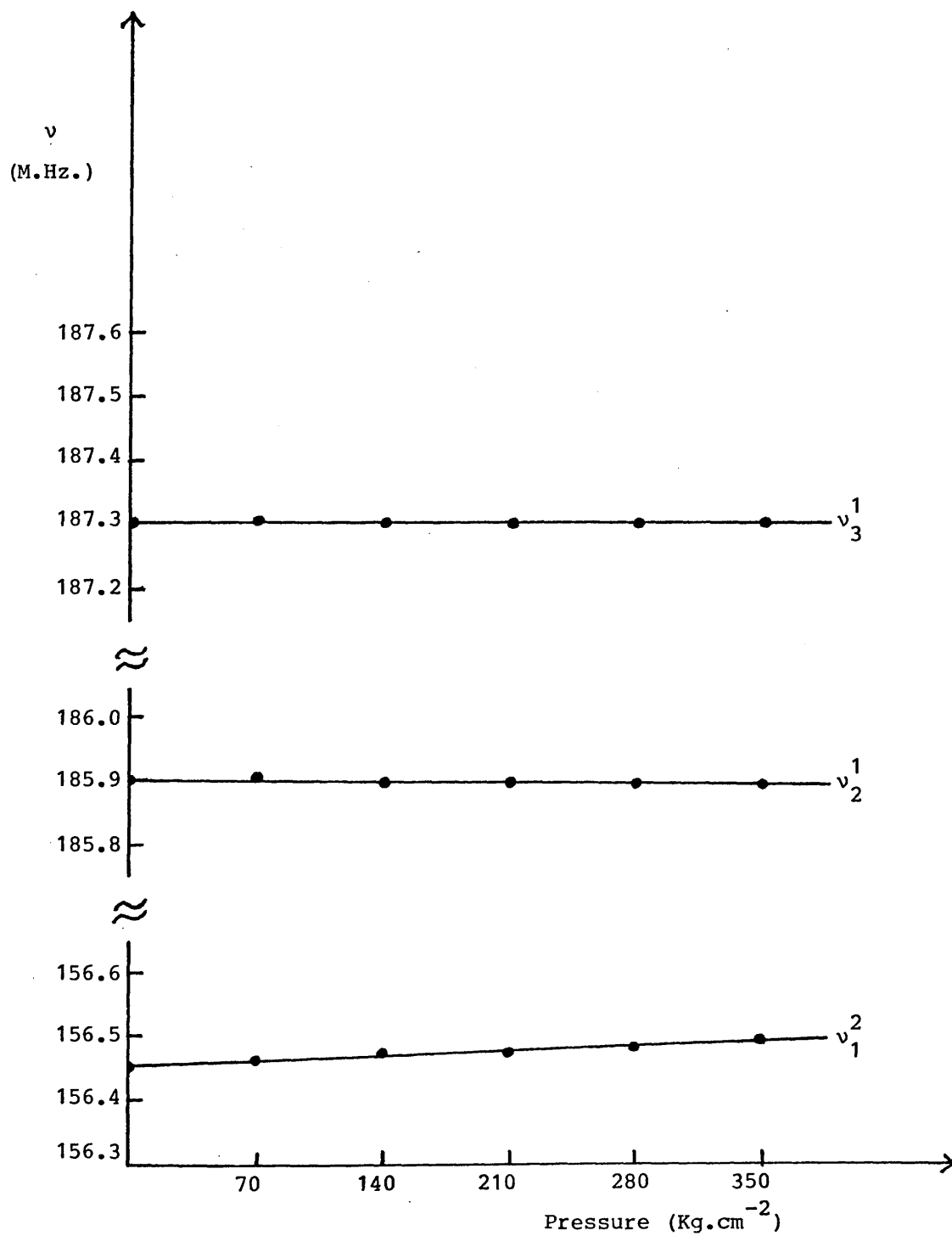


Figure 7.4 Plots of bromine-81 N.Q.R. frequencies vs. pressure for  $\text{cis-N}_3\text{P}_3\text{Br}_4(\text{NMe}_2)_2$  at 295K.

The plots of the bromine-79 quadrupole resonance frequencies in  $\text{cis-N}_3\text{P}_3\text{Br}_3\text{Ph}_3$  as a function of pressure are illustrated in figure 7.5.

It is clearly indicated in figures 7.1-7.5 that the bromine nuclear quadrupole resonance frequencies in these bromocyclotriphosphazatrienes are linear functions of the applied pressure within the pressure ranges examined. The pressure coefficients,  $(\frac{\partial\nu}{\partial P})_T$ , for these resonances are therefore independent of the applied pressure within the ranges investigated. Values of  $(\frac{\partial\nu}{\partial P})_{T=295K}$  obtained for these compounds are also given in Table 7.1.

The pressure coefficients given in this table can be simply accounted for in terms of the amplitudes of the nuclear motions in molecular solids. The nuclei in grossly overcrowded sites in molecules are less affected by the applied pressure since their motional amplitudes are relatively restricted. Furthermore, overcrowded nuclei are more protected by the presence of bulky neighbours from the effects of compression and therefore both dynamic and static effects of pressure contribute less to  $(\frac{\partial\nu}{\partial P})_T$  in overcrowded sites, and negative values of  $(\frac{\partial\nu}{\partial P})_T$  may even be obtained when the static contributions predominate.

Figures 7.1 and 7.2 together with Table 7.1 show that the  $\text{N}_3\text{P}_3\text{Br}_6$  molecule is bisected by a plane of symmetry that is retained over the pressure range examined. Furthermore, the marked differences in  $(\frac{\partial\nu}{\partial P})_T$  values given in Table 7.1 confirm that the  $(\text{N-P})_3$  ring in  $\text{N}_3\text{P}_3\text{Br}_6$  cannot be planar; it must be slightly puckered.

In  $\text{N}_3\text{P}_3\text{Br}_5\text{NHPr}^i$ , the resonance frequency,  $\nu_1$ , must be assigned to the bromine atom in the  $\equiv\text{P}(\text{Br})\text{NHPr}^i$  residue. The markedly smaller

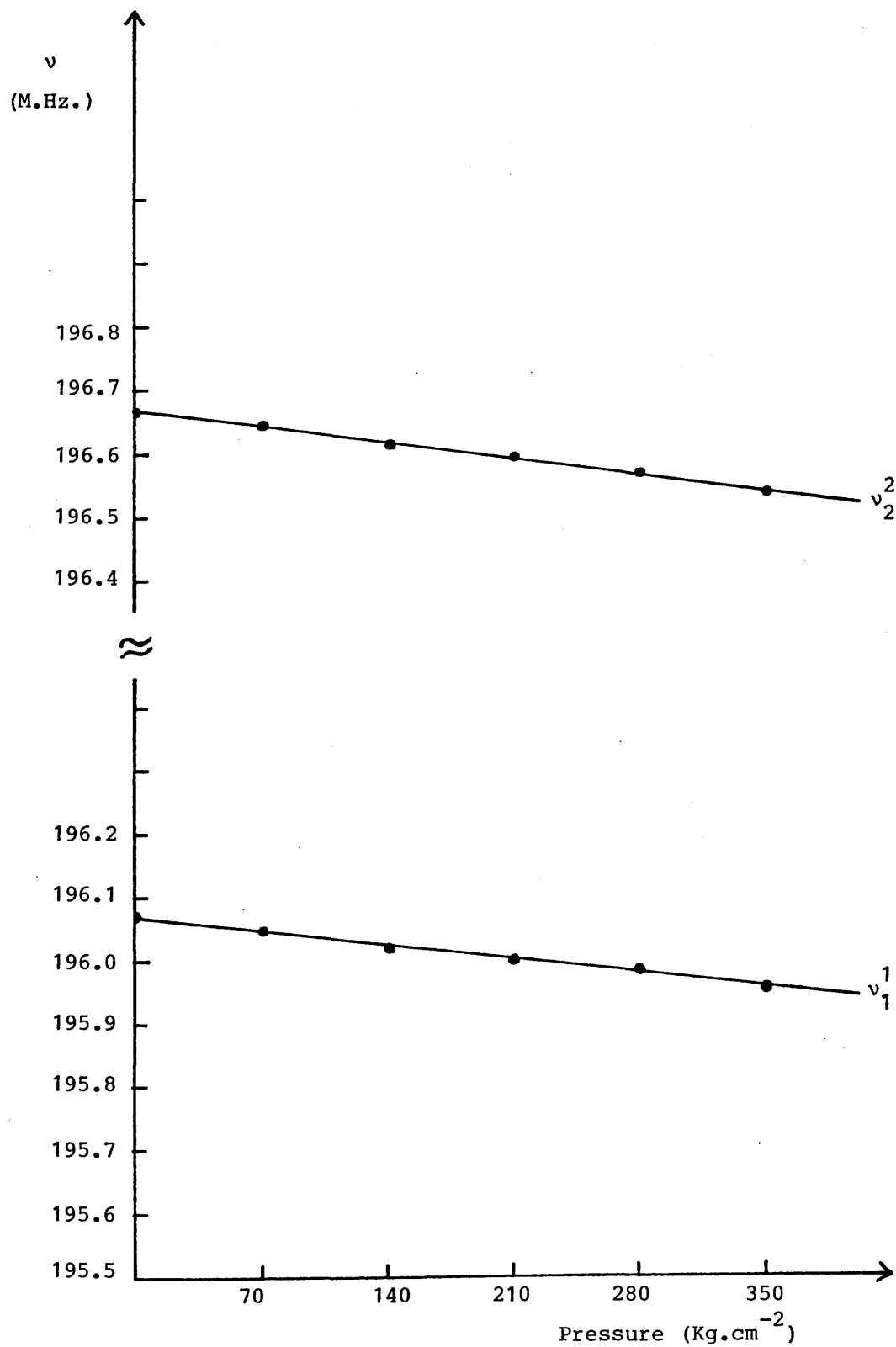


Figure 7.5 Plots of bromine-79 N.Q.R. frequencies vs. pressure for  $\text{cis-N}_3\text{P}_3\text{Br}_3\text{Ph}_3$  at 295K.

values of  $(\frac{\partial \nu_2}{\partial P})_T$  and  $(\frac{\partial \nu_3}{\partial P})_T$ , given in Table 7.1, enable  $\nu_2$  and  $\nu_3$  to be assigned to bromine nuclei on the same side of the  $(N-P)_3$  ring system as the bulky  $-NHP_r^i$  group, and therefore  $\nu_4$  and  $\nu_5$  must be assigned to the bromine atoms on the other side of the ring.

Its bromine-81 N.Q.R. spectrum shows that  $N_3P_3Br_4(NMe_2)_2$  cannot be a geminal isomer and that the two  $\equiv P(Br)NMe_2$  groups in this molecule are equivalent. The  $(N-P)_3$  ring systems in cyclotriphosphazatriene derivatives are, in general, found to be non-planar, <sup>(4,12,13)</sup> and if this is also true for our sample of  $N_3P_3Br_4(NMe_2)_2$  then this compound must have a cis-configuration. The N.Q.R. data confirm that the  $N_3P_3Br_4(NMe_2)_2$  molecule is bisected by a plane of symmetry over the pressure range  $1 \leq P \leq 352 \text{ Kg.cm}^{-2}$ . Furthermore, the smaller quadrupole resonance frequency,  $\nu_1$ , must be assigned to the bromine atoms in the  $\equiv P(Br)NMe_2$  groups. The zero value of  $(\frac{\partial \nu_2}{\partial P})_T$ , given in Table 7.1, immediately enables  $\nu_2$  to be assigned to the bromine nucleus cis to the  $-NMe_2$  groups.

Figure 7.5 and Table 7.1 suggest that over the entire pressure range examined the  $N_3P_3Br_3Ph_3$  molecule is bisected by a plane of symmetry. This molecule can therefore adopt either a cis- or a trans-configuration with respect to the bromine atoms. However, the melting point and the  $^{31}P$ -N.M.R. and infra-red data obtained for our sample are all in favour of the cis-configuration. <sup>(10,14,15)</sup> Dipole moment measurements <sup>(15)</sup> also indicate that the  $N_3P_3Br_3Ph_3$  with melting point of 194-195°C has a cis-configuration.

The small difference in the  $(\frac{\partial \nu}{\partial P})_T$  values obtained for this solid, given in Table 7.1, again imply that the three bromine atoms in the  $N_3P_3Br_3Ph_3$  molecule lie on the same side of the  $(N-P)_3$  ring.

Furthermore, figure 7.5 and Table 7.1 show that *cis*- $N_3P_3Br_3Ph_3$  is the only compound, among the cyclotriphosphazatriene derivatives studied, in which both  $\nu_1$  and  $\nu_2$  have negative pressure coefficients. The negative contributions of the static influence obviously dominate the effects of pressure on the bromine-79 quadrupole resonance frequencies in this compound. This solid should, therefore, undergo a phase transition when it is subjected to a sufficiently high pressure. However, figure 7.5 shows explicitly that the pressure system used in this work was unable to generate pressures high enough to force the predicted phase transition in *cis*- $N_3P_3Br_3Ph_3$  to take place.

In this context, figures 7.1-7.4 show that no phase transitions take place in any of these bromocyclotriphosphazatriene derivatives within the pressure ranges investigated.

The bromine-79 nuclear quadrupole resonance spectrum,  $\nu_2$ , of *cis*- $N_3P_3Br_3Ph_3$  subjected to the hydrostatic pressure of  $141 \text{ Kg.cm}^{-2}$ , at 295K, is illustrated in figure 7.6.

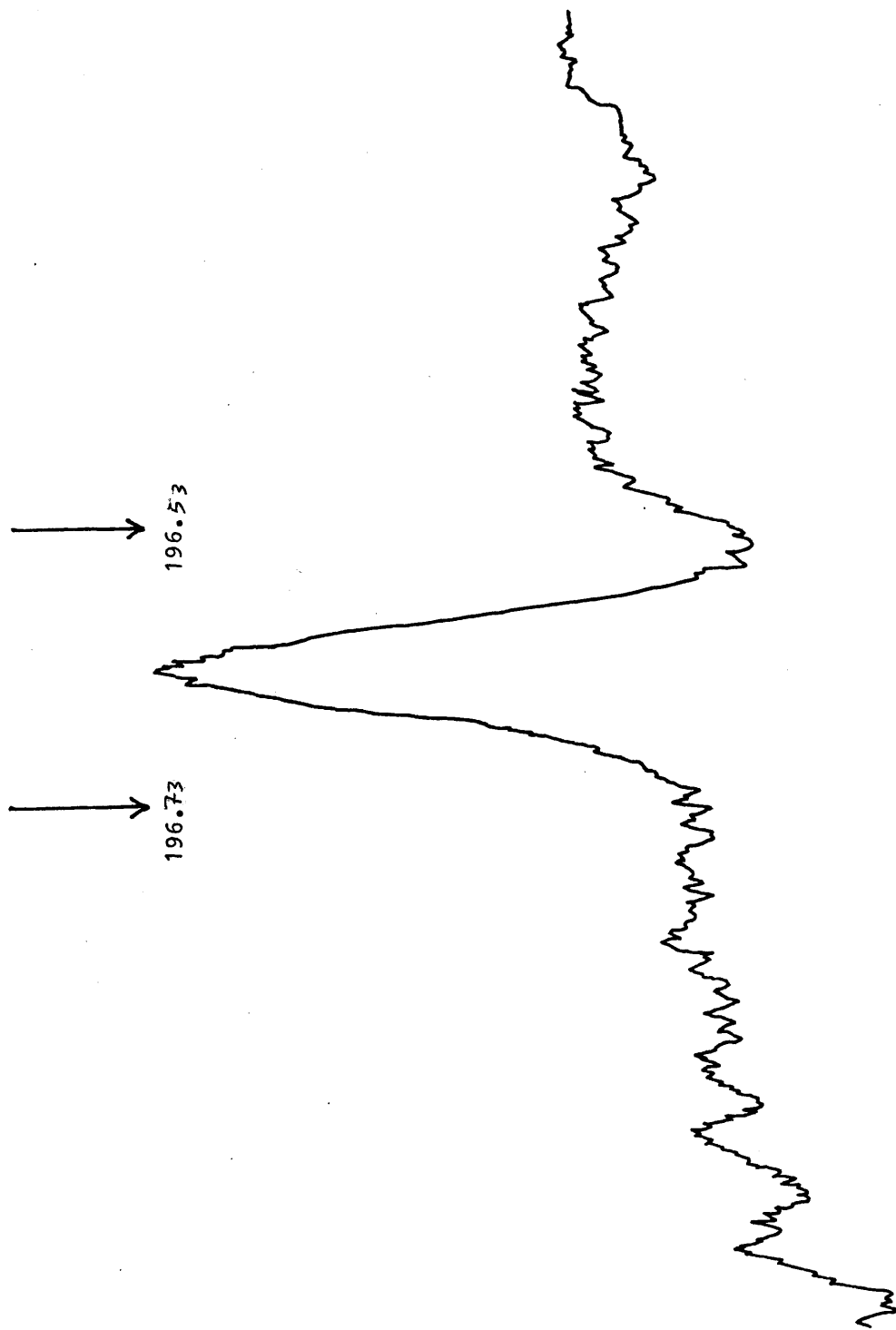


Figure 7.6 The  $\nu_2$  resonance of the bromine-79 N.Q.R. spectrum of  $\text{cis-N}_3\text{P}_3\text{Br}_3\text{Ph}_3$  under a pressure of  $141 \text{ Kg.cm}^{-2}$  at  $295\text{K}$ , recorded using Zeeman modulation. Frequencies are given in M.Hz.

7.3 TEMPERATURE DEPENDENCE OF BROMINE QUADRUPOLE RESONANCE SPECTRA

OF  $N_3P_3Br_6$ ,  $N_3P_3Br_5NHPr^i$ ,  $cis-N_3P_3Br_4(NMe_2)_2$  AND  $cis-N_3P_3Br_3Ph_3$

(i) Constant pressure conditions

The bromine quadrupole resonance frequencies, at 77K and 293K, obtained for the title compounds under constant atmospheric pressure are listed in Table 7.2. The effects of temperature variations on bromine-79 and bromine-81 quadrupole resonance frequencies in  $N_3P_3Br_6$  are shown in figures 7.7 and 7.8 respectively, and similar effects on bromine-81 quadrupole spectra of  $N_3P_3Br_5NHPr^i$  and  $cis-N_3P_3Br_4(NMe_2)_2$  are illustrated in figures 7.9 and 7.10 respectively. The temperature dependence of bromine-79 quadrupole resonance frequencies in  $cis-N_3P_3Br_3Ph_3$  is shown in figure 7.11.

Table 7.3 gives least squares fits of the bromine quadrupole resonance frequencies to polynomials of the form of equation 5.1, valid over the temperature range  $200 \leq T \leq 300K$ . Values of thermal coefficients,  $\left(\frac{\partial \nu}{\partial T}\right)_{P=1Kg.cm^{-2}; T=295K}$ , of the resonance frequencies are listed in Table 7.4. This table also includes temperature coefficients obtained for the corresponding chlorocyclotriphosphazatrienes taken from reference (4) for comparison purposes.

Figures 7.7 and 7.8 together with Tables 7.2-7.4 show that the  $N_3P_3Br_6$  molecule is bisected by a plane of symmetry that is retained over the temperature range  $77 \leq T \leq 300K$ . Furthermore, it follows from the markedly different values of the temperature coefficients

Table 7.2

Bromine quadrupole resonance frequencies.

Compound	m.p. (°C)	Isotope	Resonance <sup>I</sup>	Frequencies (M.Hz.)	
				at 77K	at 293K
$N_3P_3Br_6$	192	$^{79}Br$	$v_1^2$	234.92	229.60
			$v_2^1$	235.29	231.63
			$v_3^2$	240.76	234.64
			$v_4^1$	242.17	235.75
		$^{81}Br$	$v_1^2$	196.14	191.68
			$v_2^1$	196.48	193.50
			$v_3^2$	201.07	196.02
			$v_4^1$	202.22	196.87
$N_3P_3Br_5NHPr^i$	82-83	$^{81}Br$	$v_1^1$	173.34	168.23
			$v_2^1$	190.10	185.86
			$v_3^1$	194.63	189.75
			$v_4^1$	198.27	192.10
			$v_5^1$	199.30	193.32
cis- $N_3P_3Br_4(NMe_2)_2$	131-134	$^{81}Br$	$v_1^2$	UNOBSERVED	156.59
			$v_2^1$	AT	185.90
			$v_3^1$	77K	187.36
cis- $N_3P_3Br_3Ph_3$	193-195	$^{79}Br$	$v_1^1$	200.08	196.10
			$v_2^2$	199.05	196.63
$N_3P_3Br_5NMe_2$	112-113.5	NO SIGNALS OBSERVED IN THE RANGE $77 \leq T \leq 300K$ .			

<sup>I</sup> Superscripts to resonances indicate relative intensities.

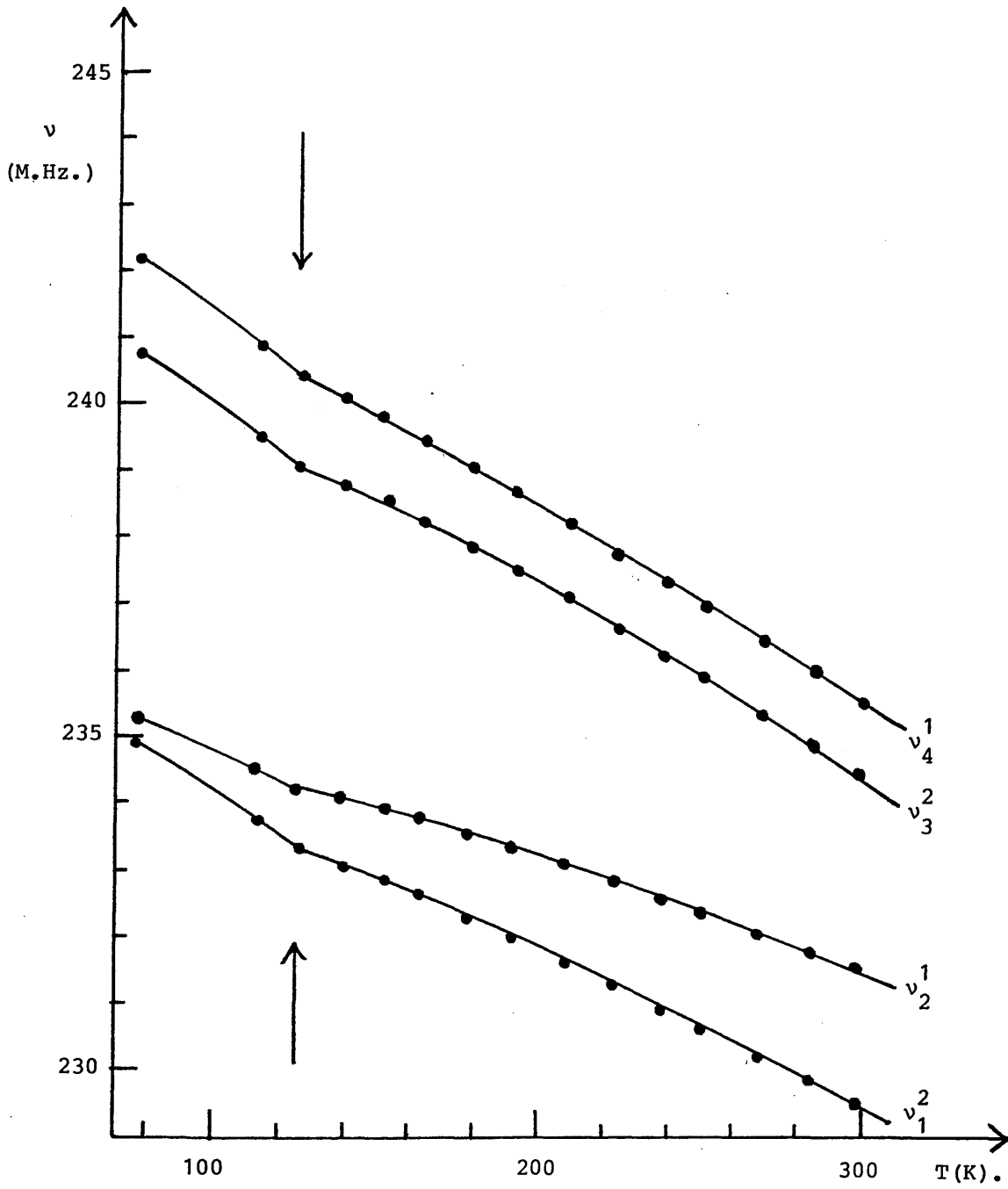


Figure 7.7 Bromine-79 N.Q.R. frequencies,  $\nu$ (M.Hz.), for  $N_3P_3Br_6$  vs. temperature (K).

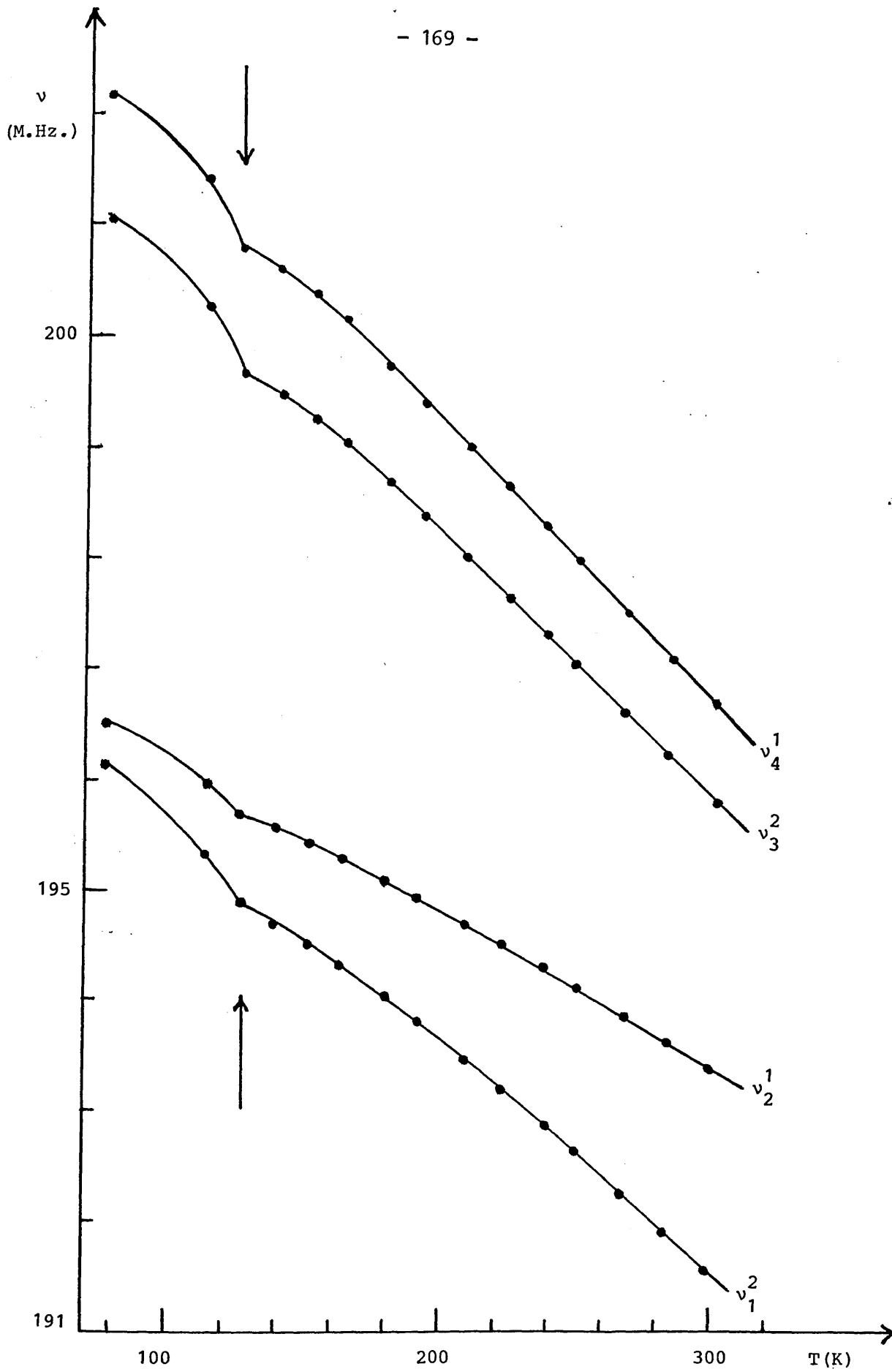


Figure 7.8 Bromine-81 N.Q.R. frequencies,  $\nu$ (M.Hz.), for  $N_3P_3Br_6$  vs. temperature (K).

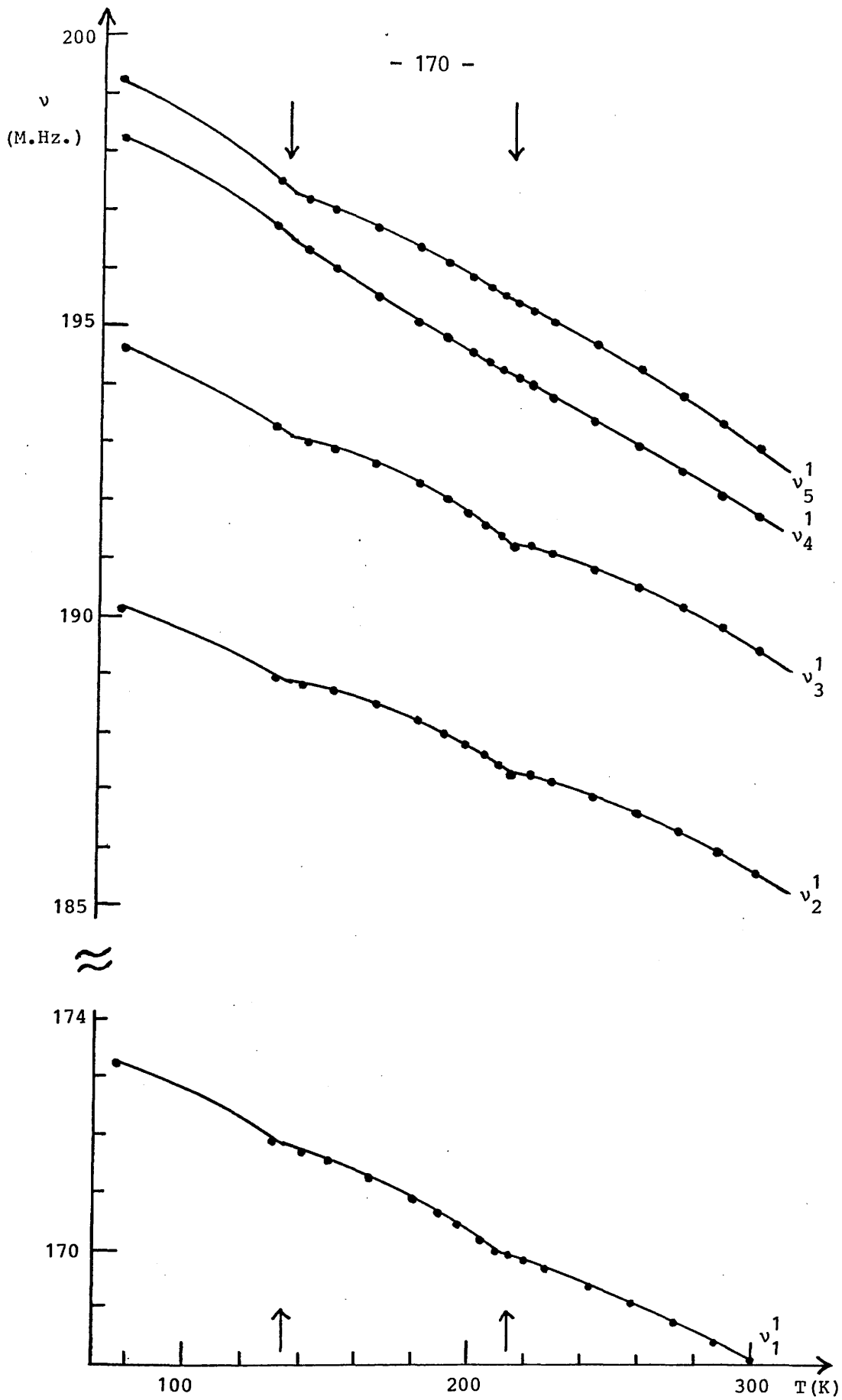


Figure 7.9 Bromine-81 N.Q.R. frequencies,  $\nu$  (M.Hz.), for  $N_3P_3Br_5NHPr^i$  vs. temperature (K).

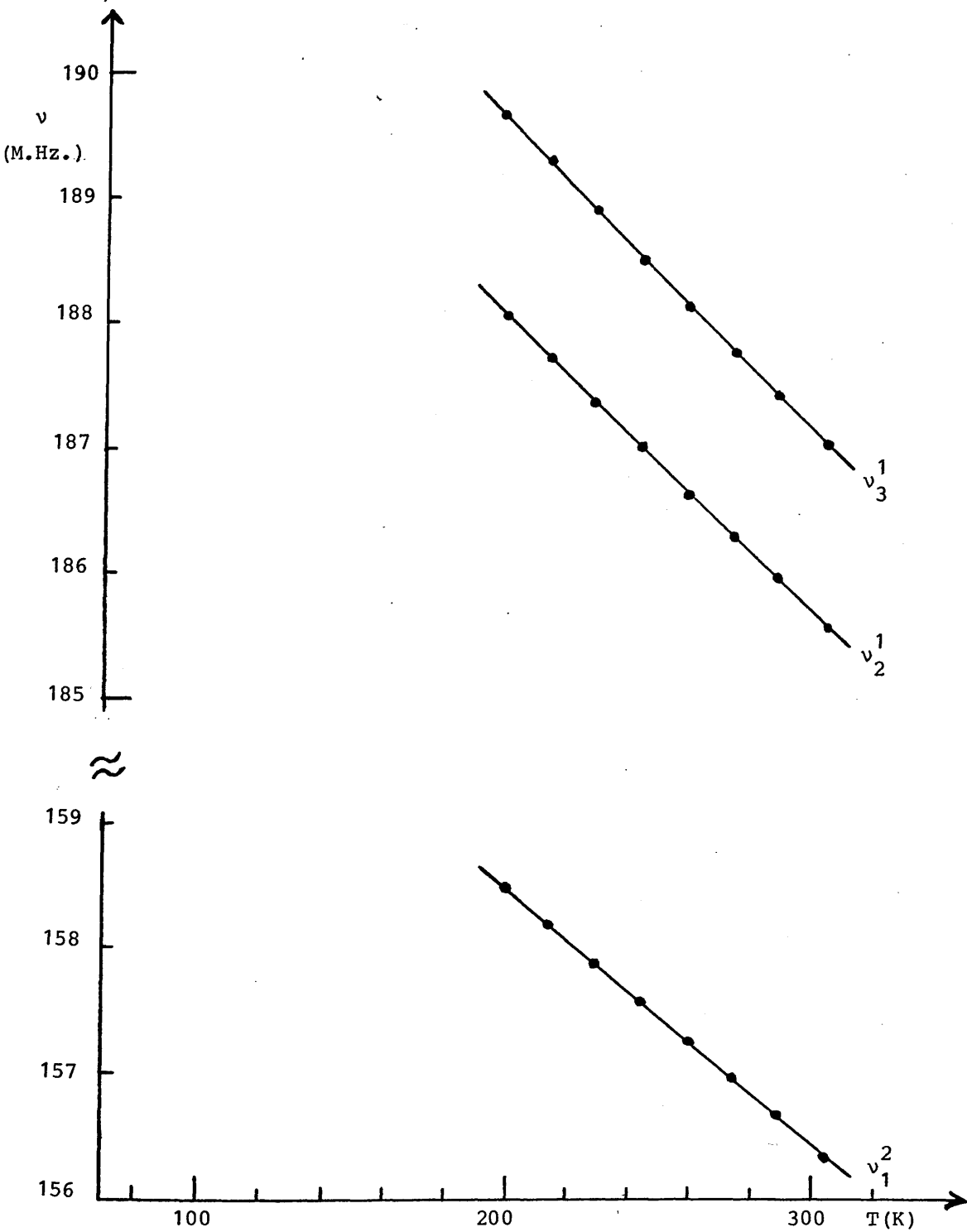


Figure 7.10 Bromine-81 N.Q.R. frequencies,  $\nu$  (M.Hz.), for  $\text{cis-N}_3\text{P}_3\text{Br}_4(\text{NMe}_2)_2$  vs. temperature (K).

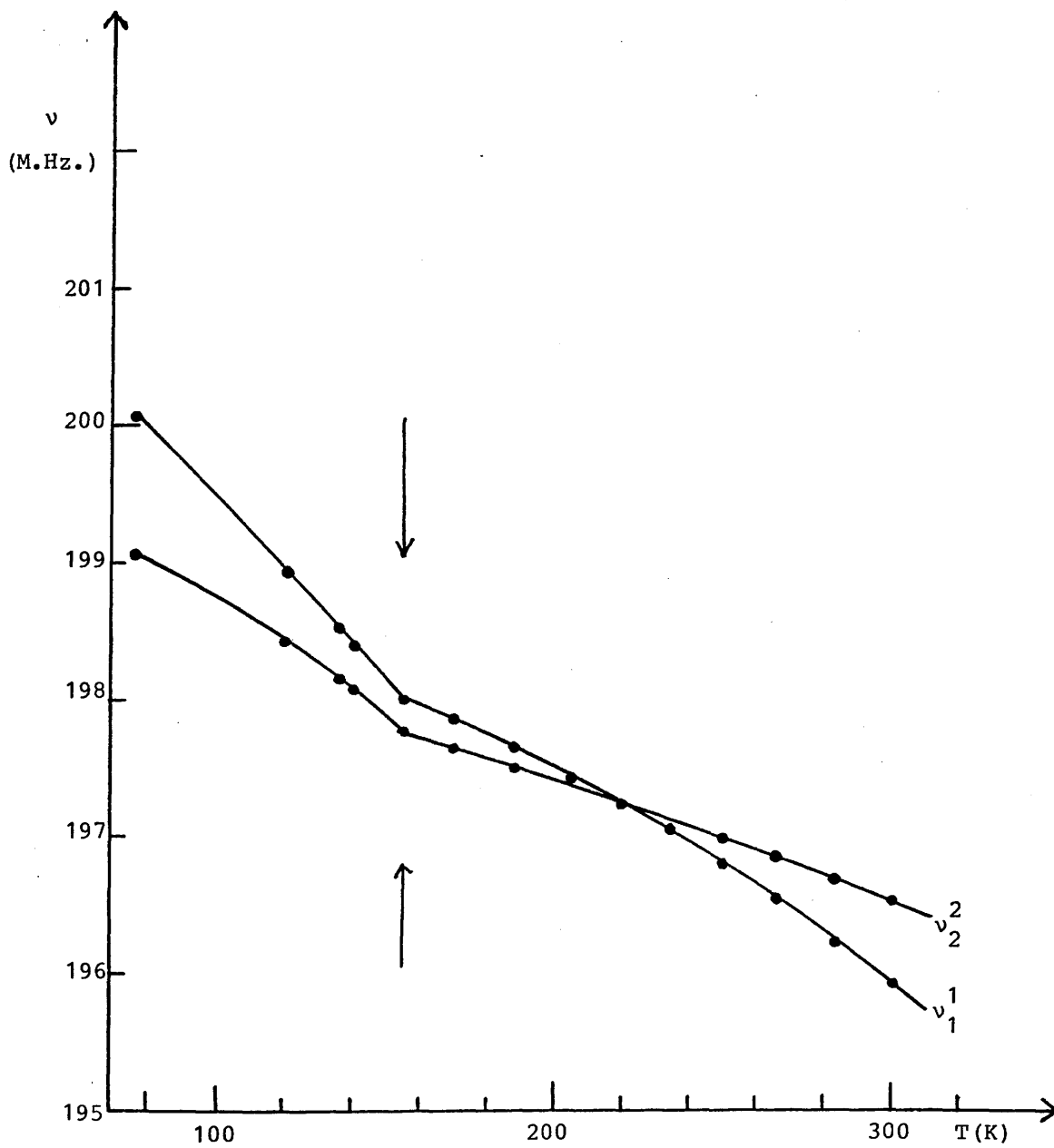


Figure 7.11 Bromine-79 N.Q.R. frequencies,  $\nu$ (M.Hz.), for  $\text{cis-N}_3\text{P}_3\text{Br}_3\text{Ph}_3$  vs. temperature (K)

Table 7.3

Coefficients calculated by fitting the best curves of the form

$$\nu = a + b'T + \frac{c'}{T}$$

to the experimental curves of N.Q.R. frequency versus temperature.

Compound	Isotope	Resonance	a	b'	c'
$N_3P_3Br_6$	$^{79}Br$	$\nu_{11}^2$	$239.25 \times 10^6$	-29110	$-340.6 \times 10^6$
		$\nu_{22}^1$	$238.63 \times 10^6$	-20800	$-252.7 \times 10^6$
		$\nu_{33}^2$	$245.55 \times 10^6$	-33240	$-318.4 \times 10^6$
		$\nu_{44}^1$	$244.56 \times 10^6$	-29880	$-5.8 \times 10^6$
	$^{81}Br$	$\nu_{11}^2$	$201.79 \times 10^6$	-28460	$-508.0 \times 10^6$
		$\nu_{22}^1$	$200.99 \times 10^6$	-20920	$-399.3 \times 10^6$
		$\nu_{33}^2$	$207.58 \times 10^6$	-33090	$-550.2 \times 10^6$
		$\nu_{44}^1$	$208.06 \times 10^6$	-32920	$-449.9 \times 10^6$
$N_3P_3Br_5NHPri$	$^{81}Br$	$\nu_{11}^1$	$176.01 \times 10^6$	-24620	$-167.5 \times 10^6$
		$\nu_{22}^1$	$194.73 \times 10^6$	-25660	$-384.7 \times 10^6$
		$\nu_{33}^1$	$196.20 \times 10^6$	-21250	$-41.0 \times 10^6$
		$\nu_{44}^1$	$199.36 \times 10^6$	-26080	$+110.2 \times 10^6$
		$\nu_{55}^1$	$204.68 \times 10^6$	-34130	$-385.1 \times 10^6$
cis- $N_3P_3Br_4(NMe_2)_2$	$^{81}Br$	$\nu_{11}^2$	$160.97 \times 10^6$	-17600	$+222.0 \times 10^6$
		$\nu_{22}^1$	$195.01 \times 10^6$	-27650	$-287.7 \times 10^6$
		$\nu_{33}^1$	$191.24 \times 10^6$	-18030	$+423.8 \times 10^6$
cis- $N_3P_3Br_3Ph_3$	$^{79}Br$	$\nu_{11}^1$	$204.17 \times 10^6$	-22910	$-410.1 \times 10^6$
		$\nu_{22}^2$	$193.27 \times 10^6$	+ 2970	$+731.2 \times 10^6$

a Values are in Hz., b' are in Hz.K<sup>-1</sup> and c' are in Hz.K.

These data are valid for temperatures greater than 200K.

Table 7.4

Thermal coefficients of halogen N.Q.R. signals in cyclotriphosphazatrienes.

Compound	Resonance	<sup>a</sup> ( $\partial\nu/\partial T$ ) <sub>P=1Kg.cm<sup>-2</sup>, T=295K</sub>		
		<sup>b</sup>		
		X = <sup>35</sup> Cl	X = <sup>79</sup> Br	X = <sup>81</sup> Br
N <sub>3</sub> P <sub>3</sub> X <sub>6</sub>	v <sub>1</sub> <sup>2</sup>	-3565	-25199	-22627
	v <sub>2</sub> <sup>1</sup>	-3120	-17898	-16328
	v <sub>3</sub> <sup>2</sup>	-3819	-29578	-26764
	v <sub>4</sub> <sup>1</sup>	-3877	-29809	-27750
N <sub>3</sub> P <sub>3</sub> X <sub>5</sub> NHPr <sup>i</sup>	v <sub>1</sub> <sup>1</sup>	-7615		-22697
	v <sub>2</sub> <sup>1</sup>	-6944		-21242
	v <sub>3</sub> <sup>1</sup>	-8926		-20777
	v <sub>4</sub> <sup>1</sup>	-7426		-27344
	v <sub>5</sub> <sup>1</sup>	-6136		-29701
cis-N <sub>3</sub> P <sub>3</sub> X <sub>4</sub> (NMe <sub>2</sub> ) <sub>2</sub>	v <sub>1</sub> <sup>2</sup>	-2673		-20153
	v <sub>2</sub> <sup>1</sup>	-3890		-24342
	v <sub>3</sub> <sup>1</sup>	-3677		-22903
cis-N <sub>3</sub> P <sub>3</sub> X <sub>3</sub> Ph <sub>3</sub>	v <sub>1</sub> <sup>1</sup>		-18197	
	v <sub>2</sub> <sup>2</sup>		-11373	

<sup>a</sup> ( $\partial\nu/\partial T$ )<sub>P=1Kg.cm<sup>-2</sup>; T=295K.</sub> Values are in Hz.K<sup>-1</sup>

<sup>b</sup> Taken from reference 4.

for the four signals that the  $(N-P)_3$  ring cannot be planar. <sup>(4)</sup> It must have a distorted slight-chair conformation, exaggerated in figure 7.12, in which  $N_1, N_3, P_4$  and  $P_6$  lie essentially in one plane,  $N_5$  lies slightly above the plane,  $P_2$  is displaced rather further below, and the resonance frequencies are assigned to the correspondingly numbered atoms as in figure 7.12. Furthermore, the relative deviations of the  $(\frac{\partial \nu}{\partial T})_{P=1\text{Kg.cm}^{-2}; T=295\text{K}}$  values from their mean, show that puckering in  $N_3P_3Br_6$  is greater than <sup>(4)</sup> in  $N_3P_3Cl_6$ . These arguments, based on quadrupole resonance data are all consistent with the X-ray analyses <sup>(16,17)</sup> carried out on this compound.

Figures 7.7 and 7.8 show explicitly that  $N_3P_3Br_6$  undergoes a single phase transition at 125K. A typical spectrum of the  $\nu_1$  resonance signal obtained for the bromine-79 nucleus in  $N_3P_3Br_6$  at 268K is illustrated in figure 7.13.

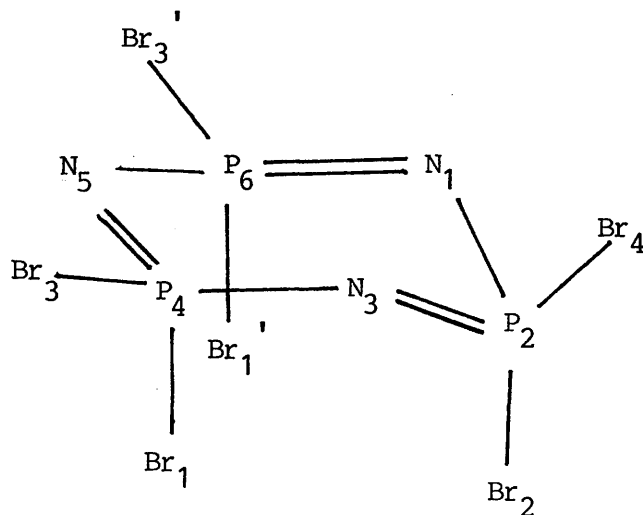


Figure 7.12 The structure of  $N_3P_3Br_6$ .

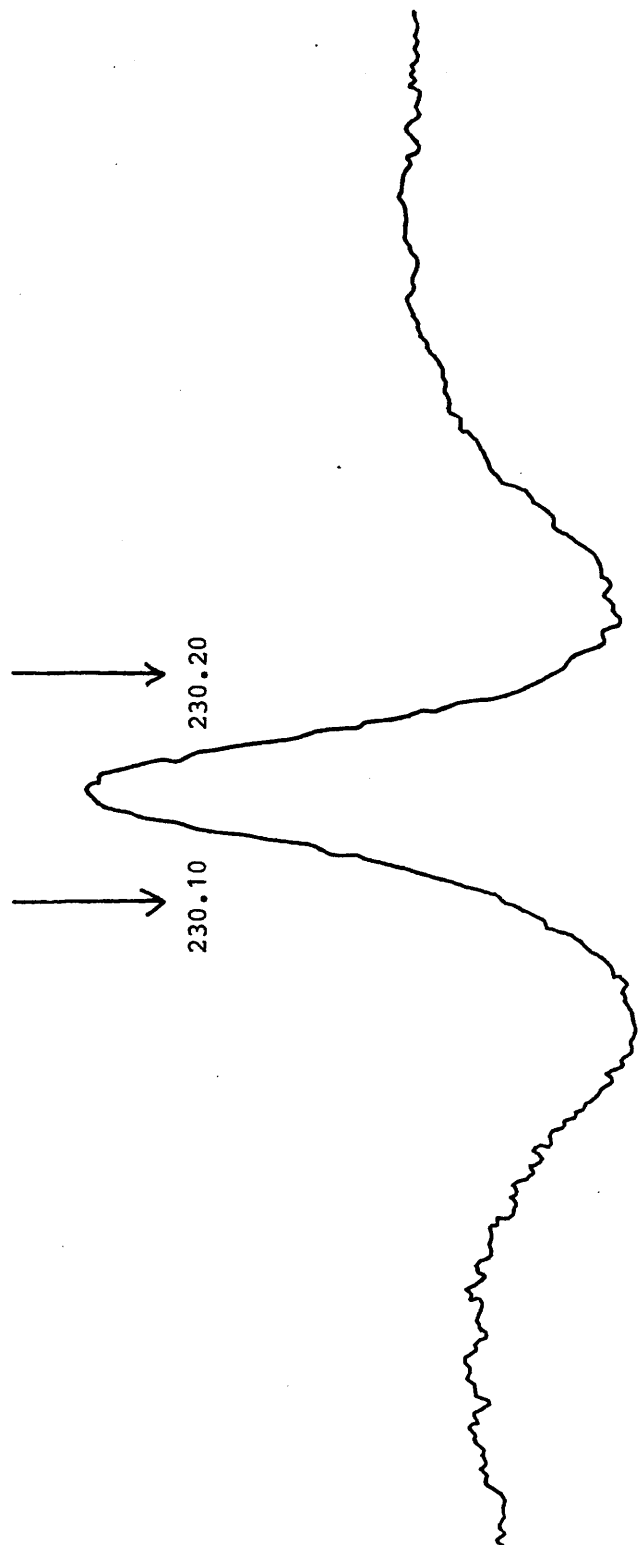


Figure 7.13 The  $\nu_1$  resonance of the bromine-79 N.Q.R. spectrum for  $N_3P_3Br_6$

at 268K recorded using Zeeman modulation.

Frequencies are given in M.Hz.

Figure 7.9 indicates that  $N_3P_3Br_5NHPr^i$  undergoes two phase transitions at 135K and 215K, but neither of these is as catastrophic as the change encountered<sup>(12)</sup> in  $N_3P_3Cl_5NHPr^i$ . The data in Table 7.4 again show that the (N-P)<sub>3</sub> ring is not planar. Furthermore, in  $\equiv PCl_2$  groups, halogen nuclei cis- to amino residues are known to have slightly lower quadrupole resonance frequencies,<sup>(4)</sup> and so  $\nu_2$  and  $\nu_3$  are assigned to the pseudo-equatorial bromine atoms cis to the  $-NHPr^i$  group. This conclusion and the data in Table 7.4 confirm the assignments of the resonances made earlier on the basis of the pressure measurements carried out on  $N_3P_3Br_5NHPr^i$ . It follows from Table 7.4 that in this molecule  $N_1$ ,  $P_2$ ,  $N_3$  and  $N_5$  are nearly coplanar,  $P_6$  moves down below this plane and  $P_4$  up, to produce a distorted slight twist-boat conformation shown in figure 7.14.

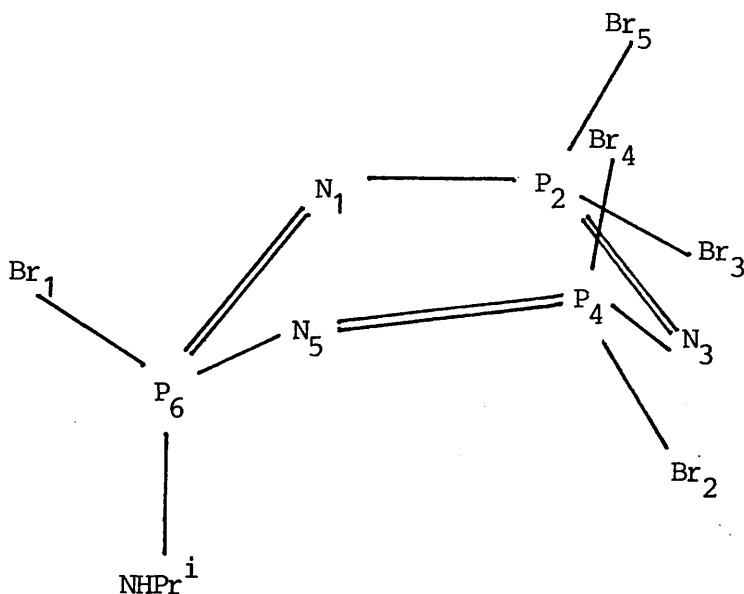


Figure 7.14 The structure of  $N_3P_3Br_5NHPr^i$ .

Figure 7.10 and Tables 7.2-7.4 indicate that the  $\text{cis-N}_3\text{P}_3\text{Br}_4(\text{NMe}_2)_2$  molecule is bisected by a plane of symmetry that is retained over the temperature range  $200 \leq T \leq 300\text{K}$  and this confirms the conclusion drawn earlier from the pressure measurements. Furthermore, Table 7.4 shows that the atoms  $\text{N}_1, \text{N}_3, \text{P}_4, \text{N}_5$  and  $\text{P}_6$  are very nearly coplanar, and  $\text{P}_2$  lies slightly above this plane as shown in figure 7.15.

Figure 7.10 shows clearly that the bromine-81 quadrupole resonance spectra of  $\text{cis-N}_3\text{P}_3\text{Br}_4(\text{NMe}_2)_2$  fade out at temperatures below 215K.

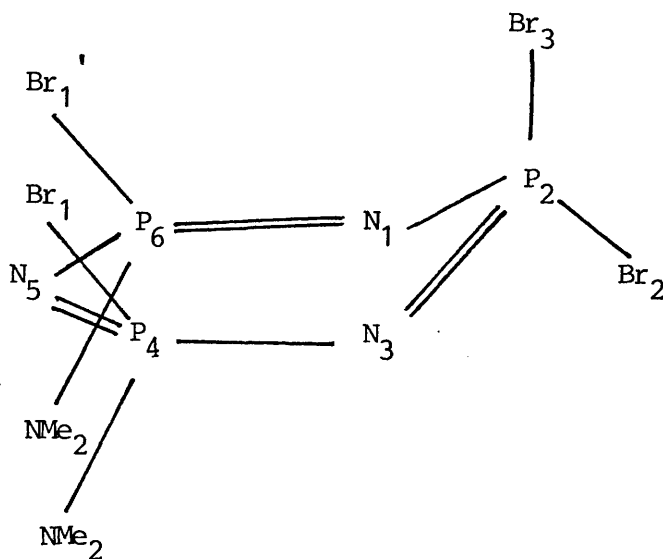


Figure 7.15 The structure of  $\text{cis-N}_3\text{P}_3\text{Br}_4(\text{NMe}_2)_2$ .

Figure 7.11 and Tables 7.2-7.4 again indicate that the  $\text{cis-N}_3\text{P}_3\text{Br}_3\text{Ph}_3$  molecule is bisected by a plane of symmetry that is retained over the entire temperature range  $77 \leq T \leq 300\text{K}$ . The data in Table 7.4 imply that in this molecule  $\text{N}_1, \text{N}_3, \text{P}_4$  and  $\text{P}_6$  lie very nearly

in the same plane,  $P_2$  lies slightly below the plane, and  $N_5$  is displaced further above to produce a slight-chair conformation exaggerated in figure 7.16. The N.Q.R. data in Table 7.4 show that the puckering in this molecule is greater than in  $N_3P_3Br_6$ .

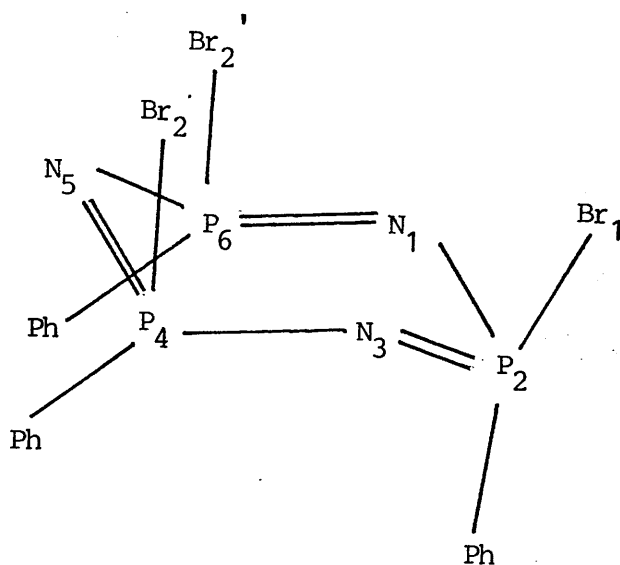


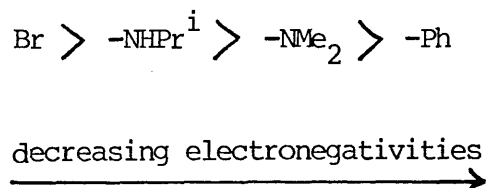
Figure 7.16 The structure of  $cis-N_3P_3Br_3Ph_3$ .

The quadrupole resonance data, therefore, imply that the molecular conformation of  $cis-N_3P_3Br_3Ph_3$  in our crystalline sample, m.p.  $193-195^\circ C$ , is similar to the molecular structure obtained from X-ray analysis<sup>(18)</sup> carried out on another crystalline system, m.p.  $162-163^\circ C$ , of  $cis-N_3P_3Br_3Ph_3$  which, unfortunately, has not been obtained in this work.

Furthermore, figure 7.11 indicates that  $\text{cis-N}_3\text{P}_3\text{Br}_3\text{Ph}_3$  undergoes a phase change at 155K: this is the phase change predicted from the pressure measurements discussed in the last section. The internal pressures generated on cooling this solid through the temperature range  $77 \leq T \leq 300\text{K}$  were high enough to force the expected phase transition to take place at the temperature indicated.

The data in Table 7.4 show that of the four bromocyclotriphosphazatriene derivatives considered in the present work, the  $(\text{N-P})_3$  ring in  $\text{cis-N}_3\text{P}_3\text{Br}_4(\text{NMe}_2)_2$  deviates least from planarity.

Furthermore, Table 7.2 shows that, in these cyclotriphosphazatrienes, amino residues are less electronegative than bromine atoms. The electronegativities of these functional groups decrease in the following order



Replacing a bromine atom by an amino residue therefore pushes the electron density on to neighbouring halogen atoms, neighbouring P-Br bonds then become more polar, the P-Br bond lengths increase, the electron densities on the remaining bromine atoms increase and hence the bromine nuclear quadrupole resonance frequencies decrease. This is an important point, since of the four commonly used electronegativity scales, the Pauling<sup>(19)</sup>, the Allred-Rochow<sup>(20)</sup>, the Sanderson<sup>(21)</sup> and the Mulliken-Jaffé scales<sup>(22,23)</sup> only the Sanderson scale places the relative electronegativities of nitrogen and bromine in an order that

is consistent with our N.Q.R. data, as shown in Table 7.5.

It should be noted that these conclusions, drawn from N.Q.R. data, are consistent with X-ray analyses<sup>(16-18)</sup> which show that the P-Br bond lengths<sup>(18)</sup> in  $\text{cis-N}_3\text{P}_3\text{Br}_3\text{Ph}_3$  (m.p. 162-164°C) are  $2.21(1)\text{\AA}$  and are significantly greater than<sup>(16,17)</sup>  $2.162(4)\text{\AA}$  found in  $\text{N}_3\text{P}_3\text{Br}_6$ .

Figure 7.17 is a plot of the bromine-81 nuclear quadrupole resonance frequencies versus the P-Br bond lengths for two compounds containing phosphorus-bromine bonds. These are approximately related by the expression

$$\nu_{81\text{Br}} \text{ (M.Hz.)} = 1903.10 - 787.48 \times d(\text{\AA}) \quad 7.1$$

so that if the bromine-81 quadrupole resonance frequency in a cyclotriphosphazatriene derivative is known then the P-Br bond length can be estimated to within  $0.004\text{\AA}$ .

Figure 7.18 shows that the bromine-81 nuclear quadrupole resonance frequencies are approximately linearly related to the corresponding chlorine-35 frequencies, within the chlorine frequency range  $19 \leq \nu \leq 29$  M.Hz., for several compounds containing halogen-phosphorus bonds. This relationship can be expressed by the following equation

$$\nu(^{81}\text{Br}) = 8.121 \nu(^{35}\text{Cl}) - 29.4 \quad 7.2$$

and it enables bromine-81 quadrupole resonance frequencies to be predicted to within a few M.Hz. if the chlorine-35 resonance frequencies in the corresponding chlorocyclotriphosphazatriene derivatives are known.

It now follows from equation 7.2 and figure 7.18 that the bromine-81 nucleus is a very much more sensitive monitor of both physical and

Table 7.5

The electronegativities of nitrogen and bromine.

Element	Scale			
	Pauling	Allred-Rochow	Sanderson	Mulliken-Jaffé
N	3.04	3.07	2.93	~12
Br	2.96	2.74	2.96	8.40

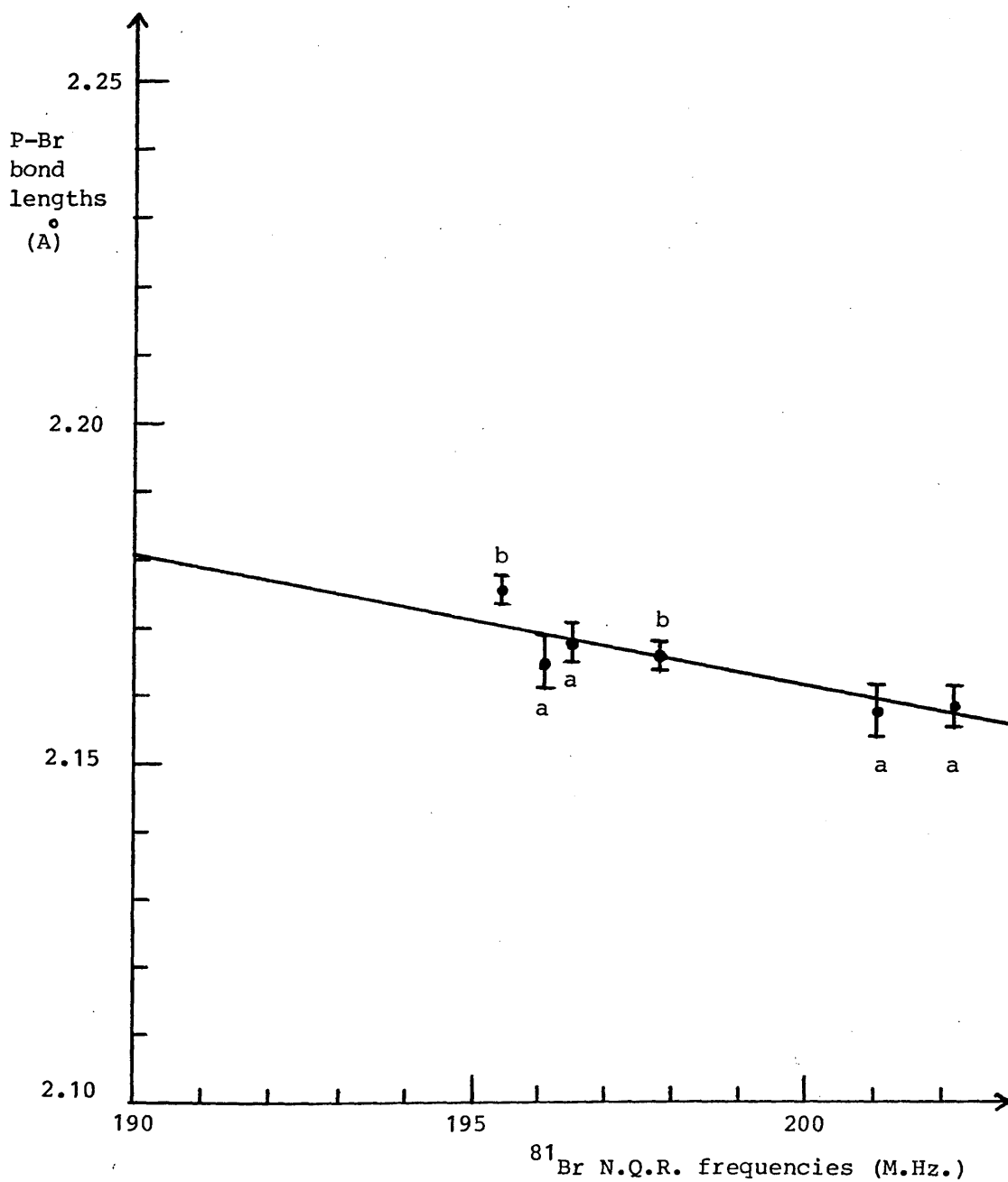


**Figure 7.17** Plot of bromine-81 N.Q.R. frequencies vs. P-Br bond lengths.

a =  $N_3P_3Br_6$  at 77K (references 16, 17 and 24)

b =  $N_4P_4Br_8$  at 297K (references 25 and 7).

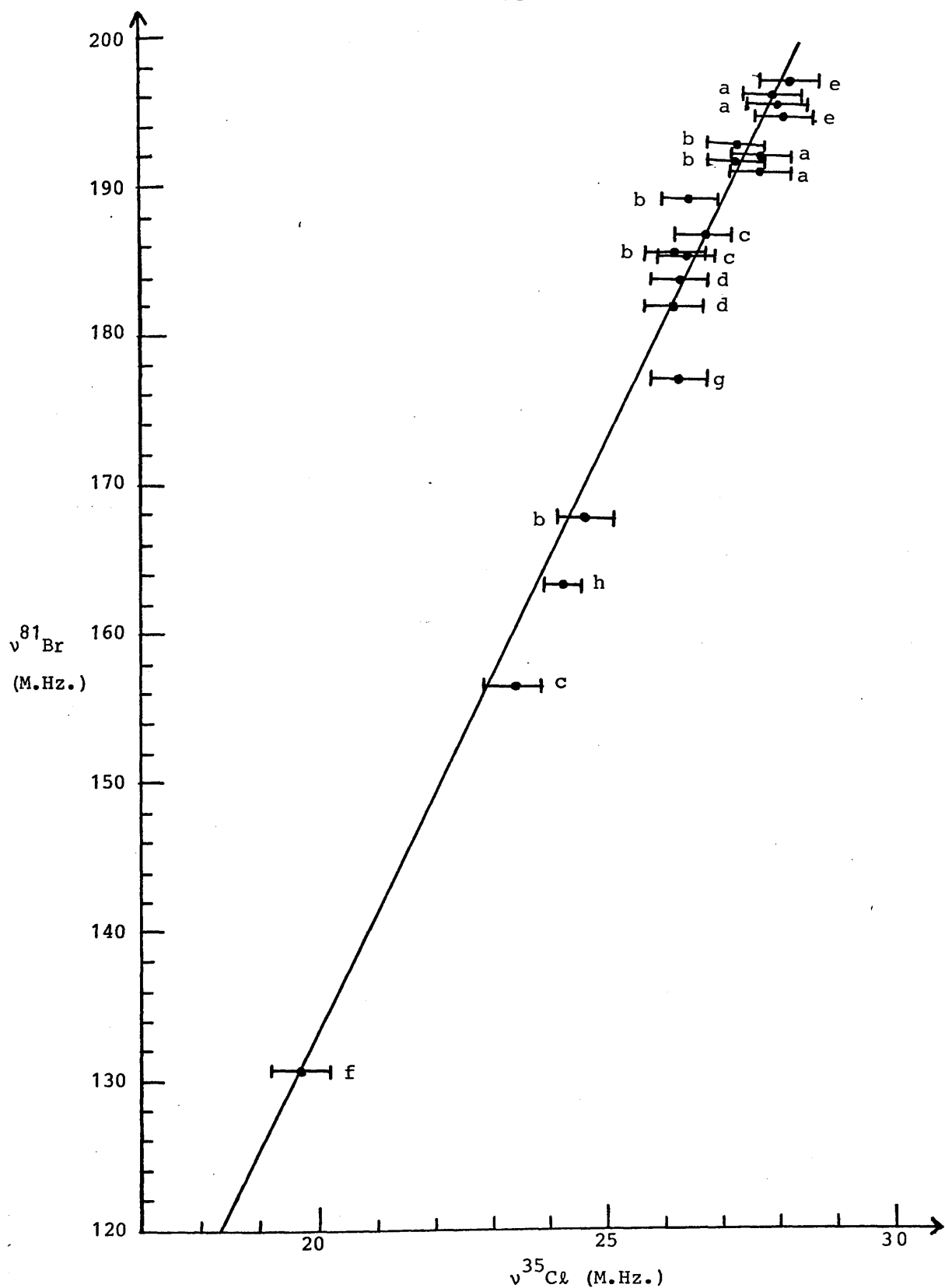


**Figure 7.18** Plot of bromine-81 vs. chlorine-35 N.Q.R. frequencies.  
 a= $N_3P_3X_6$  at 293K(ref.4); b= $N_3P_3X_5NHPr^i$  at 293K (ref.4);  
 c= $N_3P_3X_4(NMe_2)_2$  at 293K(ref.4); d= $PX_3$  at 83K (ref.26);  
 e= $N_4P_4X_8$  at 77K (refs.7 and 26); f= $N_2P_2X_2Bu^t_2$  at 293K;  
 g= $PhPX_2$  at 77K; h= $N_3P_3X_3Ph_3$  at 293K (ref. 27).

chemical changes than the chlorine-35 nucleus. Tables 7.1 and 7.4 show that the bromine nuclei are much more sensitive to changes in pressure<sup>(4,12)</sup> and in temperature than chlorine-35.

Furthermore, equation 7.2 and figure 7.18 explicitly indicate that substitution of a bromine atom in a  $\equiv\text{PBr}_2$  group by an amino residue lowers the resonance frequency of the remaining bromine nucleus by about eight times as much as is observed in the corresponding chloro-derivatives.

A comparison of the data obtained for the bromocyclotriphosphazatrienes, given in Tables 7.1 and 7.4, with similar data obtained in the case of bromocyclodiphosphazane  $(\text{BrPNBu}^t)_2$ , given in Table 6.4, shows that the N.Q.R. data cannot discriminate between phosphorus(III) and phosphorus(V) ring systems in these bromo derivatives.

(ii) Constant volume conditions

The data given in Tables 7.1 and 7.4 now enable the rate of change of frequency with temperature,  $(\frac{\partial\nu}{\partial T})_V$ , under constant volume conditions to be estimated using equation 2.48. The ratio  $\frac{\alpha}{\chi}$  required for this treatment again assumed to be  $23 \text{ Kg.cm}^{-2} \text{ K}^{-1}$ . Values of  $(\frac{\partial\nu}{\partial T})_V$  obtained for these bromocyclotriphosphazatriene derivatives are documented in Table 7.6.

The differences between the data given in the last table and the  $(\frac{\partial\nu}{\partial T})_{P,T}$  values given in Table 7.4 reveal the effects of changes in the volume of the solid, with lowering temperature, on these quadrupole resonance frequencies.

Table 7.6

Thermal coefficients, under constant volume conditions, for bromocyclotriphosphazatrienes at 295K.

Compound	Isotope	Resonance	$\left(\frac{\partial v}{\partial T}\right)_{V, T=295K}$
$N_3P_3Br_6$	$^{79}Br$	$\nu_1^2$	-19591
		$\nu_1^1$	-17898
		$\nu_2^2$	-17193
		$\nu_3^2$	-16724
		$\nu_4^1$	-16724
	$^{81}Br$	$\nu_1^2$	-18703
		$\nu_1^1$	-16328
		$\nu_2^2$	-17147
		$\nu_3^2$	-17609
		$\nu_4^1$	-17609
$N_3P_3Br_5NHPr^i$	$^{81}Br$	$\nu_1^1$	-17885
		$\nu_1^2$	-18130
		$\nu_2^1$	-18442
		$\nu_3^1$	-18839
		$\nu_4^1$	-18721
$cis-N_3P_3Br_4(NMe_2)_2$	$^{81}Br$	$\nu_1^2$	-16621
		$\nu_1^1$	-24342
		$\nu_2^1$	-21597
$cis-N_3P_3Br_3Ph_3$	$^{79}Br$	$\nu_1^1$	-25721
		$\nu_2^2$	-19550

Values of  $\left(\frac{\partial v}{\partial T}\right)_V$  are given in  $Hz.K^{-1}$ .

7.4. THE EFFECTS OF WEAK MAGNETIC FIELDS ON BROMINE-81 N.Q.R. SPECTRA  
OF  $N_3P_3Br_6$

Each bromine-81 quadrupole resonance signal obtained from a polycrystalline sample of  $N_3P_3Br_6$  was examined in applied magnetic fields within the range  $0 \leq H_O \leq 40$  Gauss, and attempts were made to use Morino and Toyama's<sup>(28)</sup> method to obtain asymmetry parameters for each bromine nucleus in this molecule.

The effects of magnetic fields on the four resonance signals,  $\nu_1, \nu_2, \nu_3$  and  $\nu_4$  are found to be identical and so the data obtained for the  $\nu_1$  resonance are discussed in detail as an example. A typical spectrum obtained for this resonance, when  $H_O = 23.85$  Gauss, is shown in figure 7.19. The spectra were all recorded using the Decca N.Q.R. spectrometer and the computer of average transients.

The asymmetry parameters,  $\eta$ , were found to be too small to be accurately measured by this method, however the results were good enough to measure the line width parameters,  $\delta$ , and plotting of  $\delta(2\nu_L)^{-1}$  against  $H_O^{-1}$  then enables an upper limit of 0.02 to be placed on the value of  $\eta$ . Values of  $\delta$  and  $\delta(2\nu_L)^{-1}$  obtained for the  $\nu_1$  resonance signal are given in Table 7.7 and the plot of  $\delta(2\nu_L)^{-1}$  versus  $H_O^{-1}$  is shown in figure 7.20. The asymmetry parameters are then measured and used, with the observed quadrupole resonance frequencies, to obtain the quadrupole coupling constants,  $\frac{eQq}{h}$ , in this solid using equation 1.32; these data are given in Table 7.8.

The data in this table and the atomic quadrupole coupling constant, 643.032 M.Hz., for the bromine-81 nucleus<sup>(29)</sup> then enable the  $\pi$ -characters

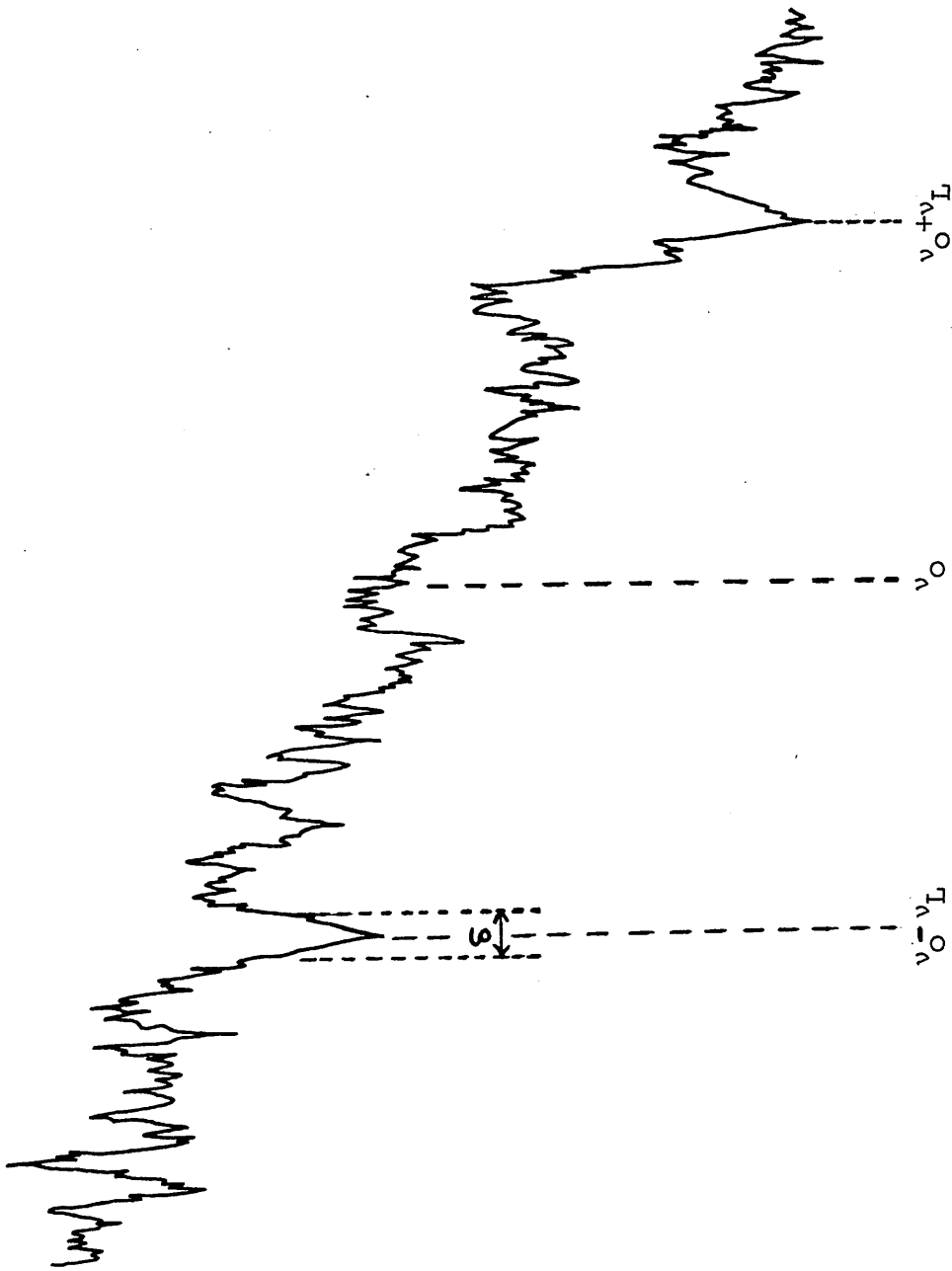


Figure 7.19 The  $\nu_1$  resonance signal of the bromine-81 quadrupole spectrum of  $N_3P_3Br_6$  subjected to a magnetic field of 23.85 Gauss.

Table 7.7

Linewidth parameters,  $\delta$ , and  $\delta(2\nu_L)^{-1}$  measured from the analysis of the  $\nu_1$  quadrupole signal of  $N_3P_3Br_6$  in weak magnetic fields.

Magnetic field (Gauss)	Larmor frequency for bromine-81 nucleus (K.Hz.)	$\delta$ (K.Hz.)	$\frac{\delta}{2\nu_L}$
12.15	13.970	4.341	0.155
16.05	18.454	4.443	0.120
20.00	22.996	4.295	0.093
23.85	27.423	4.293	0.078
27.75	31.907	4.166	0.065
31.65	36.391	4.433	0.061
35.50	40.818	4.675	0.057
39.40	45.302	4.100	0.045

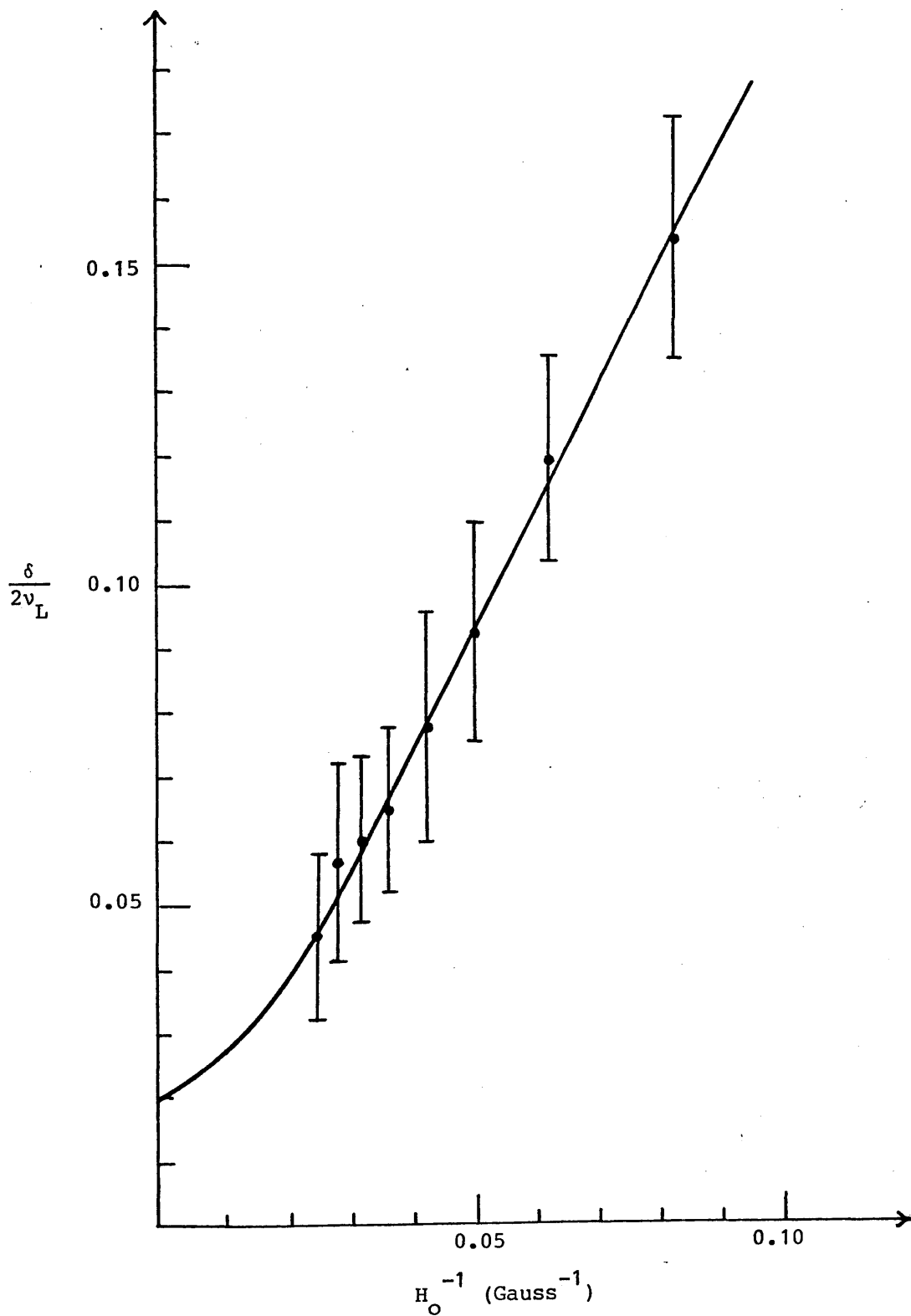


Figure 7.20 Plot of  $\delta(2\nu_L)^{-1}$  vs.  $H_0^{-1}$  for the  $\nu_1$  resonance of the bromine-81 nucleus in  $N_3P_3Br_6$  at 299K.

Table 7.8

Bromine-81 quadrupole resonance frequencies, asymmetry parameters and quadrupole coupling constants obtained for  $N_3P_3Br_6$  at 299K.

Resonance	N.Q.R. frequency at 299K (M.Hz.)	$\eta$	(eqQ/h) (M.Hz.)
$\nu_1$	$191.550 \pm 0.001$	$0.02 \pm 0.02$	$383.074 \pm 0.04$
$\nu_2$	$193.390 \pm 0.001$	$0.02 \pm 0.02$	$386.754 \pm 0.04$
$\nu_3$	$195.834 \pm 0.001$	$0.02 \pm 0.02$	$391.642 \pm 0.04$
$\nu_4$	$196.713 \pm 0.001$	$0.02 \pm 0.02$	$393.419 \pm 0.04$

in the P-Br bonds to be approximately estimated by means of equation 6.1. The  $\pi$ -bonding has turned out to contribute only about 0.4% to the nature of the P-Br bonds in the  $N_3P_3Br_6$  molecule. The N.Q.R. data, therefore, imply that the  $\pi$ -bonding in this molecule has only a very minute importance, as is found in the corresponding chloro derivative.<sup>(4)</sup>

APPENDIX - 7

PREPARATION OF THE BROMOCYCLOTRIPHOSPHAZATRIENE DERIVATIVES

7.1 Preparation of  $N_3P_3Br_6$

Hexabromotriphosphazatriene,  $N_3P_3Br_6$ , is prepared<sup>(8)</sup> by mixing 300 g (3.06 mols) of dry and finely ground  $NH_4Br$ , 300 g (1.10 mols) of  $PBr_3$  and 600 ml of dry sym-tetrachloroethane in a 2ℓ round-bottomed flask fitted with a dropping funnel containing 350 g (2.19 mols) of bromine and an efficient condenser equipped with a drying tube containing  $P_2O_5$ . The reaction is started by adding about one-half of the bromine, the mixture is then shaken thoroughly and the flask is immersed in an oil bath. The temperature of the bath is raised gradually to  $142^\circ C$ , over a period of 5 days, and maintained at this temperature for an additional 5 days. The remaining bromine is added in small portions while the reaction proceeds in order to compensate for losses from the evolution of hydrogen bromide and bromine vapours which starts at about  $100^\circ C$ .

At the end of the reaction period, the unreacted  $NH_4Br$  is removed by filtering the hot suspension through a sintered-glass funnel. The dark brown filtrate is then evaporated under reduced pressure (2mm Hg.) with a water bath, the temperature of which is raised gradually to  $80-90^\circ C$  for complete removal of the solvent.

The residue is then refluxed in 800 ml of anhydrous benzene for 12 hours using an oil bath at  $90^\circ C$ , and the benzene layer is decanted from the remaining solid. The extraction process is repeated several

times using a fresh 500 ml portion of anhydrous benzene in each extraction. The combined benzene extracts are then evaporated to give a dark semicrystalline mixture containing the trimer, the tetramer and the oily higher polymeric homologues. Subliming this mixture at 160-180°C under reduced pressure (0.25-0.50 mm Hg.) enables the trimer and the tetramer to be almost completely separated from the higher homologues which polymerize to a rubber. The coloured sublimate is resublimed to form a white crystalline mixture which contains the trimer and about 8% of the tetramer.

These components are simply separated by fractional crystallization from petroleum ether (b.p. 90-100°C). The white mixture is dissolved in sufficient hot solvent to obtain a nearly saturated solution which is cooled slowly to form the characteristic flat prismatic crystals of  $N_3P_3Br_6$  which are periodically removed from the mixture before the needle-like crystals of the tetramer are formed. The latter remain in the mother liquor which is decanted and the process is repeated with the decantate until about 70-75% of the trimer is recovered. Further recrystallizations of the trimer from the same solvent, using activated charcoal as a decolourising agent, enable pure crystals of  $N_3P_3Br_6$  to be obtained, melting point 192°C.

## 7.2 Preparation of cis-N<sub>3</sub>P<sub>3</sub>Br<sub>4</sub>(NMe<sub>2</sub>)<sub>2</sub>

This derivative is synthesised<sup>(9)</sup> by adding 18.9 ml. of 10% aqueous solution of dimethylamine (0.04 mols) dropwise, over a period of 30 minutes, to a well stirred solution of 6.15 g (0.01 mol) of N<sub>3</sub>P<sub>3</sub>Br<sub>6</sub> in 150 ml ether at 18°C. The ether layer is then separated, dried over anhydrous sodium sulphate, and evaporated to dryness to give the crystalline raw product. The product is recrystallized 4-5 times from petroleum ether (b.p. 80-100°C) to obtain pure crystals of cis-N<sub>3</sub>P<sub>3</sub>Br<sub>4</sub>(NMe<sub>2</sub>)<sub>2</sub>, melting point 131-134°C.

### 7.3 Preparation of cis-N<sub>3</sub>P<sub>3</sub>Br<sub>3</sub>Ph<sub>3</sub>

The preparation of this compound<sup>(10)</sup> is started by mixing 40 g (0.41 mols) of finely ground and dried ammonium bromide and 70 ml of dry bromobenzene in a 1ℓ three-necked flask equipped with a dropping funnel, a mechanical stirrer, and an efficient reflux condenser fitted with a drying tube containing calcium chloride. A solution of 20 g (0.075 mols) of phenyldibromophosphine in 10 ml of bromobenzene is added to the well-stirred mixture. A solution of 12 g (0.075 mols) of dry bromine in 10 ml of bromobenzene is then added dropwise, with continuous stirring, over a period of 10 hours.

The reaction flask is then placed in an oil bath which is heated gradually to 170-180°C over a period of 3-4 hours and the mixture is stirred at this temperature for 24-48 hours, until the evolution of hydrogen bromide ceases. The hot mixture is filtered through sintered glass, washed with a few millilitres of fresh dry bromobenzene and the unreacted ammonium bromide is removed. The combined filtrate and washings are transferred to a 1ℓ single-necked flask placed in an oil bath and the solvent is removed under reduced pressure (3.5 mm Hg.) while the temperature of the bath is gradually raised to 90°C and the receiving flask is cooled in a Dry Ice-acetone mixture. The dark viscous product is then extracted with five successive 70 ml portions of boiling dry n-heptane and each extract is stored separately in a refrigerator, at about 3°C, for 5-6 days. This enables a crude crystalline product to be obtained together with an oily material which solidifies slowly under n-heptane.

The combined crude product is then purified by 3-4 recrystallizations from n-heptane with activated charcoal added initially to remove traces of colour. In each crystallization, the solid product is dissolved in about 100 ml of n-heptane, boiled under reflux for few minutes and then stored in a refrigerator for 2-3 days. Pure crystals of cis-1,3,5-tribromo-1,3,5-triphenylcyclotriphosphazene are obtained, m.p. 193-195°C.

7.4 Preparation of  $N_3P_3Br_5NMe_2$

The title compound is prepared<sup>(11)</sup> by reacting 45 ml of a 2% aqueous solution of dimethylamine, (0.02 mols) with 6.15 g (0.01 mol) of  $N_3P_3Br_6$ , dissolved in 150 ml ether, at 18°C using the same preparation procedure described in 7.2. In this reaction a mono-substituted derivative,  $N_3P_3Br_5NMe_2$ , is obtained, melting point 112-113.5°C.

7.5 Preparation of  $N_3P_3Br_5NHPr^i$

This derivative was prepared by reacting isopropylamine with  $N_3P_3Br_6$ , using the procedure described in the reference (11) for preparing  $N_3P_3Br_5NMe_2$ .

59.7 ml of a 2% aqueous solution of isopropylamine (0.02 mols) is added dropwise, over 30 minutes, to a stirred solution of 6.15 g (0.01 mol) of  $N_3P_3Br_6$  in 150 ml ether at ambient temperature. The ether layer was separated, dried over anhydrous sodium sulphate, and evaporated to give a white crystalline product which gives pure  $N_3P_3Br_5NHPr^i$ , melting point  $82-83^\circ C$ , after 5-6 recrystallizations from petroleum ether (b.p.  $80-100^\circ C$ ).

R E F E R E N C E S

CHAPTER 1

1. C.P. Slichter, "Principles of Magnetic Resonance", Harper and Row, New York, N.Y., 1963, Chapter 6
2. J.A.S. Smith, J. Chem. Ed., 1971, 48, 39
3. E. Schempp and P.J. Bray, "Physical Chemistry", H. Eyring, D. Henderson and W. Jost eds., Academic Press Inc., New York, N.Y., 1970, IV, Chapter 11
4. E.A.C. Lucken, "Nuclear Quadrupole Coupling Constants", Academic Press Inc., New York, N.Y., 1969
5. F.A. Bovey, "Nuclear Magnetic Resonance Spectroscopy", Academic Press Inc., New York and London 1969

CHAPTER 2

1. E. Schempp and P.J. Bray, "Physical Chemistry", H. Eyring, D. Henderson and W. Jost eds., Academic Press Inc., New York, N.Y., 1970, IV, Chapter 11
2. H. Bayer, Z. Physik, 1951, 130, 227
3. T. Kushida, J. Sci., Hiroshima Univ., 1955, A19, 327
4. T. Kushida, G.B. Benedek and N. Bloembergen, Phys. Rev., 1956, 104, 1364

5. H.G. Dehmelt and H. Krüger, Z. Physik, 1951, 129, 401
6. M.M. McEnnan and E. Schempp, "Advances in Nuclear Quadrupole Resonance", J.A.S. Smith ed., Hyden, London, 1974, 1, 263
7. M.M. McEnnan and E. Schempp, J. Mag. Res., 1973, 11, 28
8. M.M. McEnnan and E. Schempp, J. Mag. Res., 1974, 16, 424
9. M. Zdanowska, J. Stankowski and M. Mackowiak, J. Mag. Res., 1978, 31, 109
10. W.H. Dalgleish, Ph.D. Thesis, Glasgow University, 1975
11. E.A.C. Lucken, J. Mol. Struct., 1980, 58, 121 and references therein
12. R.Sh. Lotfullin and G.K. Semin, "Advances in Nuclear Quadrupole Resonance", J.A.S. Smith ed., Hyden, London, 1975, 2, 1
13. K.W. Moore, Ph.D. Thesis, Glasgow University, 1968
14. G.A. Matzkanin, T.N. O'Neal, T.A. Scott and P.J. Haigh, J. Chem. Phys., 1966, 44, 4171 and references therein
15. T. Fuke, J. Phys. Soc. Japan, 1961, 16, 266
16. R.J.C. Brown, J. Chem. Phys., 1960, 32, 116
17. B.D. Saksena, J. Chem. Phys., 1950, 18, 1653
18. L.V. Jones, M. Sabir and J.A.S. Smith, J. Chem. Soc., Faraday II, 1978, 1723

19. G.J. D'Alessio and T.A. Scott, J. Mag. Res., 1971, 5, 416
20. T.C. Wang, Phys. Rev., 1955, 99, 566

CHAPTER 3

1. T. Kushida, Y. Koi and Y. Imada, J. Phys. Soc. Japan, 1954, 9, 809
2. S. Kojima, K. Tsukada and Y. Hinaga, J. Phys. Soc. Japan, 1955, 10, 498
3. Y. Morino, T. Chiba, T. Shimosawa and M. Toyama, J. Phys. Soc. Japan, 1958, 13, 869
4. V. Rehn, J. Chem. Phys., 1963, 38, 749
5. Y. Morino and M. Toyama, J. Chem. Phys., 1961, 35, 1289
6. J.D. Graybeal and P.J. Green, J. Phys. Chem., 1969, 73, 2948
7. Dinesh and P.T. Narasimhan, J. Chem. Phys., 1966, 45, 2170
8. J.A.S. Smith and D.A. Tong, J. Chem. Soc., 1971, A, 173
9. W.H. Dalglish, Ph.D. Thesis, Glasgow University, 1975
10. C. Dean, Phys. Rev., 1952, 86, 607
11. C. Dean, Phys. Rev., 1954, 96, 1053
12. T.P. Das and E.L. Hahn, Solid State Physics, Suppl. 1, 1958, p.7
13. M. Toyama, J. Phys. Soc. Japan, 1959, 14, 1727

14. F.J. Adrian, J. Chem. Phys., 1958, 29, 1381
15. R.B. Creel, S.L. Segel and L.A. Anderson, J. Chem. Phys., 1969, 50, 4908
16. J. Darville, A. Gerard and M.T. Calende, J. Mag. Res., 1974, 16, 205
17. J. Darville and A. Gerard, Computer Physics Communications, 1975, 9, 173

#### CHAPTER 4

1. J.A.S. Smith, J. Chem. Ed., 1971, 48, A77
2. Decca N.Q.R. Spectrometer Handbook, Decca Radar Ltd., Instrument Division, Walton-on-Thames, England
3. T.P. Das and E.L. Hahn, "Solid State Physics", Academic Press, Inc., New York, N.Y. 1958, Suppl. 1, 88
4. J.A.S. Smith and D.A. Tong, J. Phys., 1968, E1, 8
5. J.C. Carter, J.A.S. Smith, J.W.R. Cook and P.M. Butcher, "Advances in Nuclear Quadrupole Resonance", J.A.S. Smith ed., Hyden, London, 1974, 1, 191
6. A. Narath, W.J. O'Sullivan, W.A. Robinson and W.W. Simmons, Rev. Sci. Instrum. 1964, 35, 476
7. J.R. Whitehead, "Super Regenerative Receivers", Cambridge University Press, Cambridge, 1950, p.105

8. J.A.S. Smith, J. Chem. Ed., 1971, 48, A147
9. I.A. Safin, B.N. Pavlov and D. Stern, Ya. Zavod. Lab., 1964, 30, 676
10. E.S. Mooberry, H.W. Spiess, B.B. Garrett and R.K. Sheline, J. Chem. Phys., 1969, 59, 1970
11. R.E. Slusher and E.L. Hahn, Phys. Rev., 1968, 166, 332
12. D.T. Edmonds, M.J. Hunt, A.L. Mackay and C.P. Summers, "Advances in Nuclear Quadrupole Resonance", J.A.S. Smith ed., Hyden, London, 1974, 1, 145
13. D.T. Edmonds and J.P.G. Mailer, J. Mag. Res., 1977, 26, 93
14. J.A.S. Smith, J. Mol. Struct., 1980, 58, 1
15. Y. Hsieh, J.C. Koo and E.L. Hahn, Chem. Phys. Lett., 1972, 13, 563
16. D.T. Edmonds and P.A. Speight, Phys. Lett., 1971, A34, 325
17. D.T. Edmonds, M.J. Hunt and A.L. Mackay, J. Mag. Res., 1973, 9, 66
18. B. Herzog and E.L. Hahn, Phys. Rev., 1956, 103, 148

CHAPTER 5

1. R.M. Hart and M.A. Whitehead, J. Chem. Soc., 1971, A, 1738
2. R.M. Hart and M.A. Whitehead, Mol. Phys., 1970, 19, 383
3. M. Hashimoto, T. Morie and Y. Kato, Bull. Chem. Soc., Japan, 1971, 44, 1455

4. E.A.C. Lucken and M.A. Whitehead, *J. Chem. Soc.*, 1961, 2459
5. M. Kaplansky, R. Clipsham and M.A. Whitehead, *J. Chem. Soc.*, 1969, A, 584 and references therein.
6. D.U. Zakirov, I. Ya. Kuramshin, I.A. Safin, A.N. Pudovik and L.A. Zhelonkina, *J. Gen. Chem. U.S.S.R.*, 1977, 47, 1522
7. R.R. Holmes, R.P. Carter and G.E. Peterson, *Inorg. Chem.*, 1964, 3, 1748
8. H. Chihara, N. Nakamura and S. Seki, *Bull. Chem. Soc. Japan*, 1967, 40, 50
9. V.I. Svergun, V.G. Rozinov, E.F. Grechkin, V.G. Timokhin, Yu.K. Maksyutin and G.K. Semin, *Izv. Akad. Nauk. SSSR, Ser. Khim.*, 1970, 8, 1918
10. R. Keat, A.L. Porte, D.A. Tong and R.A. Shaw, *J. Chem. Soc. Dalton*, 1972, 1648
11. A.D. Gordeev, E.S. Kozlov and G.B. Soifer, *Zhur. Strukt. Khim.*, 1973, 14, 934
12. J.F. Nixon, *J. Chem. Soc.*, 1968, A, 2689
13. W. Kuchen and W. Gr<sup>u</sup>newald, *Angew. Chem. Internat. Ed.*, 1963, 2, 399
14. J. Emsley, J. Moore and P.B. Udy, *J. Chem. Soc.*, 1971, A, 2863
15. R. Livingston, *J. Phys. Chem.*, 1953, 57, 496

16. W.H. Dalgleish, Ph.D. Thesis, Glasgow University, 1975
17. H. Robinson, H.G. Dehmelt and W. Gordy, J. Chem. Phys., 1954, 22, 511
18. I.J. Colquhoun and W. McFarlane, J. Chem. Soc. Faraday Trans. II, 1977, 722
19. D.W.J. Cruickshank, Acta Cryst., 1964, 17, 671
20. M.A. Whitehead, Canad. J. Chem., 1964, 42, 1212

CHAPTER 6

1. R. Clipsham, R.M. Hart and M.A. Whitehead, Inorg. Chem., 1969, 8, 2431
2. M. Kaplansky and M.A. Whitehead, Canad. J. Chem., 1967, 45, 1669
3. W.H. Dalgleish, R. Keat, A.L. Porte and R.A. Shaw, J. Mag. Res., 1975, 20, 351
4. A. Connelly, W.H. Dalgleish, P. Harkins, R. Keat, A.L. Porte, I. Raitt and R.A. Shaw, J. Mag. Res., 1978, 30, 439
5. W.H. Dalgleish, Ph.D. Thesis, Glasgow University, 1975 and references therein.
6. R. Keat, A.L. Porte, R.A. Shaw and D.A. Tong, J. Chem. Soc. Dalton, 1972, 1648
7. A.D. Gordeev, E.S. Kozlov and G.B. Soifer, Zhur. Struct. Khim., 1973, 14, 934

8. W.H. Dalglish, R. Keat, A.L. Porte and R.A. Shaw, J.C.S. Dalton Trans., 1977, 1505
9. Kareem Sh. Ahmed, D.A. Harvey, R. Keat, A.L. Porte and D.S. Rycroft, Unpublished work
10. A.R. Davies, A.T. Dronsfield, R.N. Haszeldine and D.R. Taylor, J.C.S. Perkin I, 1973, 379
11. R. Jefferson, J.F. Nixon, T.M. Painter, R. Keat and L. Stobbs, J.C.S. Dalton, 1973, 1414
12. W. Zeiss and J. Weis, Z. Naturforsch, 1977, 32b, 485
13. K.W. Muir and J.F. Nixon, J.C.S. Chem. Comm., 1971, 1405
14. K.W. Muir, J.C.S. Dalton, 1975, 259
15. R. Livingston, J. Phys. Chem., 1953, 57, 496
16. K. Hedberg and M. Iwasaki, J. Chem. Phys., 1962, 36, 589
17. W.H. Dalglish and A.L. Porte, J. Mag. Res., 1975, 20, 359
18. R. Keat, Unpublished work
19. O.J. Scherer and W. Gläsel, Chem. Ber., 1977, 110, 3874
20. H. Robinson, H.G. Dehmelt and W. Gordy, J. Chem. Phys., 1954, 22, 511
21. Y. Morino and M. Toyama, J. Chem. Phys., 1961, 35, 1289

22. V. Rehn, J. Chem. Phys., 1963, 38, 749
23. C. Dean, Phys. Rev., 1952, 86, 607
24. C.H. Townes and B.P. Dailey, J. Chem. Phys., 1949, 17, 782
25. J.A.S. Smith, J. Chem. Ed., 1971, 48, 39
26. V. Jaccarino and J.G. King, Phys. Rev., 1951, 63, 471
27. J.G. King and V. Jaccarino, Phys. Rev., 1954, 94, 1610
28. G.B. Benedek, "Magnetic Resonance at High Pressure", Interscience, New York, N.Y., 1963
29. W. Paul and D.M. Warschauer eds., "Solids Under Pressure", McGraw-Hill Inc., New York, N.Y., 1963

CHAPTER 7

1. M. Kaplansky and M.A. Whitehead, Canad. J. Chem., 1967, 45, 1669
2. R. Clipsham, R.M. Hart and M.A. Whitehead, Inorg. Chem., 1969, 8, 2431
3. M. Dixon, H.D.B. Jenkins, J.A.S. Smith and D.A. Tong, Trans. Faraday Soc., 1967, 63, 2852
4. A. Connelly, W.H. Dalglish, P. Harkins, R. Keat, A.L. Porte, I. Raitt and R.A. Shaw, J. Mag. Res., 1978, 30, 439 and references therein

5. M.A. Whitehead, *Canad. J. Chem.*, 1964, 42, 1212
6. R. Keat, A.L. Porte, R.A. Shaw and D.A. Tong, *J. Chem. Soc. Dalton*, 1972, 1648
7. K.R. Sridharan, J. Ramakrishna, S.S. Krishnamurthy and M.N. Sudheendra Rao, *Current Science*, 1978, 47, 938
8. K. John and T. Moeller, *Inorg. Synth.*, 1963, 7, 76
9. R. Stahlberg and E. Steger, *J. Inorg. Nucl. Chem.*, 1967, 29, 961
10. P. Nannelli, S.-K. Chu, B. Manhas and T. Moeller, *Inorg. Synth.*, 1968, 11, 201
11. R. Stahlberg and E. Steger, *J. Inorg. Nucl. Chem.*, 1966, 28, 684
12. W.H. Dalglish, R. Keat, A.L. Porte and R.A. Shaw, *J. Mag. Res.*, 1975, 20, 351
13. A. Connelly, P. Harkins, A.L. Porte, R.A. Shaw and J.C. Van de Grampel, *J.C.S. Dalton Trans.*, 1980, 1012
14. T. Moeller and P. Nannelli, *Inorg. Chem.*, 1963, 2, 659
15. P. Nannelli and T. Moeller, *Inorg. Chem.*, 1963, 2, 896
16. E. Giglio and R. Puliti, *Acta Cryst.*, 1967, 22, 304
17. H. Zoer and A.J. Wagner, *Acta Cryst.*, 1970, B26, 1812
18. P.A. Kamminga and A. Vos, *Cryst. Struct. Comm.*, 1979, 8, 743

19. A.L. Allred, J. Inorg. Nucl. Chem., 1961, 17, 215
20. A.L. Allred and E.G. Rochow, J. Inorg. Nucl. Chem., 1957, 5, 264
21. R.T. Sanderson, in "Inorganic Chemistry", Van Nostrand-Reinhold, New York, 1967, pages 72-76
22. J. Hinze and H.H. Jaffé, J. Amer. Chem. Soc., 1962, 84, 540
23. J. Hinze and H.H. Jaffé, J. Phys. Chem., 1963, 67, 1501
24. Kareem Sh. Ahmed and Andrew L. Porte, J. Mol. Struct., 1980, 58, 459
25. H. Zoer and A.J. Wagner, Acta Cryst., 1972, B28, 252
26. Segel USAEC IS 520 Cat. of N.Q.R. Interpretations and Resonances in Solids, Part - I Elements and Inorganic Compounds.
27. W.H. Dalglish, Ph.D. Thesis, Glasgow University, 1975
28. Y. Morino and M. Toyama, J. Chem. Phys., 1961, 35, 1289
29. J.G. King and V. Jaccarino, Phys. Rev., 1954, 94, 1610

